Dissertation

IN SITU SPECTROSCOPY OF CATALYTICALLY ACTIVE SURFACES: FTIR AND EXAFS STUDIES OF CO OXIDATION ON PD AND AU NANOPARTICLES

ausgeführt zum Zwecke der Erlangung des akademischen Grades eines Doktors der Technischen Wissenschaften unter der Leitung von

Univ.Prof. Mag.rer.nat. Dr.rer.nat. Günther Rupprechter

E165

Institut für Materialchemie

eingereicht an der Technischen Universität Wien

Fakultät für Technische Chemie

von

Dipl.Ing. Katrin Zorn

9908781

Kalvarienberggasse 18/1/3, 1170 Wien

Wien, am 19.04.2010

ZUSAMMENFASSUNG

Ziel der vorliegenden Arbeit war, den Reaktionsmechanismus der CO Oxidation an technischen Palladium- und Gold-Nanopartikeln unter Reaktionsbedingungen zu untersuchen. Die Kombination von *in situ* Fourier-transformierter Infrarot (FTIR) Spektroskopie und *in situ* Röntgenabsorptionsspektroskopie (XAS) ermöglichte eine umfassende Charakterisierung der technischen Katalysatoren unter Reaktionsbedingungen. Durch gleichzeitige Bestimmung der katalytischen Aktivität mittels Gaschromatographie (GC) bzw. Massenspektroskopie (MS) konnten spezifische katalytische Aktivitäten mit definierten strukturellen (aber auch chemischen) Eigenschaften, sowie mit den auf der Oberfläche vorhandenen Adsorbaten (Reaktanten, Intermediate) korreliert werden. Hochauflösende Transmissionselektronenmikroskopie (HRTEM), Röntgendiffraktion (XRD), Chemisorption von H_2 oder CO, sowie (*ex situ*) FTIR Spektroskopie von CO als Sondenmolekül wurden ergänzend zur Charakterisierung der Edelmetall-Nanopartikel eingesetzt.

Zur Identifizierung der aktiven Spezies (metallisches Palladium oder Palladiumoxid) für die **CO Oxidationsreaktion an Pd-Nanopartikeln** wurde der Oxidationszustand eines technischen Pd-Al_2O_3 durch variable oxidative und reduktive Vorbehandlung variiert. Durch umfassende Charakterisierung konnte den so erhaltenen verschiedenen PdO_x Nanopartikeln (mit x=0-1) eine spezifische katalytische Aktivität für die CO Oxidation zugewiesen werden. Die beinahe äquivalente katalytische Aktivität von Substöchiometrischem Palladiumoxid PdO_x (x<1) und metallischem Pd konnte auf eine Reduktion (bereits bei Raumtemperatur) des PdO_x zu Pd in Anwesenheit von CO zurückgeführt werden. Stöchiometrisches Palladium(II)oxid wies hingegen eine signifikant niedrigere Aktivität für die CO Oxidation auf. Grund hierfür ist die deutlich höhere Stabilität gegen Reduktion durch CO, welche erst bei Temperaturen >533 K stattfindet.

Mittels *in situ* EXAFS und *in situ* FTIR spektroskopischen Untersuchungen konnte im hohen Aktivitätsbereich eine partielle Oxidation der Metall-Nanopartikel festgestellt werden. Unter hoher Aktivität kommt es somit zu einer Koexistenz von metallischem Pd und substöchiometrischem PdO_x ($x<1$). Dieses dynamische Verhalten der partiellen Ausbildung von Palladium-Suboxiden, welche sich (bereits bei relativ niedriger Temperatur) in Gegenwart von CO wieder zersetzen, führte unter spezifischen Reaktionsbedingungen zu Oszillationen der Reaktionsrate. Dadurch war ein Vergleich der katalytischen Aktivität von Pd und PdO_x unter identen Reaktionsbedingungen möglich, wobei dem (O_2-bedeckten) metallischen Pd die höchste Aktivität zugeordnet werden konnte. Für die Aktivierung von CO (bzw. O_2) und für die Aufrechterhaltung hoher katalytischer Aktivität ist somit die Anwesenheit von reduziertem, metallischem Palladium entscheidend.

Um den Reaktionsmechanismus der **CO Oxidation an Gold-Nanopartikeln** aufzuklären, wurden technische Au-TiO_2 Katalysatoren unter Reaktionsbedingungen untersucht. *In situ* FTIR spektroskopische Untersuchungen lokalisierten das CO-Adsorptionszentrum eindeutig am Au^0 (und jegliche Detektion von $Au^{\delta+}$ ging mit einer signifikanten Deaktivierung einher), wohingegen das Sauerstoff-Adsorptionszentrum am TiO_2 nachgewiesen wurde.

Weiters zeigten Versuche mit isotopenmarkiertem $^{13}C^{18}O$, dass Hydroxylgruppen (des TiO_2) katalytisch an der Reaktion teilnehmen. Dies erklärt die Aktivitätszunahme nach Zugabe einer geringen Menge Wasser, welches durch Dissoziation am TiO_2 zur Ausbildung terminaler OH- Gruppen führt. Die mittels *in situ* Spektroskopie erhaltenen Ergebnisse der CO Oxidation an Au/TiO_2 weisen daher auf eine Phasengrenzreaktion an der Oxid/Metall-Grenzfläche hin.

ABSTRACT

The objective of this thesis was to study the mechanism of CO oxidation on industrial-grade palladium and gold nanoparticles under technically relevant reaction conditions. Combining ***in situ*** **EXAFS and** ***in situ*** **FTIR spectroscopy** provided simultaneous information on the local structural properties of the active catalyst and the adsorbed surface species (reactants, intermediates). The simultaneous determination of the catalytic activity via gas phase analysis by gas chromatography (GC) or mass spectroscopy (MS) allowed to directly assign specific catalytic activity to specific structural or chemical properties. High-resolution Transmission Electron Microscopy (HRTEM), X-Ray Diffraction (XRD), chemisorption of Hydrogen or CO and CO adsorption followed by FTIR spectroscopy have been applied as complementary methods for comprehensive (*ex situ*) characterization of the noble metal catalysts. For selected systems Density Functional Theory (DFT) studies enabled a correlation of structure with adsorption properties.

In order to evaluate the nature of active sites (metallic palladium vs. palladium oxide) for **CO oxidation on palladium nanoparticles**, the activity of different PdO_x (x=0-1) species was investigated. Supported PdO_x (x=0-1) nanoparticles, obtained upon variable oxidizing and reducing pretreatments of Pd-Al_2O_3 were comprehensively characterized and the catalytic activity for CO oxidation was determined. Substoichiometric PdO_x (x<1) and metallic Pd nanoparticles showed comparable high catalytic activity, caused by the facile reduction (already at room temperature) of PdO_x to Pd upon CO exposure. In contrast, stoichiometric palladium(II)oxide exhibited lower catalytic activity. This was explained by the higher stability towards reduction by CO (up to 533 K).

In situ EXAFS and *in situ* FTIR spectroscopy, performed during steady state CO oxidation on Pd-Al_2O_3, detected a partial oxidation of the metallic nanoparticles, i.e. a coexistence of metallic palladium and substoichiometric palladiumoxide PdO_x, in the high ac-

tivity regime. The highly dynamic behaviour of partial PdO_x formation, that can be easily decomposed/reduced (at low temperature) in the presence of CO to metallic palladium, led under very specific conditions to oscillatory behaviour. This allowed an unambiguous comparison of the specific activities of metallic palladium and palladium(sub)oxide, and conclusive evidence for oxygen-covered metallic Pd being the active phase for CO oxidation was found. The *in situ* spectroscopic study of CO oxidation on Pd-Al_2O_3 indicated that metallic Pd was essential for the activation of CO (and oxygen), and thus required for high catalytic activity.

In order to elucidate the nature of the catalytically active sites and the mechanism for **CO oxidation on Au nanoparticles**, CO oxidation was studied on industrial-grade Au-TiO_2 under technically relevant conditions. *In situ* FTIR spectroscopic studies identified zero-valent gold atoms as the main CO adsorption site (any detection of oxidized $Au^{\delta+}$ was paralleled by deactivation), whereas the O_2 adsorption sites were localized on the TiO_2 support.

Adsorption experiments with isotopically labelled $^{13}C^{18}O$ clearly demonstrated the involvement of support hydroxyl groups in the catalytic reaction. This also explained the increase in catalytic activity observed upon addition of small amounts of water, that dissociated on titania producing an increased number of terminal OH groups. The results of the *in situ* FTIR spectroscopy study of CO oxidation on Au-TiO_2 strongly supported a “phase boundary-mechanism”, with the reaction taking place at the metal/oxide interface.

I would like to thank…

*… my supervisor **Günther Rupprechter** for proposing an exciting project. I am grateful for his guidance, the valuable discussions and for his support- particularly in the final level of this work.*

*… **Suzanne Giorgio** and **Claude Henry** for the HR-TEM measurements performed at the CNRS and their support during my stay in Marseille.*

*… **Jeroen van Bokhoven** for guiding the EXAFS analysis and for the helpful discussions during my stay in his group at the ETH Zürich.*

*… **Henrik Grönbeck** for the DFT calculations, **Erich Halwax** for the XRD and **Jose Juan Calvino** for the HAADF-STEM measurements.*

… Österreichische Forschungsgemeinschaft, Österreichischer Austauschdienst, Marietta Blau Mobilitätsstipendium, Gesellschaft österr. Chemiker, VFA der TU Wien, Deutsche Bunsengesellschaft, EU Travel support and COST for financially supporting my research at other institutions and the attendance of several conferences.

*… **all colleagues at the institute**, for the great working atmosphere and for the welcome (coffee)breaks in between.*

*… **my family and friends** for always being there.*

TABLE OF CONTENTS

1

INTRODUCTION

The objective of heterogeneous catalysis has been drastically changed within the last decades. In the beginning of catalysis, the main focus was to maximize the activity of a catalyst, in order to increase the yield of a particular product. However, this was often accompanied by the production of significant amounts of (hazardous) waste, formed by unselective side reactions. Nowadays, the highest priority is rather to obtain the desired product with maximum selectivity, in order to use raw materials most efficient. This development of environmentally-benign technologies is part of a concept that is usually referred to as "green chemistry".

However, in order to "tune" the selectivity of a heterogeneous catalyst (such as oxide supported noble metal nanoparticles) in the desired direction, fundamental knowledge of the processes occurring on the catalyst surface, i.e. a molecular level understanding of the reaction mechanism, is required. Since the catalytic performance strongly depends on the structural and chemical properties, the key goal is to correlate distinct catalyst properties with a certain catalytic activity and/or selectivity, for which comprehensive catalyst characterization is essential. Industrial catalysis usually takes place at relative high temperature and/or pressure. Under such conditions many processes such as sintering, restructuring, reduction or oxidation of the catalyst may occur that can strongly alter the catalytic performance. In many cases the active sites may even be created during the reaction. Such information is not accessible when catalysts are characterized only before or after reaction (by so called "*ex situ"* characterization techniques) or studied under conditions far from technical relevance. Therefore, there is definitely need for "*in vivo"* studies, i.e. *in situ* investigation of the working catalyst under technically relevant reaction conditions. It should be noted that within this thesis "*in*

situ" is used in its strictest sense i.e. "*in situ*" refers to spectroscopy performed on the working catalyst during CO oxidation, paralleled by simultaneous activity measurements. This approach is also referred to as "operando" spectroscopy in the literature.

In situ Fourier-Transform Infrared (FTIR) spectroscopy is a well-established method for this purpose. It provides information on species adsorbed under reaction conditions and the (active) adsorption site, and the nature and location of intermediates may be identified. The application of X-ray Absorption spectroscopy (XAS), such as EXAFS (Extended X-Ray Absorption Fine Structure), is less frequently applied (mostly due to the requirement of a synchrotron facility), but is a very valuable analytical tool in catalysis. EXAFS spectroscopy provides detailed information on the local structure of the catalyst (without the need of long-range order), which is especially suitable for nanoparticles and amorphous phases. Since both methods exclusively probe photons, they are applicable under technically relevant (high pressure) conditions. Therefore, FTIR and EXAFS belong to the most important *in situ* spectroscopic methods.

CO oxidation is *the* prototypical reaction for mechanistic studies and the most investigated catalytic reaction in heterogeneous catalysis. However, the exact reaction mechanism and the nature of active sites under technically relevant reaction conditions are still debated.

For CO oxidation on palladium (or on Pt group metals), metallic Pd was identified being the active site. However, in the recent years increasing attention has been drawn towards a so-called "oxide model", in which the catalytic activity is assigned to a surface oxide formed under reaction conditions. A vivid debate has started on the nature of the active sites (metallic palladium vs palladium oxide) for CO oxidation on Pd.

For CO oxidation on gold the situation is even "worse" and CO oxidation on Au seems to be a mystery after all. Small gold nanoparticles are able to catalyze CO oxidation at temperatures as low as 203 K but the origin of this exceptional high catalytic activity and the reaction mechanism (which may also strongly depend on the support) are still ambiguous.

This thesis was thus aiming at a fundamental investigation of the reaction mechanism of CO oxidation on industrial-grade Pd and Au catalysts, using *in situ* FTIR and EXAFS spectroscopy. The concept of *in situ* spectroscopy under technically relevant conditions was combined with isotope adsorption studies in order to answer fundamental questions concerning the relevant active site and reaction mechanism under technical (industrial) conditions.

Following an Introduction of experimental methods, Chapter 3 of this thesis is dedicated to a comprehensive characterization of different oxidized and reduced PdO_x (x=0-1) nanoparticles. Systematic oxidation studies were performed to elucidate the nature of PdO_x (x=0-1) that may be present under reaction conditions. The behaviour of the particular species in a CO atmosphere or under CO oxidation conditions was then investigated by *in situ* FTIR spectroscopy, in order to correlate the palladium oxidation state with a specific catalytic activity.

Chapter 4 of this thesis is concerned with the mechanism of oscillatory CO oxidation on palladium nanoparticles. The structural properties and the adsorbates during an oscillation period were identified by *in situ* EXAFS and *in situ* FTIR spectroscopy. Via a simultaneous determination of the catalytic activity of oscillatory CO oxidation, the nature of active site (palladium vs palladiumoxide) for CO oxidation was elucidated.

Finally, Chapter 5 is dedicated to CO oxidation on gold nanoparticles. Systematic adsorption studies of isotopically labelled and unlabelled CO and CO_2 were performed to obtain mechanistic information on the CO adsorption site, the gold oxidation state and the nature of possible intermediates. Again, *in situ* FTIR spectroscopy was applied under variable reaction conditions to study the nature of surface species during reaction and to gain insight in the reaction mechanism of CO oxidation on gold.

Chapter 6 is a concise summary of the most important results. Although CO oxidation on noble metals is a seemingly “simple” reaction, with its elucidation awarded with the Nobel Prize 2007, under technically relevant reaction conditions the influence of surface oxidation adds significant complexity, that can only be tackled by *in situ* observations of “catalysts at work”.

2

EXPERIMENTAL

One of the main goals in heterogeneous catalysis is to correlate specific catalyst properties with resulting catalytic activity and/or selectivity. Therefore, a comprehensive catalysts characterization, preferentially *under reaction conditions*, is essential. This experimental chapter gives a short introduction to the most important characterization methods applied in this thesis. Extended X-Ray Absorption Fine Structure (EXAFS) Spectroscopy will be discussed as a method that provides structural and chemical information of catalysts via interference of scattered radiation. (High Resolution) Transmission Electron Microscopy (HR-TEM) reveals information about the size and shape of supported nanoparticles, but also about their composition and internal structure, and X-ray fluorescence or diffracted electrons can be analyzed. Finally, Infrared spectroscopy will be discussed, likely being the most important spectroscopic technique in catalysis, which provides information of adsorbates and the catalyst itself. After a brief theoretical background of each method, an overview of the type of accessible information will be given and limitations are discussed, focussing mainly on the applicability for technical supported metal catalysts. The experimental details of the particular experiments will be provided in the corresponding sections.

2.1 Extended X-Ray Absorption Fine Structure (EXAFS)

Extended X-ray Absorption Fine Structure (EXAFS) Spectroscopy is an X-Ray absorption technique which provides detailed information on the local structure of catalysts. Due to the fact that EXAFS exclusively probes photons, it is a very important *in situ* spectroscopic method that can be applied under technically relevant reaction conditions.

The method is based on the absorption of X-rays (photons with wavelengths ranging from ~25 Å to 0.25 Å) through the photoelectric effect: photoelectrons are created that are scattered by nearby atoms, which leads to interference effects that show up in the X-ray absorption spectrum. This phenomenon was already known since the 1920s but the application of EXAFS had to wait until tunable X-ray sources became available at synchrotron facilities in the 1970s.

The basic physics

According to Lambert's law (equation (2-1)) the incident intensity I_0 of an X- ray beam is reduced to I_t when it passes through a material. The extent of attenuation depends on the path length x of the radiation through the material (i.e. the sample thickness) and the linear absorption coefficient μ(E), which is a function of the photon energy E:

$$I_t = I_0 e^{-\mu(E)x} \qquad (2\text{-}1)$$

An X-Ray absorption spectrum (see Figure 2-1) typically exhibits an intensity smoothly decreasing to higher energy. As soon as the energy of an incoming photon is high enough to excite an electron from the inner core levels to an unoccupied electronic state or to the continuum, a sharp increase in the absorption intensity is observed. This increase is the so-called absorption edge. Depending on the shell from which the electrons are released, the edges are called K- or L-edges for the most strongly bonded (n=1) and next most strongly bonded (n=2) shells, respectively. Assuming that the absorbed photon with the energy E_{hv} excites a single core electron, the kinetic energy of the electron E_{kin} is given by the difference between the photon energy E_{hv} and the binding energy in the atom E_b: $E_{kin} = E_{hv} - E_b$.

The linear absorption coefficient μ(E) is proportional to the transition probability of the photoelectric event. According to Fermi´s Golden Rule (equation 2-2) the transition probability is a function of the initial ψ_i- and final-state wave functions ψ_f.

$$\mu(E) = C\left|\langle \psi_f | \hat{e}r | \psi_i \rangle\right|^2 \delta(E_f - E_i - hv) \qquad (2\text{-}2)$$

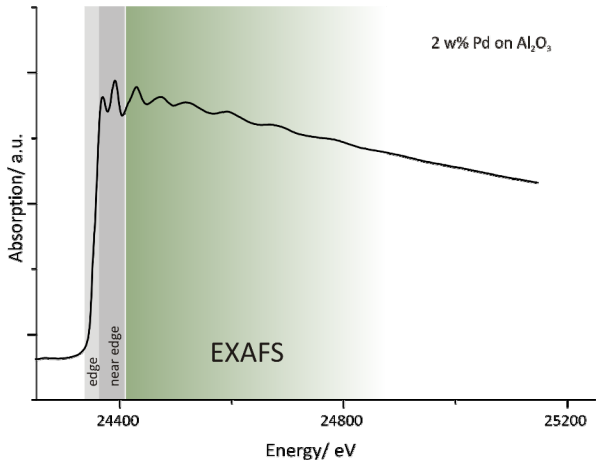

Figure 2-1 X-Ray Absorption spectrum as a function of photon energy at the Pd K-edge of Pd particles supported on γ- Al_2O_3. Assignment of the edge, near edge and EXAFS region.

The created outgoing photoelectron must be quantum mechanically treated as a wave whose wavelength is given by the de Broglie relation (see equation (2-3) where ħ is the reduced Planck constant and p is the momentum of the photoelectron). Due to it's wave character it can be scattered at a neighboring atom and interfere with the outgoing wave, upon which the two waves can enhance or cancel each other.

$$\lambda = \frac{\hbar}{p} \tag{2-3}$$

Since the final-state wave function ψ_f consists of the outgoing *and* the backscattered electron wave (equation (2-4)), the transition probability and therefore the absorption coefficient μ(E) are modulated by the interference between these two waves.

$$\psi_f = \psi_{outgoing} + \psi_{backscattered} \tag{2-4}$$

The final phase is (apart from the wavelength of the photoelectron and the phase-shift caused by the scattering event) defined by the path lengths of both waves. Thus, the distance to the neighboring atoms determines the interference pattern. This interference pattern is visible in the X- Ray Absorption spectrum where fine structure is observed that extends up to several hundred electron volts above the absorption edge (marked by the green area in Figure 2-1).

The EXAFS function: In a mono-atomic solid the EXAFS function χ(k) (equation (2-5)) is the sum of the scattering contributions of all neighboring coordination shells and can be extracted from an absorption spectrum by removing the parabolic background and the absorption step (i.e. the spectrum of a free atom). The EXAFS function can be expressed as a function of the wave number of the photoelectron k, where i labels the coordination shells around the electron emitting atom, $A_i(k)$ is the amplitude (equal to the scattering intensity due to the i^{th} coordination shell), r_i is the distance between the central atom and atoms in the i^{th} shell and Φ_i is the total phase shift.

$$\chi(k) = \sum_i A_i(k) \sin\left[2kr_i + \Phi_i(k)\right] \tag{2-5}$$

Qualitative interpretation of the EXAFS function: In the following, a qualitative interpretation of the parameters appearing in the EXAFS function is provided. For detailed information refer to the literature (see [1] and references therein).

Every coordination shell contributes a sine function multiplied by an amplitude A_i to the EXAFS function. The amplitude A_i contains the number of neighbors in the coordination shell N_i as the most important information (see equation (2-6)):

$$A_i(k) = N_i \frac{e^{2r_i/\lambda(k)}}{kr_i^2} S_0^2(k) F_i(k) e^{2k^2\sigma_i^2} \tag{2-6}$$

Other terms include e.g. the attenuation of the electrons when traveling through the solid (first exponential term) or relaxation effects of the emitting atoms (S_0). The back-scattering factor F_i is a very important quantity: it's dependency on energy is characteristic for an element and is recognizable in the envelope of the EXAFS contribution from a specific neighbor. Thus, a scattering atom can be identified via F_i. Finally, the so-called Debye-Waller Factor σ_i^2 is included in the last exponential term: it is the root mean square deviation of the interatomic distance r_i and therefore a measure for the fluctuations in r_i, either due to thermal motion or structural disorder.

EXAFS analysis: Apparently, a great deal of information about the material studied is included within the EXAFS equation and the main goal in EXAFS analysis is to retrieve three key items of information for every single coordination shell: namely the intera-

tomic distances r_i, the coordination numbers N_i and the Debye Waller Factors σ_i^2. In order to retrieve this information all sine contributions of the EXAFS function must be determined. Fourier Analysis is thus performed which converts the EXAFS function $\chi(k)$ to a radial distribution function $\Theta_n(r)$ (equation (2-7)), which represents the probability of finding an atom at a distance r, modified by two r-dependent terms which progressively decrease the intensity of distant shells.

$$\Theta_n(r) = \frac{1}{\sqrt{2\pi}} \int_{k_{min}}^{k_{max}} k^n \chi(k) e^{2ikr} dk \qquad (2\text{-}7)$$

The argument of each sine contribution (see again equation (2-5)) depends on k (which is known), on r (to be determined) and on the phase shift Φ_i. The phase shift is a characteristic property of the scattering atom in a certain environment and can be derived from the EXAFS spectrum of a reference compound for which all distances r_i are known. Additionally, n is an integer and can be chosen n=1 to selectively emphasize light or n=2 or 3 to emphasize heavy scatterers.

Information Content and Limitations of EXAFS:

As already mentioned, EXAFS is an ideal probe for local structures of catalytic materials under reaction conditions. It provides information on the number and kind of neighboring atoms, and their distances. One main advantage of this method is the high penetrating power of the X-rays, which makes this technique ideal for *in situ* studies. X-ray Diffraction (XRD) is similar in this regard, but it requires long-range order and is therefore especially less suitable for small particles (below 3 nm particle size) or for amorphous phases. Thus, EXAFS is particularly usefull to study the structure of supported metal nanoparticles and opens e.g. the possibility to determine their dispersion, since it was shown that the coordination number, which is directly accessible via EXAFS analysis, is a linear function of the particle size [2, 3]. Consequently, EXFAS represents an alternative to dispersion analysis via chemisorption [4], with the advantage that no adsorption stoichiometry of the probe molecule needs to be assumed. However, EXAFS is only meaningful assuming monodisperse particles, i.e. that the average environment is the same throughout the entire catalyst. Furthermore, data analysis can become very

complicated and time consuming for multi-component catalysts and strong expertise is required. Finally, since EXAFS is an inherently short-range order probe and does not give any information on long-range order, it can not replace diffraction techniques such as XRD, but rather complements them.

2.2 Transmission Electron Microscopy (TEM)

Historically, Electron Microscopes were developed because of the limited image resolution of light microscopes. After Louis de Broglie 1925 first stated that electrons also have wave-like characteristics with a wavelength substantially smaller than that of visible light, Knoll and Ruska developed the idea of an electron microscope already in 1932, for which Ruska received the Nobel Prize in 1986. Nowadays, Electron Microscopy is a well-developed technique for the determination of particle size and shape of supported catalyst particles. Even though the main motivation for the development of the first electron microscopes was to improve image resolution, it was soon realized that many other (secondary) signals were produced upon interaction of a high-energy electron beam with a specimen. Most of them are utilized in so-called analytical electron microscopes (AEM), providing complementary information [5, 6].

The basic physics

Interaction of electrons with matter: Figure 2-2 gives a schematic overview of the signals that are generated upon interaction of a high-energy electron beam with a specimen.

a) *Transmitted electrons* (direct beam): Fraction of primary electrons that passes the sample without energy loss.

b) *Diffracted (coherently elastically scattered) electrons*: Electrons are diffracted at crystal planes of particles that are favorably oriented towards the electron beam (Bragg condition).

c) *Inelastically Scattered Electrons*: Electrons can interact inelastically with the specimen, the corresponding energy loss is characteristic for the affected elements.

d) *Backscattered Electrons*: Belong to the part of incoherently elastically scattered electrons (that collide with single nuclei) that are reflected from the sample; the backscattering is more efficient for heavy atoms.

e) *X- Ray and Auger Electrons*: The emission of X- rays and Auger electrons, which takes place upon relaxation of core-ionized atoms, contains elemental information.

f) *Secondary Electrons*: Created as ionization products upon inelastic collisions.

g) *Cathodoluminescence*: Photons are emitted (from UV to IR) by the recombination of electron-hole pairs created in the sample.

Operating modes and analysis options: The different operating modes and analysis options will be briefly introduced to demonstrate how the particular species, created upon interaction of the electron beam with the specimen, contribute to provide information on crystallography, chemical composition and morphology of a sample.

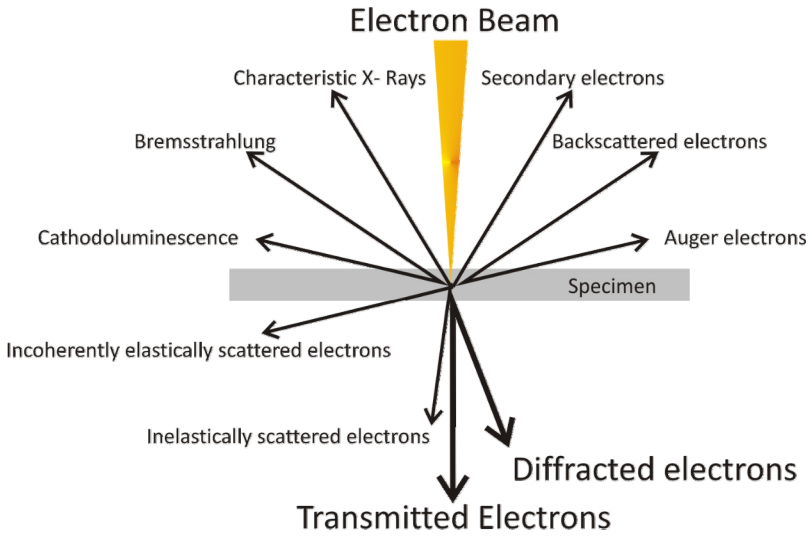

Figure 2-2 Signals generated upon interaction of a high-energy electron beam with matter.

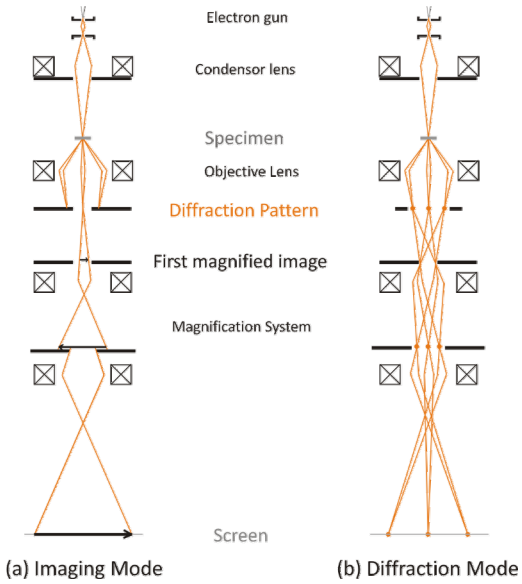

Figure 2-3 Schematic illustration of the two different TEM operating modes: the Imaging (a) and the Diffraction mode (b).

A) *Transmission Electron Microscopy (TEM) operating modes*: Basically, there are two main modes of a transmission electron microscope. The *Imaging mode* (bright field and dark field imaging) and the *Diffraction mode* (see Figure 2-3):

a) The *Imaging mode* (see Figure 2-3a) is similar to an optical microscope: an electron beam passes through a condenser which produces parallel rays that impinge on the specimen. When the transmitted electrons (of the direct beam) are used to form a two-dimensional projection of the sample this is called “bright field imaging” and contrast is caused due to different sample thickness, different sample density and regions that scatter (diffract) a portion of the beam away from the axis. Contrast is created when using an objective aperture (in the back focal plane of the objective lens) which removes diffracted electrons so they cannot contribute to the image formation anymore. In the “dark field imaging” mode the diffracted (elastically scattered) electrons are used to form the image. This can be realized by shifting the objective aperture off-centre, to remove the direct beam from subsequent imaging. High resolution imaging is possible in both modes (bright and dark field), in which lattice planes may be studied to resolve crystal structure and defects.

b) In the *Diffraction mode* (see Figure 2-3b) the image from the back focal plane of the objective lens is magnified. This gives a diffraction pattern that contains crystallographic information about the specimen. By analyzing the spot pattern dimensions and directions it is possible to deduce exact crystallographic information of a specimen.

B) Scanning Transmission Electron Microscopy (STEM): In STEM the electron microscope is operated in scanning mode, with a converged electron beam scanned across a defined sample area. Figure 2-4 schematically illustrates the location of the diverse detectors used for imaging and chemical analysis of the following probes:

a) *Transmitted electrons*: the "primary electrons" are projected onto a bright field detector (BF) for space-resolved bright field imaging.

b) *Diffracted electrons* are projected on the dark field detector (DF) for space-resolved dark field imaging.

c) *Incoherently elastically scattered electrons* are projected on a high-angle annular dark field (HAADF) detector. Heavier elements scatter more efficient, thus space-resolved elemental information of the sample is obtained.

d) *Backscattered electrons* originate from deeper specimen regions and can be detected using a backscattered electron detector (BSED): heavier elements scatter more efficient and appear brighter in the image and therefore information on the composition of the sample is obtained.

e) *Secondary electrons* usually exhibit low kinetic energies and can therefore only escape if they were created close to the specimen surface. Thus, a high-resolution topographic image of the specimen surface can be obtained using a secondary electron detector (SED).

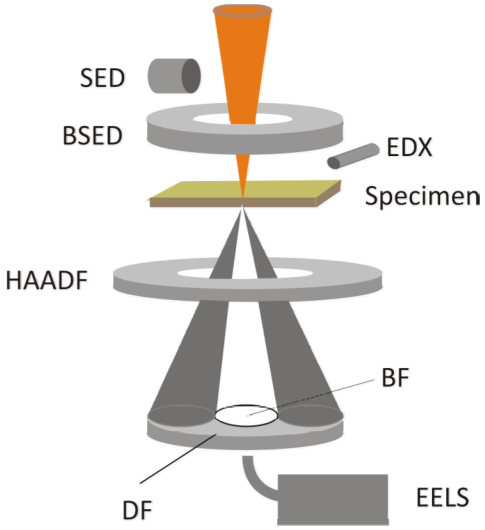

Figure 2-4 Location of the various detectors for imaging and elemental analysis: Bright field (BF), Dark field (DF), High-angle annular dark field (HAADF), Secondary electron (SED), Backscattered electron (BSED) and X-ray (EDX) Detector and the Electron Energy Loss Spectrometer (EELS).

f) *X- rays*: By using an EDX detector the characteristic X-rays can be detected to gain information on the chemical composition of a selected part of the sample. The analysis of Auger electrons, which are created simultaneously with X-rays (but with a higher efficiency for lighter elements), is not commonly used since their detection requires UHV conditions.

g) *Inelastically scattered electrons*: Electron Energy-Loss Spectroscopy (EELS) is applied to determine the energy distribution of the inelastically scattered electrons. Detailed information on the elemental, structural and electronic properties of a specimen can be obtained. The main advantage of EELS compared to EDX is the higher sensitivity for lighter elements, since they generally exhibit a low X-ray fluorescence efficiency.

Information Content and Limitations of TEM

Transmission electron microscopy belongs to the most often used characterization techniques for catalysts. The determination of particle size distributions has become a matter of routine, as long as sufficient contrast between the particles and the support is obtained and uniform detection probability for all particles applies. Additionally, diffrac-

tion pattern analysis provides comprehensive structural information on grain sizes, shapes and distributions. Point and space groups can be determined and defects such as dislocations, stacking faults or grain boundaries can be identified. Via EDX and EELS analysis also elemental information on the investigated specimen is accessible. However, several limitations of the method need to be discussed: first of all, high resolution means also that only a small part of the specimen can be observed at a time, with the assumption that the imaged part of the catalyst is representative for the entire material. Secondly and probably the major limitation in TEM is the requirement of thin specimen. Sample preparation methods that affect the specimen may change both structure and its chemistry. Finally, due to the fact that the method involves electrons, beam damage can create difficulties, especially with increasing accelerating voltage. The use of electrons also implies that imaging needs to be performed in vacuum (to give sufficiently long mean free path for the electrons). This is another problem since the morphology of small particles may critically depend on the gaseous environment [7, 8]. However, this limitation was partially overcome by the development of so-called environmental high resolution transmission electron microscopes (ETEM), when special “high pressure cells” allow measurements at a background pressure of several mbar.

2.3 Infrared Spectroscopy

Infrared spectroscopy can be considered the most important spectroscopic technique in catalysis, with the first commercial infrared instruments being available in the 1940s [9]. The first studies of adsorption on supported metals were done in the pioneering work of Eischens *et al.* [10, 11] already during the 1950s. The method is based on the excitation of intramolecular vibrations by the absorption of photons with wavelengths in the mid- IR, ranging between 50 and 2.5 μm. The most common application in catalysis is to identify adsorbed species and to characterize the nature of the corresponding adsorption sites on the catalyst surface.

The basic physics

Molecules possess discrete levels of vibrational energy. Transitions between different vibrational energy levels occur upon absorption of photons with wavelength in the mid-IR range (50-2.5 μm). As a general selection rule for the absorption of a photon the (dynamic) dipole moment of the molecule must change during the vibration.

Normal vibration modes: In general, the description of a molecule consisting of N atoms requires 3N coordinates. Three coordinates are necessary to describe the translational motion and three (or two for linear molecules) extra coordinates are required for the description of the rotational motion. The remaining 3N-6 (3N-5 for linear molecules) coordinates are used to describe the motions of the atoms relative to one another, the so-called vibrational modes. The description of these modes is simplified when only normal modes of vibrations are considered. A normal mode of vibration is one when each nucleus executes simple harmonic oscillations around the equilibrium position. All nuclei move with the same frequency and are in-phase and the center of mass of the molecule remains unaltered. Each normal mode of vibration is treated as a simple harmonic oscillation of a so-called normal coordinate. The normal coordinate is constructed such that it expresses all individual displacements of the nuclei involved. In the following, a diatomic molecule will be considered for which the (unique) normal coordinate corresponds to the internuclear distance/bond.

The harmonic approximation: The simplest model of a diatomic vibrating molecule is the harmonic oscillator, which can be described by two masses m_1 and m_2 connected via a weightless spring with the force constant k, which is a measure of the bond strength. The force dF necessary to move the atom by a certain distance dx from the equilibrium position is proportional to the force constant k according to Hook's law (equation (2-8)), with the corresponding "harmonic" potential energy V representing a parabola (equation (2-9)):

$$dF = -kdx \tag{2-8}$$

$$V = \frac{1}{2}kx^2 \tag{2-9}$$

Solving Schrödinger´s Equation for the harmonic oscillator leads to equidistant vibrational energy levels E_n (equation (2-10)), with a fixed separation of hν (as schematically illustrated in Figure 2-5a). The vibrational frequency ν (equation (2-11)) is related to the atomic masses m_1 and m_2 via the reduced mass m, and the force constant k of the oscillation.

$$E_n = (v_i + \frac{1}{2})h\upsilon \quad \text{with } v_i = 0,1,2,\ldots \tag{2-10}$$

$$\upsilon = \frac{1}{2\pi}\sqrt{\frac{k}{m}} \quad \text{with } \frac{1}{m} = \frac{1}{m_1} + \frac{1}{m_2} \tag{2-11}$$

Allowed transitions in the harmonic approximation are those for which the vibrational quantum number v_i changes by ± 1, while overtones (i.e. transitions with $\Delta v_i > \pm 1$) are forbidden.

The harmonic potential is a useful approximation for small deviations of the atoms from their equilibrium position but it completely fails for larger deviations. The most obvious shortcome of the harmonic potential is that the bond between two atoms cannot break. However, for the interpretation of IR spectra the harmonic oscillator description is usually sufficient. Thus, the vibrational frequency increases with increasing bond strength and decreasing masses of the vibrating atoms, and the force constant of a molecule can be calculated when the vibrational frequency is known.

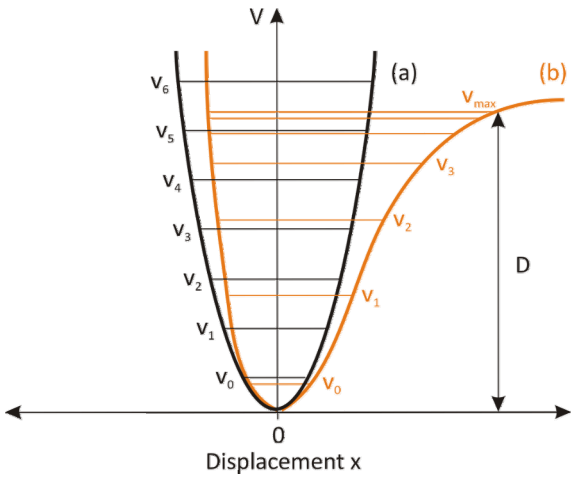

Figure 2-5 The harmonic (a) and anharmonic potential (b) with their corresponding energy states according to quantum mechanics.

The anharmonic approximation: A real molecule performs an anharmonic vibration. Therefore, Hook's law is no longer correct since the force needed to compress a bond is larger than to stretch the bond by the same distance. Anharmonic potentials can be represented by approximate functions, e.g. a physically more realistic potential is the Morse potential (equation (2-12)), where f is the force constant near the potential minimum, D stands for the dissociation energy of the vibrating bond and x again describes the deviation from the equilibrium position. Note that the corresponding vibrational energy levels are no longer equally spaced (see Figure 2-5b). In addition, the number of vibrational energy levels is finite. Dissociation of the chemical bond can take place and overtones with transitions $\Delta v_i > \pm 1$ are allowed (however with a small transition probability).

$$V(x) = D(1 - e^{-\sqrt{f/2D}x})^2 \qquad (2\text{-}12)$$

Vibrational Transitions: Electromagnetic radiation can induce vibrational transitions only for vibrational modes that induce changes in the molecular dipole moment. Such vibrations are called infrared active and the intensity of absorption is proportional to the change in dipole moment. Therefore, species with polar bonds such as CO, NO or OH exhibit strong IR bands, whereas covalent bonds such as C-C or N=N absorb IR light only weakly and homonuclear diatomic molecules such as H_2 or N_2 are infrared inactive. For complex molecules, an analysis of the symmetry of the normal modes is necessary to define the active normal modes.

In terms of selection rules, allowed transitions are defined by $\Delta v_i = \pm 1$. From the Boltzmann distribution it follows for almost all molecules that only the vibrational ground state (v_0) is populated at room temperature. The IR spectrum is then dominated by the fundamental transition from the vibrational ground state E_0 to the first vibrational excited state E_1.

CO adsorption on supported metal catalysts followed by IR

The most common application of infrared spectroscopy in catalysis is to identify adsorbed species and to study the way in which they are chemisorbed on the catalyst. Especially the adsorption of probe molecules such as CO and NO, followed by IR spectros-

copy, is a widely used technique for supported metal catalysts: the vibrational frequency (i.e. the absorption band position) of the probe molecules is strongly influenced by the properties of the substrate. Thus, indirect information on the catalyst can be obtained. The general physical principles, leading to the differing stretching vibrations of adsorbed molecules on supported metal catalysts, will be discussed below, using the example of CO as the most common probe molecule, being also the probe molecule of choice within this thesis.

The Blyholder model: Blyholder [12] qualitatively explained the shift of the infrared band position as a function of adsorption sites and CO coverage , considering CO adsorption on metals in the light of Hückel molecular orbitals. First an isolated (gas phase) CO molecule is considered: the carbon atom, which is sp_z- hybridized forms a σ- bond with the p_z orbital of the oxygen atom, while the p_x and p_y orbitals produce two π bonds. This leads to electron lone pairs in the oxygen 2s orbital and in the carbon sp_z hybrid orbital. This sp_z hybrid orbital has a slightly antibonding character and can form a coordinative bond with a suitable acceptor orbital. Blyholder therefore treats the metal atom as a central atom of a complex, where the d-orbital acts as an acceptor orbital, with the other surrounding metal atoms and the adsorbed CO molecule acting as its ligands. The electron lone pair on the carbon atom forms a σ-bond to the central metal atom which in the first instance strengthens the C-O bond due to the slightly antibonding character of the sp_z orbital. However, this also leads to a large negative charge on the central metal atom. Therefore, back donation from the d-orbital of the central atom to the antibonding π^*-molecular orbital of CO occurs which stabilizes the coordinate bond and consequently the whole complex. Due to this transfer of electron density into the antibonding π^*-orbital, the carbon-oxygen bond is finally weakened, which can be observed in the infrared absorption spectrum by a red shift (i.e. a shift to lower wave number or energy) compared to the gasphase (isolated) CO molecule. Thus, whatever influences the degree of back donation will influence the attenuation of the CO bonding strength, observable by a shift of the absorption band. Therefore, the exact band position contains information on following properties:

a) *Coordination number of the adsorption site*: the surrounding metal atoms ("ligands") compete for electrons and back donation is decreased with an increasing metal coordination number: therefore, the CO absorption band is sensitive to the location of the CO adsorption site (facet, corner, edge, …)

b) *CO coverage*: an increasing number of coordinated CO molecules ("ligands") leads to decreased back donation to the individual CO molecule: the CO absorption band therefore contains information on the CO coverage

c) *CO adsorption geometry*: multiple coordination of a single CO molecule to the metal surface enhances back donation: therefore atop-, bridge- or three-fold-adsorbed CO can be distinguished

d) *Co-adsorbates:* co-adsorbates may also remove or add electrons from/to the metal d-band and therefore also influence the degree of back donation: information about the presence and nature of co-adsorbates is provided

e) *Metal oxidation state*: With increasing positive charge of a metal ion, back donation decreases and may become so weak that the CO absorption band is even blue shifted compared to the isolated (gas phase) molecule. In this case the CO-bond is strengthened by the transfer of the lone pair electrons of the slightly antibonding sp_z-orbital) to the substrate. Therefore, the band position provides information about the metal oxidation state.

Thus, CO adsorption followed by infrared spectroscopy yields a vast variety of indirect information about the chemical nature and structure of catalysts, and a number of reviews are available concerning the characterization of metallic [10, 13-17] and oxidic [14] surfaces.

Many effects influencing the vibrational frequency of CO are successfully explained by the rather simple Blyholder theory. However, the CO absorption spectrum is additionally influenced by the response of the conducting metal substrate to the varying electromagnetic field. The adsorption of CO on a metal surface leads to oscillations of the electrons in the metal conduction band, sympatically with respect to the dipole of the adsorbate. Therefore, an image dipole is created equal to the real one, but opposite in sign

(see Figure 2-6a). Even though the following principles are strictly applicable to an infinite and perfectly conducting sheet only, it turned out that they are an adequate approximation for explaining the behaviour of CO on small supported metal particles, too. In the following a short overview of the physical principles are given, that strongly influence the spectrum of CO molecules adsorbed on metals, and therefore provide comprehensive information on both the adsorbate and the substrate.

The metal-surface selection rule: This rule, first explicitly invoked by Pearce *et al.* [18], states that only vibrational modes that possess vibrational dipole moments with components perpendicular to the surface have measurable intensities. This is explained by the fact that a "real" dipole which is oriented parallel to the metal surface produces an image dipole that exactly opposes it (Figure 2-6b): thus the interaction of both dipoles (real and image) with the IR radiation cancel each other and no absorption can occur. In contrast, a "real" dipole perpendicular to the surface is reinforced by the created image dipole (see Figure 2-6c) and enhanced absorption is observed. This effect leads to a restricted number of observable vibration modes on metal surfaces which results in two important consequences: 1) the IR spectra of complicated molecules are simplified and 2) the analysis of IR (in)active molecular modes of the adsorbates yields information on the exact adsorption geometry on the surface.

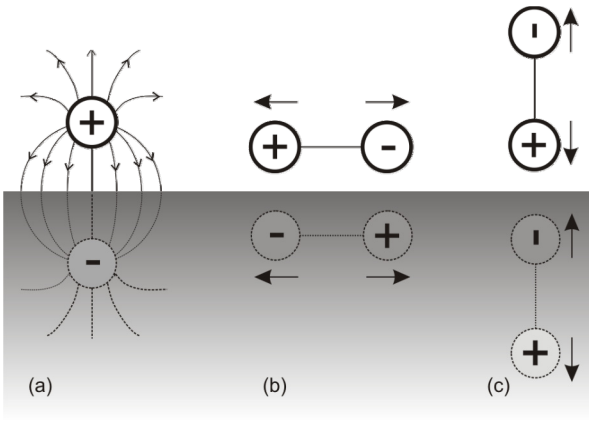

Figure 2-6 Real and image dipoles at metal surfaces: image effect for a single charge (a), the image of a dipole parallel to the surface opposes the original (b) and the image of a dipole perpendicular to the surface enhances the original (c) (Reproduced by permission of Elsevier Science from Pearce *et al* [18]).

Dipolar coupling effects: Hammaker *et al.* [19] found similar cancelling and enhancement effects upon interaction of individual molecular dipoles of adjacent adsorbed molecules:

a) *Coverage dependent wave number shift*: coupling of the dipoles of two identical molecules can give rise to two different modes of collective vibrations: they can vibrate in phase at a wave number slightly higher, or they can vibrate out of phase at a wave number slightly lower than the single molecule. While in the second case the dipoles cancel each other (and the vibration mode is IR inactive), in the first case they reinforce each other and enhanced absorption with a absorption band slightly shifted to higher wave numbers is observed. The number of collective modes increases with the number of coupling molecules, but only the collective mode where all molecules vibrate in-phase is IR active with the wave number continuously blue shifted (i.e. shifted to higher wave numbers). This coupling was shown to be proportional to the product of the dynamic dipoles and inversely proportional to x^3 of their distance x. Since the distance x between the adsorbed molecules varies with coverage, the exact band position provides information on the degree of surface coverage.

b) *Coverage dependent molecular absorptivity*: Dipolar coupling also changes the electronic polarizability of individual molecules. Therefore, the polarizability is also a function of coverage, or more precise: the molecular absorptivity decreases with coverage [20]. As a consequence the absorption band is not proportional to the number of adsorbed molecules and a quantitative interpretation of IR spectra is rather difficult.

c) *Intensity transfer*: Last but not least, coupling between different species (i.e. molecules with different vibrational frequencies) strongly influences the relative intensity of their individual bands: A characteristic transfer of intensity is observed from the low-frequency to the high frequency mode. The reason for this effect is obvious: The collective in-phase vibration (dominated by the high wave

number species) possesses enhanced absorptivity due to the reinforcement of the dipoles. In contrast, the collective out-of phase vibration (dominated by the low wave number species) looses intensity because of the opposing dipoles. This effect can become so strong that a minor high frequency species (of only a few percent) dominates the absorption spectrum of a major low frequency species [20]. This demonstrates that even a qualitative conclusion on the relative amounts of different species is very difficult.

Applications and limitations in catalysis

Infrared spectroscopy is uniquely valuable for the investigation of powder catalyst samples and can give information about the chemical nature of the catalysts or adsorbed species and about their structures and the strengths of chemical bonds. For example, the IR spectrum of an activated sample can provide direct information about the surface hydroxyl groups of the support or other stable surface species such as sulphate groups. Additionally, IR spectroscopy is often applied during catalyst preparation when e.g. the decomposition of a catalyst precursor is followed during drying, calzination or reduction steps. Also intermediate species, formed under reaction conditions, can be identified via *in situ* IR measurements. However, probably the most powerful tool is the application of probe molecules such as CO or NO that provides a vast quantity of indirect information on the adsorption sites (chemical and structural properties) and adsorbates (adsorption geometry, surface coverage and co-adsorbates).

Infrared spectroscopy is certainly a very powerful method for *qualitative characterization* of available adsorption sites, adsorption geometries of reactants, products or intermediates. However, the main limitation is the *quantitative information* about these species. As already discussed, dipole coupling effects may influence the absorption coefficients of the adsorbed species and therefore clearly preclude a quantitative analysis. Sometimes neither the absolute amount nor the relative ratio of different surface species is obtained. Additionally, infrared spectroscopy gives rather poor direct information about the substrate itself (the active material) due to the fact that e.g. the metal-oxide vibrations are well below 1000 cm^{-1} where measurements are difficult due to the ab-

sorption by the support. Finally, the absorption spectrum of a technical catalyst (possessing a certain particle size distribution with a large number of different adsorption sites) represents a superposition of many different species and interpretation becomes very challenging.

References

[1] D.C. Koningsberger, and R. Prins, X- Ray Absorption: Principles, Applications, Techniques of EXAFS , SEXAFS and XANES. Wiley, New York, 1988.

[2] B.J. Kip, F.B.M. Duivenvoorden, D.C. Koningsberger, and R. Prins, Journal of Catalysis 105 (1987) 26.

[3] P.W.J.G. Wijnen, F.B.M. Vanzon, and D.C. Koningsberger, Journal of Catalysis 114 (1988) 463.

[4] H.L. Gruber, Journal of Physical Chemistry 66 (1962) 48.

[5] D.B. Williams, and B.C. Carter, Transmission Electron Microscopy, A Textbook for Materials Science. Plenum Press, New York, 1996.

[6] S. Amelinckx, D. van Dyck, J. van Landuyt, and G. van Tendeloo, Handbook of Microscopy. VCH, Weinheim, 1997.

[7] P.L. Gai, E.D. Boyes, S. Helveg, P.L. Hansen, S. Giorgio, and C.R. Henry, MRS Bulletin 32 (2007) 1044.

[8] P. Nolte, A. Stierle, N.Y. Jin-Phillipp, N. Kasper, T.U. Schulli, and H. Dosch, Science 321 (2008) 1654.

[9] B. Schrader, Infrared and Raman Spectroscopy, Methods ans Applications. VCH, Weinheim, 1995.

[10] R.P. Eischens, and W.A. Pliskin, Advances in Catalysis 10 (1958) 1.

[11] R.P. Eischens, W.A. Pliskin, and S.A. Francis, Journal of Chemical Physics 22 (1954) 1786.

[12] G. Blyholder, Journal of Physical Chemistry 68 (1964) 2772.

[13] R.R. Ford, and H.P.a.P.B.W. D.D. Eley, Advances in Catalysis, Academic Press. 51.

[14] K.I. Hadjiivanov, and G.N. Vayssilov, Advances in Catalysis, Vol 47 47 (2002) 307.

[15] P. Hollins, Surface Science Reports 16 (1992) 51.

[16] J.T. Yates, Surface Science 300 (1994) 731.

[17] G. Rupprechter, Advances in Catalysis, Academic Press. 133.

[18] H.A. Pearce, and N. Sheppard, Surface Science 59 (1976) 205.

[19] R.M. Hammaker, S.A. Francis, and R.P. Eischens, Spectrochimica Acta 21 (1965) 1295.

[20] P. Hollins, and J. Pritchard, Chemical Physics Letters 75 (1980) 378.

3

OXIDATION OF PD NANOPARTICLES

3.1 Introduction

The oxidation of carbon monoxide is of great practical importance and is, for example, employed in commercial three-way-catalysts (TWC) to reduce automotive emissions. Palladium represents a major constituent of the TWC catalyst and it is well-known that the catalytic properties of the noble metal strongly depend on its oxidation state. Whereas it is accepted that e.g. for the combustion of methane Pd-oxide is the "active phase" (although mechanistic details are still debated) [1], the specific activity of Pd vs. Pd-oxide for CO oxidation at moderate temperatures is still controversially discussed in literature [2-12] (the same holds for Pt, Rh and Ru catalysts [13-28]). Significant efforts have thus been made to study the nature and activity of various oxide surfaces for catalytic CO oxidation, in order to correlate the oxidation state with its corresponding activity.

In the following a relatively simple but straightforward approach to the problem will be shown. By using well-defined high surface area Pd-Al_2O_3 catalysts, the effect of the oxygen atmosphere present during typical CO oxidation conditions will be examined. The resulting Pd oxidation state must represent an upper limit of oxidation, because in the presence of the reducing agent CO the noble metal can only be less oxidized. In a following step, the reduction (reaction) of various Pd-oxides by (with) CO was examined. In order to monitor the behaviour of different PdO_x ($0 \leq x \leq 1$) species under reaction conditions and to identify the species active in CO oxidation, *in situ* FTIR spectroscopy was combined with catalytic activity measurements by gas chromatography (GC). The FTIR/GC results were complemented by *ex situ* HRTEM, XRD, BET, and H_2 chemisorption.

Whereas the interaction of CO, O_2 and CO/O_2 has been intensively studied for palladium model catalysts (single crystals, supported nanoparticles) (see [29, 30] and references therein), systematic studies of "seemingly simple" technological Pd catalyst are surprisingly scarce for this reaction. The well-defined Pd-Al_2O_3 catalysts described below are thus intended to represent a link between industrial-grade catalysts and UHV-based model catalysts, contributing to a better understanding of active phases of CO oxidation.

3.2 Experimental

Catalyst preparation

All experiments were performed using a 5 w% Pd catalyst that was synthesized via incipient wetness impregnation of a commercial γ-Al_2O_3 support from Sasol (~250 m^2/g). As a precursor for the noble metal $Pd(NO_3)_2*2H_2O$ in aqueous solution was used. The samples were stirred for 1h at room temperature and then dried at 373 K overnight. Calcination was carried out at 773 K for 3 hours in static air. The oxidation state of the resulting palladium nanoparticles was varied by different "activation" (i.e. pretreatment) procedures in reducing or oxidizing atmosphere, performed before characterization and catalytic measurements. Pure γ-Al_2O_3, calcined at 773 K, and commercial PdO (Sigma Aldrich; ~5 m^2/g) were used for reference measurements.

Characterization methods and theoretical calculations

The BET surface area of the catalysts was obtained with a Quantasorb apparatus. Palladium dispersion was determined via H_2-chemisorption in a volumetric system according to the sorption-backsorption method to differentiate surface-adsorbed and dissolved hydrogen [31].

High resolution transmission electron microscopy (HRTEM) (Jeol 3010 operated at 300 kV) was applied to determine the morphology, microstructure and oxidation state of the nanoparticles. After appropriate *ex situ* activation or reaction, catalysts were deposited on a microscope grid covered with holey-carbon film. To determine lattice spacings

and angles between atomic planes, Fast Fourier Transforms (FFTs) of digital HRTEM images of atomically-resolved individual particles were used.

X-ray diffraction (XRD) patterns were collected using a Phillips X'Pert PRO diffractometer with CuK_α radiation. Estimation of crystallite size was carried out using the Rietveld method (program TOPAS R 2.1, Bruker, 2003).

FTIR spectroscopy of adsorbed CO was applied to characterize the accessible adsorption sites on metallic and oxidic palladium. Samples were prepared as self-supporting wafers (0.8 cm diameter, <0.5 mm thickness and typically 8-10 mg/cm^2), and were placed inside an IR cell (high vacuum (HV; <10^{-5} mbar) up to 1 bar; 100 K to 873 K). Infrared spectra were recorded by a Bruker IFS 28 FTIR spectrometer equipped with an MCT detector (resolution 4 cm^{-1}). Following a specific reductive/oxidative pre-treatment (in the same cell), adsorption experiments were carried out under static pressure at 100 K, utilizing the HV-compatible IR cell. For CO oxidation studies, *in situ* FTIR spectra of the working catalysts were collected in a second IR flow cell, with time-resolved spectroscopy being combined with on-line gas chromatography. This methodology has also been termed "*operando*" [32, 33].

XPS spectroscopy, which would be the apparent choice to examine oxidation, turned out to be incapable of determining the exact surface oxidation state. Using non-monochromatized MgK_α radiation (1254 eV) resulted in a kinetic energy of Pd3d electrons around 920 eV, which leads to an inelastic mean free path of ~1.5 nm. Consequently, both the surface and "bulk" of the particles contributed to the spectra. Furthermore, X-ray induced reduction [34] and charging prevented unambiguous assignments. Consequently, as described below, FTIR (CO) was mainly used to characterize surface oxidation states.

DFT was applied with the gradient corrected exchange- correlation functional according to Perdew, Burke and Ernzerhof (PBE) [35]. The single- electron Kohn- Sham orbitals were expanded in a local numerical basis set [36, 37]. In particular, a double numerical basis set was used together with polarization functions. A semicore pseudopotential was applied for Pd to describe the interaction between the valence electrons and

the core. The Kohn- Sham equations were solved self-consistently using an integration technique based on weighted overlapping spheres centred at each atom. In all calculations, repeated slabs were separated by about 12 Å. Reciprocal space integration over the Brillouin zone is approximated with finite sampling using the Monkhorst-Pack scheme. The stretch vibrations were calculated by finite differences.

Activity measurements

The temperature-dependent activity of CO oxidation was investigated (in addition to reactivity measurements in the IR flow cell) in a fixed-bed flow reactor. As usual, activation procedures were performed in the reactor prior to the reaction. CO oxidation was carried out at atmospheric pressure, with the feed gas controlled by mass flow controllers (50 mbar CO, 50 mbar O_2, He added up to 1 bar). The flow of CO relative to palladium weight was $2.7x10^{-3}$ mol/(g s), which for 5 nm Pd particles is equivalent to 1.3 CO molecules/(Pd surface atom s) (not to be confused with the impingement rate). The outlet gas composition was analyzed *on-line* by gas chromatography, using HP-PLOT Mole-Sieve and HP-PLOT Q columns and a thermal conductivity detector.

3.3 Results and Discussion

In the following, the preparation/characterization of supported Pd nanoparticles of various oxidation state will be discussed. Second, their interaction (reduction) with CO will be described, followed by *in situ* studies of $CO+O_2$ reaction on the various catalysts.

3.3.1 Preparation and characterization of different PdO_x (x=0-1) nanoparticles on Al_2O_3

Various reducing and oxidizing activation pretreatments were applied in order to modify the oxidation state of the catalyst (5 wt% Pd on γ-Al_2O_3):

I) Reduction in 1 bar hydrogen flow at 573 K: denoted "Pd-Al_2O_3"

II) Oxidation in 1 bar oxygen flow at 1073-1273 K: denoted "PdO-Al_2O_3"

III) Oxidation in 1 bar oxygen flow at 673 K: denoted "PdO_x-Al_2O_3" (x<1)

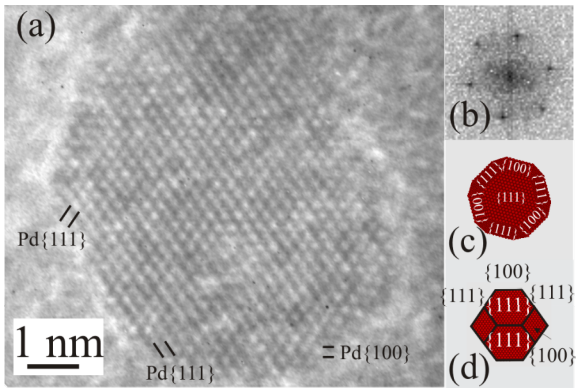

Figure 3-1 (a) High-resolution TEM image of a reduced Pd particle supported on Al_2O_3: (a) experimental image, (b) fast Fourier transform (FFT; rotated), and sketches showing a cuboctahedral particle (c) in side-view and (d) in [110] zone axis orientation.

Comprehensive structural characterization by HRTEM, XRD and FTIR spectroscopy (CO adsorption) revealed the following characteristics of the different catalysts:

1) The reduced Pd-Al_2O_3 catalyst

After reductive treatment, 5 wt% Pd-Al_2O_3 exhibited faceted (metallic) Pd^0 particles of ~5 nm mean diameter, mainly exposing {111}, {100} and a smaller fraction of {110} facets, typical of cuboctahedral shape [38] (see the lattice image and sketches in Figure 3-1). Hydrogen chemisorption indicated a Pd dispersion of 23% which correlates with 5 nm particle size (assuming spherical shape).

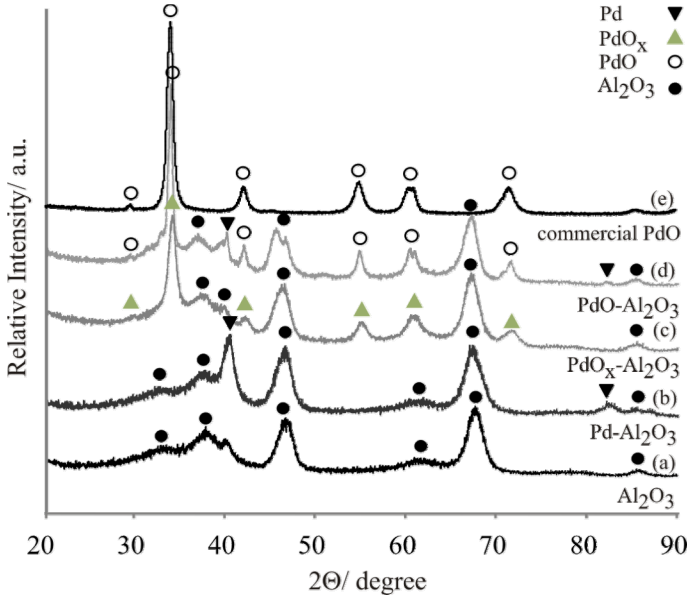

Figure 3-2 XRD analysis of (a) support, (b) reduced Pd-Al_2O_3, (c) substoichiometric PdO_x-Al_2O_3, (d) fully oxidized PdO-Al_2O_3 and (e) commercial PdO.

The mean diameter of 5 nm was further confirmed by analysis of XRD line broadening (Figure 3-2b). The specific surface area of the catalyst, as determined via the BET isotherm, was 250 m^2/g.

The FTIR spectrum of CO adsorbed at 0.5 mbar gas pressure at 100 K (Figure 3-3a) exhibited peak maxima at 2100 and 1998 cm^{-1}, with a broad shoulder extending to below 1998 cm^{-1}. The assignment of the CO (carbonyl) bands to metallic Pd^0 nanoparticles is based upon results obtained from UHV-prepared/grown model catalysts (single crystals, nanoparticles) as well as from powder catalysts, and has been described in detail in [39-42]. In brief, the main bands in the C-O stretching frequency range correspond to bridge-bonded CO at particle edges, steps and (100) facets (1998 cm^{-1}), to bridge- and hollow-bonded CO at (111) facets (terraces) of the nanoparticles (low-frequency tail around 1950 cm^{-1} and extending to 1900 cm^{-1}, respectively), and to on-top (linearly) bonded CO (2100 cm^{-1}) at (111) terraces and low-coordination (corner) sites. Additionally, carbonate species were formed on the alumina support by reaction of CO with surface hydroxyl groups [43], leading to several different absorption bands between 1700 cm^{-1} and 1200 cm^{-1} (not shown).

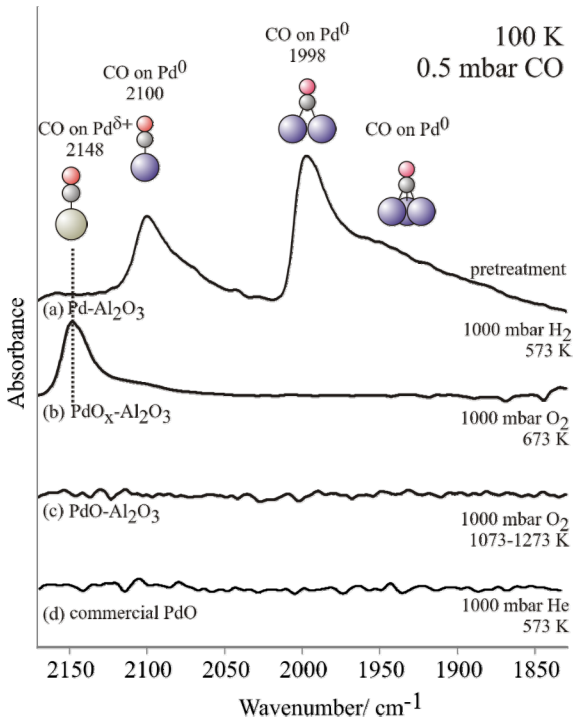

Figure 3-3 FTIR spectra of 0.5 mbar CO adsorbed at 100 K on (a) reduced Pd-Al_2O_3, (b) substoichiometric PdO_x-Al_2O_3, (c) the fully oxidized PdO-Al_2O_3 and (d) a commercial PdO.

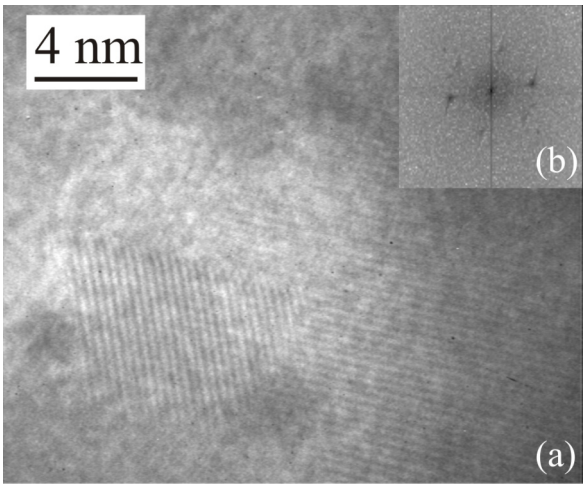

Figure 3-4 HRTEM image of a fully oxidized PdO particle on Al_2O_3: (a) Experimental image and (b) fast Fourier transform (FFT).

2) The fully oxidized PdO-γ-Al_2O_3 catalyst

As indicated by the HRTEM micrograph in Figure 3-4, oxidation in 1 bar oxygen at 1073-1273 K resulted in fully oxidized PdO particles. The main reflections in the XRD pattern of the PdO-Al_2O_3 catalyst (Figure 3-2d) were assigned to PdO and Al_2O_3, based on reference measurements of the γ-Al_2O_3 support (Figure 3-2a) and commercial PdO (Sigma Aldrich; Figure 3-2e). Additionally, a small contribution of metallic palladium was observed, indicating that some metallic Pd was retained upon oxidation.

FTIR spectra of 0.5 mbar CO at 100 K demonstrated that the PdO-Al_2O_3 catalyst did not adsorb CO (Figure 3-3c). It was thus concluded that the fraction of metallic palladium (detected by XRD) was located inside the PdO particles and not at their surface, i.e. the PdO particles had a small metallic core.

This is due to heating the catalyst in O_2 beyond the PdO decomposition temperature (~1073 K), followed by cooling in O_2 to ~373 K, which is sufficient to convert the particle surface to PdO (but retains a small metallic core).

The absence of CO adsorption on PdO is in variance to former reports of a band at 2148 cm^{-1} that was assigned to CO adsorbed on Pd(II)O. However, it was also stated in [44] that the appearance of this band was always accompanied by a partial reduction of oxidized palladium, indicated by CO bands ≤2100 cm^{-1} (typical of Pd^0). Reference meas-

urements using commercial PdO verified, however, that CO did not adsorb on the PdO surface, not even at 100 K (Figure 3-3d). Furthermore, the DFT results presented below also confirm the low binding energy of CO on PdO. The suggested CO adsorption on PdO reported in [44] is thus likely due a partially reduced sample with Pd oxidation state lower than +2.

3) The "substoichiometric" PdO_x-γ-Al_2O_3 catalyst

Oxidation in 1 bar oxygen flow at 673 K produced "substoichiometric" PdO_x particles, the identification of which was mainly based upon FTIR of CO adsorption (Figure 3-3b) and upon their facile reducibility (see below). The FTIR spectrum of 0.5 mbar CO at 100 K in Figure 3-3b displays a band at 2148 cm^{-1}, which is characteristic of CO adsorbed on substoichiometric PdO_x with $x<1$.

Whereas CO-FTIR showed a clear difference between supported PdO_x and PdO particles, the XRD pattern of the "substoichiometric" PdO_x (Figure 3-2c) basically resembled that of fully oxidized PdO (Figure 3-2d). The broader reflections of substoichiometric PdO_x indicated smaller crystallite size but the positions of the reflections were almost identical. The lattice parameters of the substoichiometric oxide PdO_x seem to differ only slightly from those of (bulk) PdO and XRD was thus not able to differentiate the two oxide phases. This was also true for HRTEM images of PdO_x particles (Figure 3-5) with the lattice distances being very similar to those of PdO.

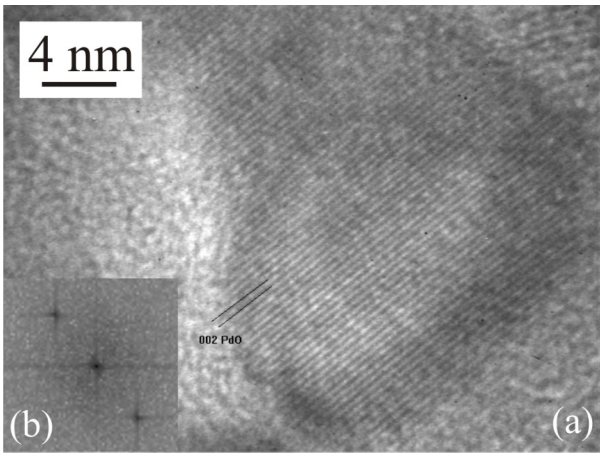

Figure 3-5 HRTEM image of a substoichiometric PdO_x particle on Al_2O_3: (a) Experimental image and (b) fast Fourier transform (FFT).

In order to monitor the transition from Pd^0 to PdO_x in more detail, i.e. to study the effect of lower oxygen partial pressure and lower temperatures that are more similar to the reaction conditions of CO oxidation, additional FTIR studies were carried out (CO adsorption at 100 K after variable pretreatments). Figure 3-6a shows spectra acquired after oxidizing the (reduced) Pd-Al_2O_3 (as shown in Figure 3-3a) in 50 mbar oxygen at increasing temperature (298 to 673 K). Already after pretreatment at 298 K, small amounts of PdO_x can be detected (small peak at 2160 cm^{-1}). However**,** the major part of palladium remained metallic (integrated areas of 1996+2109:2160 = 24:1; assuming similar IR cross sections). With increasing temperature the amount of substoichiometric oxide increased at the expense of metallic palladium, but even after pretreatment at 503 K the palladium remained mostly metallic (integral areas of 1996+2109:2160 = 1.8:1). A temperature of 503 K corresponds to CO oxidation reaction conditions above ignition (see below) and therefore represents an *upper limit* of the Pd oxidation state under working conditions. Heating to 673 K in 50 mbar oxygen was necessary to obtain a catalyst with only weak contributions of metallic Pd left (shoulder at 2107 cm^{-1} in Figure 3-6a).

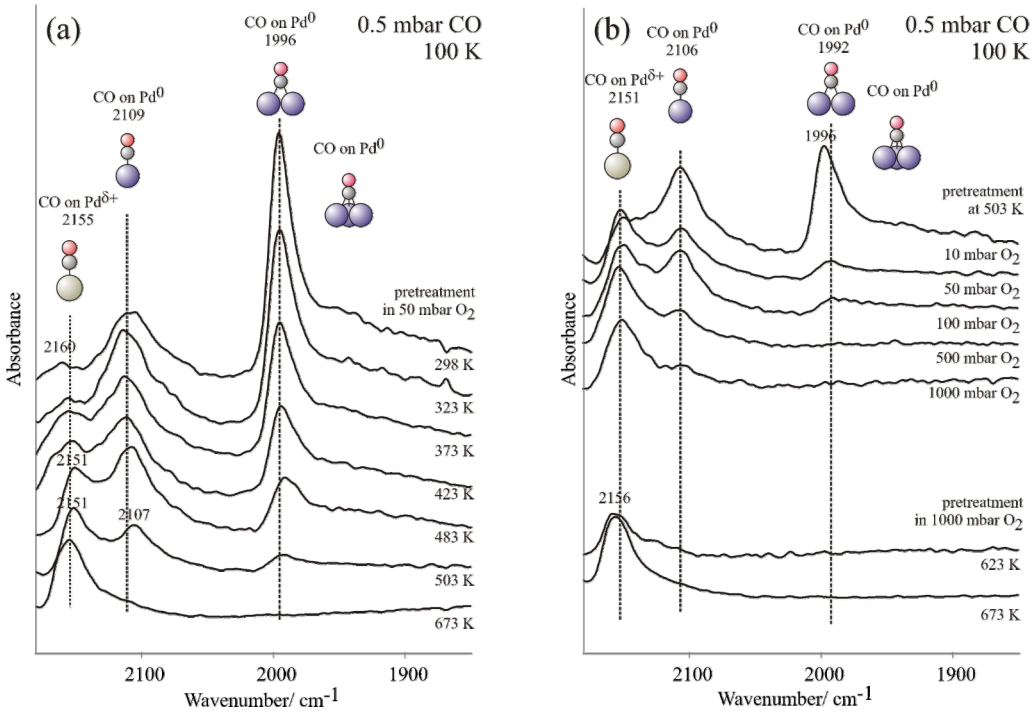

Figure 3-6 FTIR spectra of 0.5 mbar CO adsorbed at 100 K after different pretreatments of the reduced Pd-Al_2O_3: (a) influence of the temperature at 50 mbar O_2 pressure on the oxidation behaviour and (b) influence of the O_2 pressure at 503 K and identification of conditions for complete metal removal.

The extent of surface oxidation at a given temperature was also strongly dependent on the oxygen pressure, as shown for 503 K in Figure 3-6b. Whereas the upper limit of surface oxidation under reaction conditions (50 mbar oxygen at 503 K) still represents mainly metallic Pd particles (integral areas of 1996+2106:2151 = 1.8:1), upon increasing the oxygen pressure to 1000 mbar at 503 K the particle surface can be largely converted to substoichiometric PdO_x (integral areas of 2106:2151 = 0.4:1). However, as displayed at the bottom of Figure 3-6b, metallic contributions are even left upon heating to 623 K in 1 bar oxygen. Temperatures as high as 673 K in 1 bar oxygen were necessary to finally obtain a catalyst with no metallic palladium left.

Altogether, the oxidation experiments clearly indicated that the catalyst surface remained mainly metallic (~66% metallic contributions) under reaction conditions. A fraction of ~34 % substoichiometric oxide represents the upper limit in the absence of CO. Even though minor amounts of the substoichiometric oxide was already detected after pre-treatment at room temperature, rather "harsh" oxidizing conditions were required to obtain a "metal-free" oxidic catalyst surface. The temperature rather than the oxygen pressure determined the extent of oxidation. Apparently, oxidation in ≤1 bar oxygen below 673 K always leads to a coexistence of metallic Pd^0 and substoichiometric PdO_x ($x<1$).

3.3.2 Confirmation of IR band assignments by DFT calculations

HRTEM and XRD were unable to differentiate between (surface) substoichiometric PdO_x ($x<1$) and fully oxidized PdO. Nevertheless, their CO adsorption properties were markedly different and FTIR spectroscopy of adsorbed CO was thus applied to differentiate the two oxidation states. A band at 2148 cm^{-1} was assigned to CO adsorbed on PdO_x ($x<1$) ($Pd^{\delta+}$) whereas PdO (Pd^{2+}) was characterized by the absence of CO adsorption (no CO band detected even at 100 K). The band assignment, although reasonable, is not unambiguous because the band at 2148 cm^{-1} has typically been assigned (with few exceptions) to CO adsorbed on Pd^{2+} (see e.g. [44] and references therein).

Using DFT, Yudanov *et al.* [45] showed that the adsorption properties of (111) and (100) facets on nanosized 3-D (cubo-octahedral) Pd clusters (with more than 80 Pd atoms) were very similar to corresponding ideal (infinite) Pd single crystal surfaces. Hence it should be feasible to apply results obtained for Pd single crystal surfaces to our catalysts, containing well-defined nanoparticles which preferentially expose {111}, {100} and {110} facets. In addition to DFT calculations of CO adsorption on Pd(111), Pd(100) and Pd(110), calculations for the corresponding surface oxides and for PdO were also performed, in order to validate the band assignments. The CO vibrational frequencies were calculated for the most stable adsorption sites with the CO coverage set to 0.25 ML.

Due to the strong dependence of the CO stretching frequency on CO coverage for palladium [39, 42, 46-51], a direct correlation between *calculated* frequencies (for 0.25 ML CO coverage) and *experimental* frequencies observed in low temperature/high coverage experiments (performed at 100 K with 0.5 mbar CO background pressure) is difficult to achieve. It is rather the analysis of relative shifts of the C-O stretching frequencies induced by changes in the palladium oxidation state that yields valuable information.

Table 3-1 summarizes the calculated C-O bond distances d(C-O), the adsorption energies E_{ads}, and the corresponding CO vibrational frequencies for stable adsorption sites (0.25 ML CO coverage) for different (reduced) metallic and oxidized palladium facets.

Surface		d(C-O) Å	E_{ads} eV	ν (C-O) cm^{-1}
100 top		1.157	1.47	2058
100 bridge		1.174	1.86	1922
100 top	oxidized	1.148	0.69	2085
100 bridge	oxidized	1.169	0.97	1927
110 top		1.158	1.44	2054
110 bridge		1.175	1.77	1925
110 top	oxidized	1.148	0.65	2092
111 top		*	*	*
111 bridge		*	*	*
111 top	oxidized	*	*	*
PdO top		1.138	0.19	2156

* calculations currently performed

Table 3-1 Calculated C-O bond distances d(C-O), adsorption energies E_{ads} and the corresponding CO vibrational frequencies for different metallic and oxidic palladium facets.

1) CO adsorption on Pd(100), Pd(110) and corresponding surface oxides

Bridge sites were the most stable adsorption sites for both Pd(100) and Pd(110), exhibiting adsorption energies that were 0.39 eV and 0.33 eV higher, respectively, than those of the corresponding on-top adsorption sites. The results are consistent with previous theoretical [7, 52, 53] and experimental work [54, 55].

For the $(\sqrt{5}x\sqrt{5})R27°$ surface oxide on Pd(100) the bridge site was still energetically favoured by 0.28 eV over top-site adsorption, However, for the Pd(110)-surface oxide bridge adsorption turned out unstable and only the top site was available.

Both for Pd(100) and Pd(110), surface oxidation induced a blue-shift of the on-top CO stretching frequency: 27 cm^{-1} and 38 cm^{-1} for oxidation of Pd(100) and Pd(110), respectively. In contrast, the stretching frequency of bridge-bonded CO was almost unaffected (blue shift of only 5 cm^{-1}).

2) CO adsorption on Pd(111) and the corresponding Pd_5O_4 surface oxide

For Pd(111) the situation was different: on reduced Pd(111) the 3-fold hollow was the most stable adsorption site and energetically favoured by 0.6 eV over the top site. This again agreed with earlier theoretical [56] and experimental work [57-59]. However, for the Pd_5O_4 surface oxide the calculations again identified top-site adsorption as the only stable configuration. Preliminary results again suggested a blue-shift with respect to atop CO on Pd(111). Experimental IR observations of CO adsorption on Pd_5O_4 have been hampered by its high reactivity.

3) CO adsorption on PdO

Finally, the PdO surface was theoretically investigated as a model for fully oxidized PdO nanoparticles (Table 3-1). The results indicated that only the top-site was available for adsorption (2156 cm^{-1}), but its adsorption energy was very low (0.19 eV). Consequently, CO adsorption on PdO can be excluded for temperatures higher than 40 K, in agreement with the experimental findings.

It can be summarized that on the $(\sqrt{5}x\sqrt{5})R27°$ surface oxide on Pd(100) the bridge and top adsorption sites were stable (with the bridge site being favoured), whereas on all other oxidized surfaces only on-top adsorption should occur. For all surfaces, the vibrational frequencies of on-top CO were blue-shifted by ~30-40 cm^{-1} upon (surface) oxidation. CO adsorbs on PdO with a vibrational frequency of 2156 cm^{-1} but due to the low adsorption energy this species is only stable below 40 K.

The theoretical work corroborated the FTIR assignments, attributing the band at 2148 cm^{-1} to CO adsorbed on substoichiometric PdO_x (blue shifted by 43 cm^{-1} as compared to atop CO on Pd^0). Additionally, the absence of CO adsorption at 100 K is an indication for a fully oxidized PdO surface (CO adsorption only below 40 K).

3.3.3 Interaction of PdO_x and PdO with CO studied by FTIR spectroscopy

FTIR spectroscopy demonstrated a coexistence of metallic palladium and substoichiometric PdO_x ($x<1$) when the O_2 pressure (0.05-1 bar) and temperature (503 K) were similar to typical reaction conditions (Figure 3-6). As a next step, the interaction of alumina supported PdO_x ($x<1$) with CO was studied by FTIR spectroscopy, in order to examine the properties of PdO_x under reaction-like conditions. Corresponding experiments were also performed for PdO.

Figure 3-7a shows a typical FTIR spectrum when 0.5 mbar CO were exposed to alumina supported PdO_x ($x<1$) particles at 100 K. As mentioned, the band at 2145 cm^{-1} was assigned to CO adsorbed on $Pd^{\delta+}$. The band at 2196 cm^{-1} was due to weak CO adsorption on alumina (verified by reference measurements of the alumina support- not shown) and immediately disappeared upon raising the temperature. The 2196 peak was not included in Figure 3-3 and 3-6 to avoid confusion (but it was present for all samples except unsupported commercial PdO).

The adsorption spectrum remained unchanged as long as the temperature was kept constant at 100 K. Increasing the temperature to 295 K (Figure 3-7b) led to a red-shift (from 2145 cm^{-1} to 2139 cm^{-1}) and continuous decrease of the band corresponding to CO adsorbed on $Pd^{\delta+}$. Simultaneously, a band at 2106 cm^{-1} (CO linearly bonded to Pd^0)

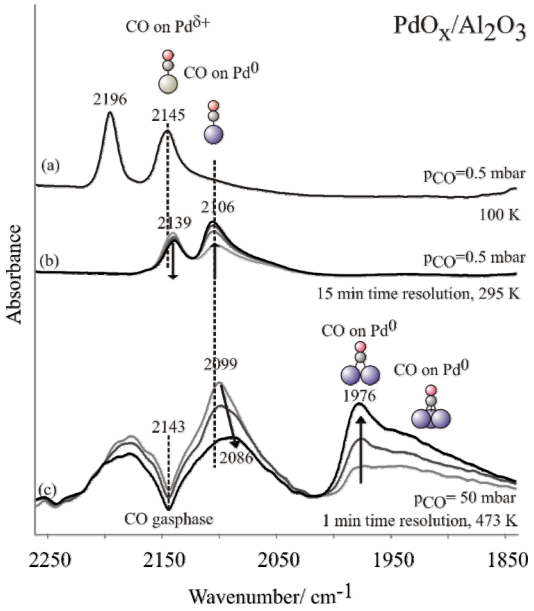

Figure 3-7 FTIR spectra of 0.5 mbar CO adsorbed on the substoichiometric PdO_x particles at (a) 100 K and (b) 295 K. Reduction at 295 K was followed with a time resolution of 15 min. (c) At 473 K and 50 mbar CO, reduction was complete within 3 min (spectra collected with a time resolution of 1 min).

developed. This experiment verified that partially oxidized palladium PdO_x does not react with CO at 100 K, but reduction already started at 295 K even at this low CO partial pressure. Under these conditions oxide reduction was slow, with the spectra in Figure 3-7b being collected in intervals of 15 minutes. However, experiments at higher CO partial pressure and temperature (comparable to reaction conditions) revealed that the reduction of PdO_x was much faster. For example, at 50 mbar CO and 473 K, reduction was complete within 3 minutes (see Figure 3-7c).

The reactivity of substoichiometric PdO_x seems comparable to the reactivity of the Pd_5O_4 monolayer surface oxide on Pd(111). Gabasch *et al.* [2] reported that reaction with ~10^{-4} mbar CO produced CO_2 at temperatures as low as ~330 K.

Analogous experiments were also performed for the supported PdO nanoparticles that exhibited no CO adsorption capacity at 100 K. Both the catalyst oxidized at 1073-1273 K in 1 bar O_2, yielding fully oxidized PdO (surfaces), and commercial (unupported) PdO were stable against room temperature reduction in a CO atmosphere (not shown). According to Gabasch *et al.* [2], PdO crystallites did not react with 10 mbar CO at 473 K within 1h, and a temperature of 523 K was required to produce metallic Pd.

3.3.4 Catalytic activity for CO oxidation

Finally, the CO oxidation activity of the 3 different supported catalysts and commercial PdO were compared in the temperature range 400-543 K, for a mixture of 50 mbar CO and 50 mbar O_2, with He balanced to 1000 mbar. Commercial unsupported PdO was basically unreactive (not shown) with a reaction rate at least 4 orders of magnitude smaller than that of PdO_x-Al_2O_3 (reduced and oxidized). Pd-Al_2O_3, PdO_x-Al_2O_3 and PdO-Al_2O_3 exhibited typical light-off (ignition) profiles (Figure 3-8), with light-off temperatures of 498 K and 535 K (for 50% CO conversion). Below 535 K, the alumina supported reduced Pd^0 particles and the PdO_x particles (Figure 3-8a, b) exhibited higher CO conversion than the fully oxidized PdO particles (Figure 3-8c). *In situ* FTIR spectra, acquired during the reaction, are also included in Figure 3-8 (acquired before and after ignition), and pre- and post-reaction XRD pattern are compared in Figure 3-9.

The substoichiometric PdO_x nanoparticles (Figure 3-8b) had basically the same activity profile as the Pd^0 catalyst (Figure 3-8a). Note that the FTIR studies of the interaction of PdO_x with CO (Figure 3-7) had indicated that PdO_x was easily reduced by CO. This was corroborated by the *in situ* IR spectra of Pd and PdO_x catalyst collected under low conversion (low activity) reaction conditions at 498 K (Figure 3-8, spectra A and C, respectively) which were almost identical. The bands at 2170 cm^{-1} and 2105 cm^{-1} (with the minimum at 2143 cm^{-1}) originated from CO gas phase absorption.

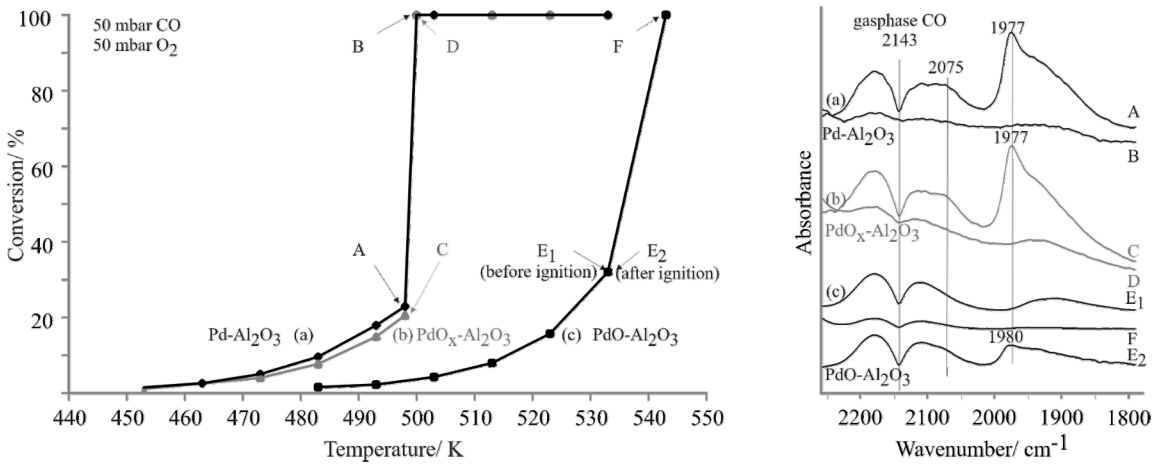

Figure 3-8 CO oxidation (conversion) and *in situ* FTIR spectra at different temperatures: Comparison of (a) reduced Pd-Al_2O_3, (b) substoichiometric PdO_x-Al_2O_3 (x<1) and (c) fully oxidized PdO-Al_2O_3. Capital letters mark conditions under which *in situ* FTIR spectra were acquired.

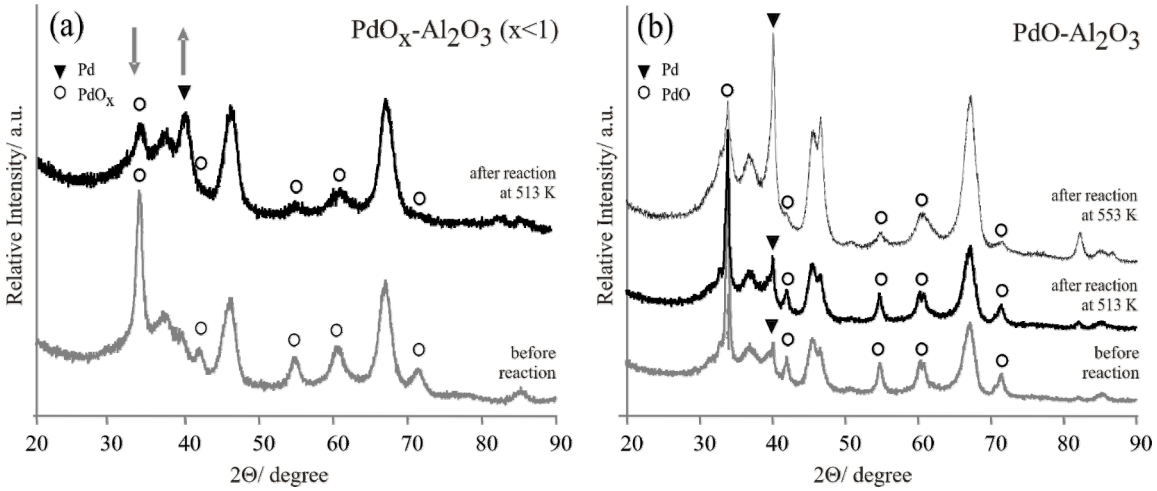

Figure 3-9 XRD analysis of (a) substoichiometric PdO_x-Al_2O_3 (x<1) before and after reaction at 513 K (above ignition), and of (b) PdO-Al_2O_3 before and after reaction at 513 K (below ignition) and after reaction at 553 K (above ignition). Reflections of the alumina support are not marked.

CO desorption from Pd particles supported on Al_2O_3 [60], FeO [61] or Nb_2O_5 [62] thin film exhibited a maximum at ~470 K. CO-TPD measurements on technical alumina supported Pd catalysts performed by Lear and coworkers [63] reported a CO desorption maximum around 498 K. This indicates that at temperatures below 498 K the palladium surface is covered (self-poisoned) by CO, explaining the low conversion. Under these conditions the reaction rate is thus controlled by dissociative oxygen adsorption and this step is inhibited by adsorbed CO.

In situ IR spectra of Pd-Al_2O_3 and PdO_x-Al_2O_3 at higher reaction temperature (i.e. at higher or even 100 % conversion; see spectra B and D in Figure 3-8, respectively), when both catalysts again showed identical activity, detected CO adsorbed on metallic Pd, although with a very low intensity (coverage) at this high temperature.

The reduction of the substoichiometric PdO_x particles under reaction conditions was further confirmed by XRD measurements (Figure 3-9a). After reaction in the high activity regime at 513 K, the reflections of PdO_x had almost disappeared and mainly metallic palladium was detected (reflex at 40°).

For Al_2O_3 supported PdO particles, *in situ* FTIR spectroscopy under reaction conditions (spectrum E_1 in Figure 3-8c) suggested that the activity again arose from metallic palladium, detected via small signals of CO adsorbed on Pd^0. The surface of supported PdO nanoparticles was thus partially reduced under reaction conditions. Because PdO reduction by CO occurs around 523 K for CO pressures of 10 mbar (and higher), as reported in [2], for supported PdO ignition occurred around 533 K (Figure 3-8c). Apparently, a partially reduced surface is responsible for the activity, which was further confirmed by the XRD observation of PdO (cores):

XRD measurements after reaction in the low activity regime (513 K) did hardly detect any change in composition, when compared to the diffraction pattern collected before the reaction (Figure 3-9b). However, the XRD pattern acquired after reaction at 553 K (in the high activity regime) showed a partial reduction of the PdO particles, indicated by the appearance of the intense reflex centred at 40° corresponding to Pd^0. This partial reduction was further confirmed by *in situ* FTIR spectroscopy of PdO-Al_2O_3 during reaction (Figure 3-8c). Whereas metallic Pd was hardly detectable below ignition (spectrum E_1 at 533 K), the spectrum obtained after reaction at 543 K (i.e. above ignition) and cooling back to 533 K (spectrum E_2) clearly showed a pronounced CO adsorption band at 1980 cm^{-1}, i.e. the palladium oxide was partially reduced. However, upon decreasing the reaction temperature, no hysteresis in the reaction rate was observed, i.e. simple PdO to Pd reduction alone can not explain the effect.

The exact origin of the PdO activity remains unclear but may involve the formation and decomposition of carbonates on alumina, oxygen spillover from and re-oxidation of PdO (defects must play an important role since PdO is not easily reduced and reoxidized).

Before turning to the final conclusions, previous model studies will be recalled. Molecular beam experiments on model catalysts demonstrated a significant catalytic activity of Pd suboxides. Gabasch and coworkers [2] characterized a two-dimensional Pd_5O_4 surface oxide on Pd(111) which was easily reduced by CO already at 330 K. Although the Pd_5O_4 surface oxide was quite active as compared to bulk PdO, it was still five times less active than chemisorbed oxygen on metallic Pd(111). Schalow and coworkers [8] studied

the relationship between the formation of Pd surface oxides and the reaction kinetics of CO oxidation, using a model catalyst of Pd nanoparticles supported on a Fe_3O_4 thin film. They demonstrated that Pd surface oxides can form and decompose dynamically during the reaction, depending on the reaction environment (CO/O_2 ratio). Nevertheless, the formation of Pd surface oxide was always paralleled by a decrease of CO oxidation catalytic activity.

Coming back to the phases present on technological catalysts during CO oxidation at high conversion, such as at 50 mbar CO and 50 mbar O_2 (He balance to 1000 mbar) at 503 - 533 K. The oxidation experiments (Figure 3-6) revealed that under oxygen partial pressures (50 mbar) and temperatures (503 K) typical for CO oxidation, the alumina supported nanoparticles are neither fully converted to PdO_x nor to PdO. The complete transformation to PdO_x or PdO would require oxidation in 1 bar O_2 at 673 K and >1073 K, respectively. This demonstrates that under reaction conditions (ignoring CO for the moment) there may be a coexistence of Pd and PdO_x ($x<1$). However, taking into account the reducing agent CO (50 mbar), the metallic phase is certainly favoured.

It is hard to imagine that the PdO_x phase constitutes the major active phase when it represents a minor fraction even in pure O_2. It is even harder to imagine that PdO_x represents the active phase in the presence of CO, which rapidly reduces PdO_x even around room temperature and at low CO partial pressure (under reaction conditions of 50 mbar CO at 503 K PdO_x is reduced instantaneously). In other words, when PdO_x formation is slower than its reduction (removal), PdO_x can not be the active phase.

This also explains the identical high catalytic activity of the initial PdO_x-Al_2O_3 and the Pd^0-Al_2O_3 catalysts because under reaction conditions both catalysts transform to the same (mostly metallic) state. CO oxidation proceeds by reaction of CO with the oxygen-covered metallic surface that is able to dissociate oxygen (and also allows for CO adsorption). Together with the molecular beam results (also showing that metallic palladium is the more active phase for CO oxidation) it can only be concluded that metallic palladium is mainly responsible for the catalytic activity under realistic conditions and at temperatures up to 533 K.

3.4 Conclusions

Well-defined high surface area palladium catalysts were prepared and alumina supported palladium nanoparticles were created in 3 different oxidation states: Pd^0, PdO_x (x<1) and PdO. Metallic Pd^0 particles were obtained upon reduction in 1 bar H_2 at 573 K. The reduced Pd particles were subsequently oxidized to higher oxidation state: heating in 50 mbar O_2 to 503 K led to a coexistence of Pd and PdO_x (x<1) but the surface remained mainly metallic. Temperatures as high as 673 K in 1 bar O_2 were required to obtain substoichiometric palladium particles PdO_x (x<1) with no metallic palladium left on the surface. The PdO_x (x<1) particles were characterized by a CO adsorption band in the FTIR spectrum at 2148 cm^{-1}, corresponding to CO adsorbed on $Pd^{\delta+}$, and by their facile reduction by CO even at low CO partial pressure (0.5 mbar CO) and low temperature (295 K). This suggests that the PdO_x particles behave similar to a Pd_5O_4 surface oxide on Pd(111). The reduced catalysts with Pd^0 particles and the oxidized catalyst with PdO_x (x<1) particles exhibited the same high catalytic activity for CO oxidation. This was explained by both catalysts finally reaching the same oxidation state under reaction conditions, i.e. metallic Pd covered by chemisorbed oxygen. Heating in 1 bar O_2 at 1073-1273 K produced fully oxidized supported PdO particles, characterized by the absence of CO adsorption. Furthermore, the PdO particles were stable towards room temperature reduction by CO. Supported PdO particles required temperatures higher than 483 K to exhibit catalytic activity, explained by the onset of pronounced PdO surface reduction to Pd^0. DFT calculations of CO adsorption on different Pd single crystal surfaces, and on the corresponding surface oxides and PdO, corroborated the FTIR band assignments. The high surface area catalysts are indeed an important link between industrial-grade catalysts and UHV-based model catalysts. The current results showed strong resemblance with previous model studies. Strong oxidizing conditions were required to obtain (metal-free) oxidic particle surfaces, even in the absence of the reducing agent CO. Consequently, under technically relevant conditions metallic palladium will always dominate whereas PdO_x phases are unstable due to their facile reducibility. Based on these and previous molecular beam results, the highest catalytic activity is assigned to oxygen-covered metallic palladium.

References

[1] D. Ciuparu, M.R. Lyubovsky, E. Altman, L.D. Pfefferle, and A. Datye, Catalysis Reviews-Science and Engineering 44 (2002) 593.

[2] H. Gabasch, A. Knop-Gericke, R. Schlogl, M. Borasio, C. Weilach, G. Rupprechter, S. Penner, B. Jenewein, K. Hayek, and B. Klotzer, Physical Chemistry Chemical Physics 9 (2007) 533.

[3] F. Gao, M. Lundwall, and D.W. Goodman, Journal of Physical Chemistry C 112 (2008) 6057.

[4] F. Gao, Y. Wang, Y. Cai, and D.W. Goodman, Journal of Physical Chemistry C 113 (2009) 174.

[5] X.Q. Gong, Z.P. Liu, R. Raval, and P. Hu, Journal of the American Chemical Society 126 (2004) 8.

[6] B.L.M. Hendriksen, S.C. Bobaru, and J.W.M. Frenken, Surface Science 552 (2004) 229.

[7] J. Rogal, K. Reuter, and M. Scheffler, Physical Review B 75 (2007).

[8] T. Schalow, B. Brandt, M. Laurin, S. Schauermann, J. Libuda, and H.J. Freund, Journal of Catalysis 242 (2006) 58.

[9] J. Szanyi, and D.W. Goodman, Journal of Physical Chemistry 98 (1994) 2972.

[10] J. Szanyi, W.K. Kuhn, and D.W. Goodman, Journal of Physical Chemistry 98 (1994) 2978.

[11] C.J. Zhang, and P. Hu, Journal of the American Chemical Society 123 (2001) 1166.

[12] G. Zheng, and E.I. Altman, Journal of Physical Chemistry B 106 (2002) 1048.

[13] M.D. Ackermann, T.M. Pedersen, B.L.M. Hendriksen, O. Robach, S.C. Bobaru, I. Popa, C. Quiros, H. Kim, B. Hammer, S. Ferrer, and J.W.M. Frenken, Physical Review Letters 95 (2005).

[14] A. Bottcher, H. Conrad, and H. Niehus, Journal of Chemical Physics 112 (2000) 4779.

[15] F. Gao, S.M. McClure, Y. Cai, K.K. Gath, Y. Wang, M.S. Chen, Q.L. Guo, and D.W. Goodman, Surface Science 603 (2009) 65.

[16] F. Gao, Y.L. Wang, Y. Cai, and W. Goodman, Surface Science 603 (2009) 1126.

[17] J. Gustafson, R. Westerstroem, A. Mikkelsen, X. Torrelles, O. Balmes, N. Bovet, J.N. Andersen, C.J. Baddeley, and E. Lundgren, Physical Review B 78 (2008).

[18] B.L.M. Hendriksen, S.C. Bobaru, and J.W.M. Frenken, Catalysis Today 105 (2005) 234.

[19] B.L.M. Hendriksen, and J.W.M. Frenken, Physical Review Letters 89 (2002).

[20] S.M. McClure, and D.W. Goodman, Chemical Physics Letters 469 (2009) 1.

[21] S.M. McClure, M. Lundwall, Z. Zhou, F. Yang, and D.W. Goodman, Catalysis Letters 133 (2009) 298.

[22] H. Over, O. Balmes, and E. Lundgren, Surface Science 603 (2009) 298.

[23] H. Over, O. Balmes, and E. Lundgren, Catalysis Today 145 (2009) 236.

[24] H. Over, and M. Muhler, Progress in Surface Science 72 (2003) 3.

[25] K. Reuter, and M. Scheffler, Physical Review B 73 (2006).

[26] M. Rossler, S. Gunther, and J. Wintterlin, Journal of Physical Chemistry C 111 (2007) 2242.

[27] C. Stampfl, and M. Scheffler, Surface Science 377 (1997) 808.

[28] X.C. Su, P.S. Cremer, Y.R. Shen, and G.A. Somorjai, Journal of the American Chemical Society 119 (1997) 3994.

[29] M. Baumer, J. Libuda, K.M. Neyman, N. Rosch, G. Rupprechter, and H.J. Freund, Physical Chemistry Chemical Physics 9 (2007) 3541.

[30] J. Libuda, and H.J. Freund, Surface Science Reports 57 (2005) 157.

[31] J.E. Benson, H.S. Hwang, and M. Boudart, Journal of Catalysis 30 (1973) 146.

[32] M.O. Guerrero-Perez, and M.A. Banares, Chemical Communications (2002) 1292.

[33] B.M. Weckhuysen, Physical Chemistry Chemical Physics 5 (2003) 4351.

[34] Y. Suchorski, L. Rihko-Struckmann, F. Klose, Y. Ye, M. Alandjiyska, K. Sundmacher, and H. Weiss, Applied Surface Science 249 (2005) 231.

[35] J.P. Perdew, K. Burke, and M. Ernzerhof, Physical Review Letters 77 (1996) 3865.

[36] B. Delley, Journal of Chemical Physics 92 (1990) 508.

[37] B. Delley, Journal of Chemical Physics 113 (2000) 7756.

[38] G. Rupprechter, Physical Chemistry Chemical Physics 3 (2001) 4621.

[39] F.M. Hoffmann, Surface Science Reports 3 (1983) 107.

[40] N. Sheppard, and C. De la Cruz, Advances in Catalysis, Vol 42 42 (1998) 181.

[41] N. Sheppard, and C. DelaCruz, Advances in Catalysis, Vol 41 41 (1996) 1.

[42] G. Rupprechter, Advances in Catalysis, Academic Press. 133.

[43] K. Foettinger, R. Schloegl, and G. Rupprechter, Chemical Communications (2008) 320.

[44] K.I. Hadjiivanov, and G.N. Vayssilov, Advances in Catalysis, Vol 47 47 (2002) 307.

[45] I.V. Yudanov, R. Sahnoun, K.M. Neyman, N. Rosch, J. Hoffmann, S. Schauermann, V. Johanek, H. Unterhalt, G. Rupprechter, J. Libuda, and H.J. Freund, Journal of Physical Chemistry B 107 (2003) 255.

[46] A.M. Bradshaw, and F.M. Hoffmann, Surface Science 72 (1978) 513.

[47] J.C. Cook, S.K. Clowes, and E.M. McCash, Journal of the Chemical Society-Faraday Transactions 93 (1997) 2315.

[48] R. Raval, S. Haq, M.A. Harrison, G. Blyholder, and D.A. King, Chemical Physics Letters 167 (1990) 391.

[49] J. Szanyi, and D.W. Goodman, Catalysis Letters 14 (1992) 27.

[50] H. Unterhalt, G. Rupprechter, and H.J. Freund, Journal of Physical Chemistry B 106 (2002) 356.

[51] D. Loffreda, D. Simon, and P. Sautet, Surface Science 425 (1999) 68.

[52] A. Eichler, and J. Hafner, Physical Review B 57 (1998) 10110.

[53] P. Hu, D.A. King, S. Crampin, M.H. Lee, and M.C. Payne, Chemical Physics Letters 230 (1994) 501.

[54] R.J. Behm, K. Christmann, G. Ertl, and M.A. Vanhove, Journal of Chemical Physics 73 (1980) 2984.

[55] G. Ertl, and P. Rau, Surface Science 15 (1969) 443.

[56] P. Sautet, M.K. Rose, J.C. Dunphy, S. Behler, and M. Salmeron, Surface Science 453 (2000) 25.

[57] M. Beutl, and J. Lesnik, Vacuum 61 (2001) 113.

[58] H. Conrad, G. Ertl, J. Koch, and E.E. Latta, Surface Science 43 (1974) 462.

[59] X.C. Guo, and J.T. Yates, Journal of Chemical Physics 90 (1989) 6761.

[60] M. Baumer, and H.J. Freund, Progress in Surface Science 61 (1999) 127.

[61] R. Meyer, D. Lahav, T. Schalow, M. Laurin, B. Brandt, S. Schauermann, S. Guimond, T. Kluner, H. Kuhlenbeck, J. Libuda, S. Shaikhutdinov, and H.J. Freund, Surface Science 586 (2005) 174.

[62] F. Hobel, A. Bandara, G. Rupprechter, and H.J. Freund, Surface Science 600 (2006) 963.

[63] T. Lear, N.G. Hamilton, and D. Lennon, Catalysis Today 126 (2007) 219.

4

OSCILLATIONS ON PD-ALUMINA

4.1 Introduction

The oxidation of carbon monoxide on noble metals is *the* prototypical reaction for mechanistic studies in heterogeneous catalysis. The reaction steps of non-dissociative CO adsorption and dissociative O_2 adsorption, of CO+O co-adsorption and reaction on single crystal surfaces have been studied in great detail under ultrahigh vacuum (UHV; reactant pressures around 10^{-6} mbar). CO oxidation follows a Langmuir-Hinshelwood mechanism with asymmetric competitive adsorption of reactants: whereas adsorbed CO (coverage >0.6 ML [1]) inhibits oxygen adsorption, a 2x2 (0.25 ML) saturation coverage of adsorbed (atomic) oxygen does not inhibit CO adsorption on e.g. Pt surfaces. The oxygen-covered metallic noble metal surface is therefore most active. On Pt(110) single crystals, the interplay between preferential CO adsorption on the reconstructed ("missing row") surface, accompanied by CO adsorption lifting the reconstruction and increasing the oxygen sticking probability, as well as the fast and facile CO+O reaction recreating the clean reconstructed surface, lead to oscillatory behavior of the reaction rate, that was thoroughly investigated and fully explained by Ertl and coworkers (see [2] and references therein).

In recent years the interest in the "seemingly simple" CO oxidation was renewed by single crystal studies utilizing *in situ* spectroscopic (Surface X-ray Diffraction, SXRD) or microscopic (Scanning Tunneling Microscopy, STM) methods that could be operated in the mbar range, i.e. at reactant pressures similar to technological CO oxidation (automotive three-way catalysts, industrial catalysis, etc). Under mbar oxygen pressure, surface oxides were observed to be present and, based on an activity increase during oxide for-

mation, the surface oxides were suggested being the (more) active phases of CO oxidation, whereas the metallic surface was assigned being less active or even inactive [3-6]. Although these (batch reactor) studies failed to show a high steady-state activity of the oxidic surface, the picture of high oxide activity was extended to other metals such as Pd and Rh [3, 5, 7-11]. Apart from being in variance with "classical" surface science results, recent molecular beam studies of absolute reaction probabilities of CO with oxygen-covered metallic and with (partially) oxidized PdO_x/Pd single crystal surfaces and PdO_x/Pd nanoparticles assigned ~5 times higher activity to the oxygen-covered metal [12, 13]. One has to confess, however, that UHV conditions were applied in these studies. *In situ* infrared (PM-IRAS) studies on noble metal single crystals at mbar pressure also reported lower oxide activity [14-18], starting a vivid debate on the (more) active phase.

The *in situ* spectroscopic study on industrial-grade Pd-Al_2O_3, as discussed in the previous chapter 3, was carried out below and above the ignition ("light-off") temperature. While in the low activity regime the catalyst was fully reduced, in the high activity regime a coexistence of metallic and oxidic palladium was observed. One could thus argue that a partially oxidized catalyst surface is more active than a metallic catalyst surface. However, in the low activity steady-state regime the metallic surface is poisoned by CO and is rather inactive, whereas above ignition the steady-state activity is so high that the surface is partly oxidized. It is, however, not appropriate to determine inherent activities by comparing a CO-poisoned metallic surface with a partially oxidized surface at *different* temperature. A meaningful comparison requires comparing the two different states at identical conditions (partial pressure of reactants, temperature). This is in principle possible when changes of the catalyst structure/composition lead to a hysteresis effect with respect to reaction temperature (ignition/extinction). Nevertheless, one still has to cope with comparing a self-poisoned with an active surface. Alternatively, examining the bistable region of CO oxidation, i.e. the conditions of catalytic rate oscillations, allows a direct comparison of the two different states under identical conditions (partial pressure of reactants, temperature).

Following these considerations, the mechanism of catalytic oscillations on Pd-Al_2O_3 catalysts was investigated by *in situ* FTIR and *in situ* XAS spectroscopy, combined with gas chromatographic and mass spectrometric gas phase analysis, in order to deduce conclusive evidence whether the oxygen-covered metallic surface or a palladium-surface oxide is the most active phase. All spectroscopic and kinetic experiments were performed in the same tubular flow reactor, avoiding inherent limitations of batch reactor studies.

4.2 Experimental

The 2 wt% Pd-Al_2O_3 catalyst was prepared by incipient-wetness impregnation of high-purity alumina (sulphate- and sodium-free; 180 m^2/g) using $Pd(NH_3)_4(NO_3)_2$ dissolved in water as precursor. The sample was dried overnight at 373 K and then reduced at 523 K in 1 bar H_2. A mean palladium particle size of 1.3 nm was determined by scanning transmission electron microscopy (STEM; JEM- 2010F FasTEMm FEI) by High-angle annular dark field (HAADF) imaging [19].

The *in situ* FTIR experiments were performed in a flow cell, connected to mass flow controllers, allowing to mix ultrapure reactant gases in the desired ratio. The reactor outlet was connected to a gas chromatograph (using a HP-PLOT Molesieve, a HP PLOT Q column and a thermal conductivity detector) for online gas phase analysis. The gas phase CO band (measured by FTIR) was calibrated by gas chromatography. Simultaneous *in situ* monitoring of the gas phase CO and adsorbed CO bands by FTIR during the oscillations allowed an unambiguous correlation between the catalytic activity and the surface properties. Infrared spectra were recorded by a Bruker IFS 28 FTIR spectrometer equipped with an MCT detector (resolution 4 cm^{-1}) with a time resolution of 3 s. The catalyst was prepared as self-supporting wafer (0.8 cm diameter, <0.5 mm thickness and typically 8-10 mg/cm^2), placed inside the IR cell. Additionally, FTIR spectroscopy of adsorbed CO was applied to characterize the available adsorption sites on metallic and oxidic palladium (shown in Figure 4-3). For these experiments a high-vacuum IR cell was used, with the catalyst again prepared as self-supporting wafer. Adsorption experiments

were carried out under static pressure in high vacuum (HV; background pressure $<10^{-5}$ mbar) at 100 K.

In situ QEXAFS (Quick EXAFS) experiments were carried out in transmission mode (Pd K-edge) at the superXAS beamline of the Swiss Light Source (SLS) in Villigen, Switzerland. The QEXAFS experiments were performed in the same FTIR flow cell by using aluminium foil windows (instead of KBr). The outlet of the reactor was connected to a QIC-20 mass spectrometer (Hiden Analytical) to monitor the outlet gas composition. To obtain sufficient signal, the pellet weight was increased by a factor of 10 in comparison to the pellet used for the FTIR studies, as was the total gas flow. The CO and O_2 partial pressure ratio was kept constant at $CO:O_2$ = 3:2, to obtain conditions comparable to the FTIR experiments. The ring current was approximately 400 mA and operated in top-up mode. The polychromatic radiation from a superbend magnet, with a magnetic field of 2.9 T and critical energy of 11.9 keV, was monochromated using a channel cut Si(111) crystal in the QEXAFS monochromator [20, 21]. The energy scale was calibrated with a palladium foil measured simultaneously. The QEXAFS monochromator was oscillating with 1 Hz, resulting in two spectra per second (i.e. a time resolution of 0.5 seconds). QEXAFS spectra were collected below and above ignition, as well as under oscillating conditions.

4.3 Results and Discussion

Figure 4-1 displays the oscillatory CO_2 reaction rate (CO_2 concentration) for CO oxidation on 2 wt% Pd-Al_2O_3 (mean Pd particle size 1.3 nm, $CO:O_2$:He = 3:2:25 ml/min; total pressure 1 bar; T=523 K). This $CO:O_2$-ratio was chosen because oscillations were more pronounced compared to a $CO:O_2$-ratio of 1:1; not shown. Longer time-regimes of high activity (~15 sec) are interrupted by shorter rate minima of ~5 sec. Also included in Figure 4-1 is the time-resolved integrated intensity of adsorbed CO, as determined by *in situ* FTIR spectroscopy, that oscillated in reverse to the CO_2 rate. Corresponding IR spectra, acquired during the oscillation period τ, are displayed in Figure 4-2a and compared to *in situ* spectra collected before and after ignition under steady state (i.e. at low and high catalytic activity, respectively). The vibrational frequencies (1920-1960 cm^{-1}) are

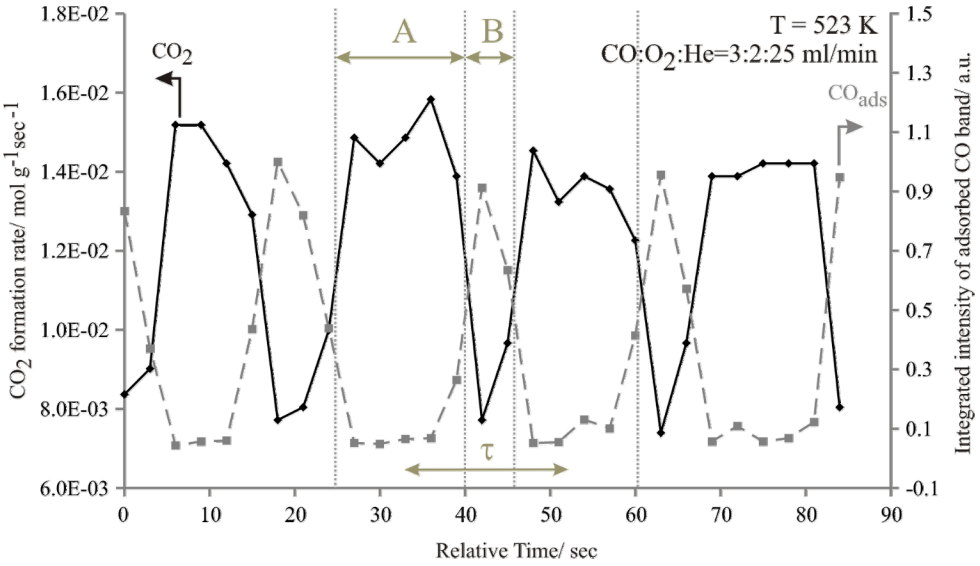

Figure 4-1 Oscillatory CO oxidation on Pd-Al_2O_3: CO_2 formation rate and integrated CO-FTIR intensity vs. time; Reaction conditions: $CO:O_2$:He = 3:2:25 ml/min at 523 K with regimes A and B indicating high and low activity, respectively. Additionally, the oscillation period τ is indicated. The corresponding FTIR spectra are shown in Figure 4-2a.

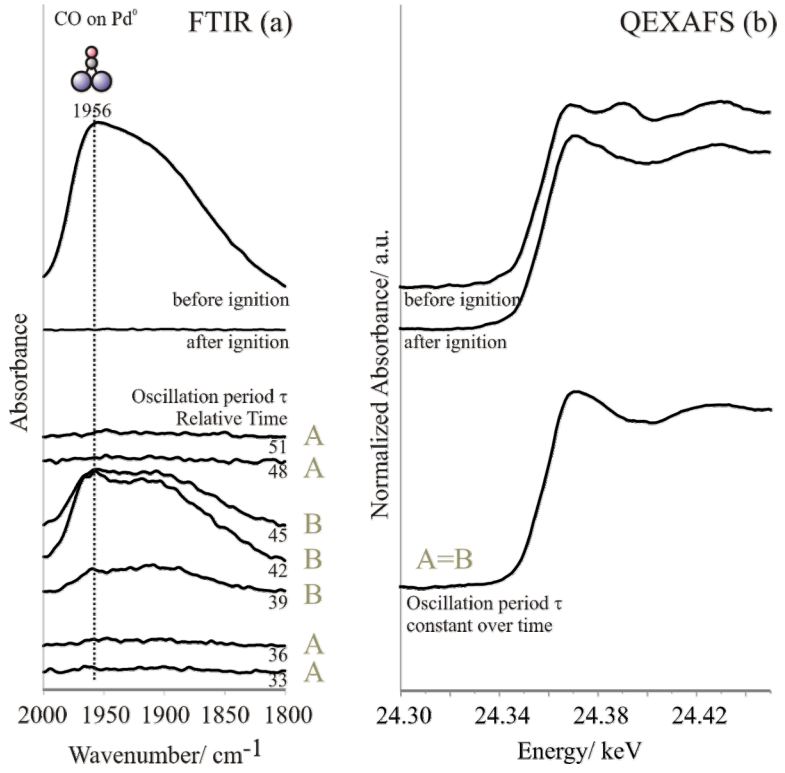

Figure 4-2: (a) *In situ* FITR spectroscopy of adsorbed CO during CO oxidation on Pd-Al_2O_3 at 523 K, collected before and after ignition and during the oscillation period τ (labels A and B indicate the corresponding activity regimes in Figure 4-1; (b) *in situ* QEXAFS spectra collected during CO oxidation on Pd-Al_2O_3 acquired before and after ignition, and during the oscillation period τ (representative spectrum; no changes were observed in time) indicate the coexistence of metallic and oxidic Pd.

characteristic of CO on metallic Pd (CO-Pd^0), presumably co-adsorbed with oxygen, whereas no bands characteristic for CO adsorbed on (partially) oxidized Pd (CO-$Pd^{\delta+}$) were observed under reaction conditions. For CO-$Pd^{\delta+}$, bands were observed at ~2130 cm^{-1} (Figure 4-3), due to the lower binding energy as compared to CO-Pd^0. Note that the integrated CO-IR intensity never reached zero (hardly observable in the expanded spectra in Figure 4-2a), which indicates a permanent *co-existence* of metallic and oxidic Pd, the latter presumably being a Pd_5O_4-like surface oxide which is easily reduced by CO even at room temperature (see Figure 4-3b). The coexistence of metal and oxide is further evident from *in situ* QEXAFS (Figure 4-2b), however without being able to resolve the structural changes during the fast oscillation. The observed spectra correspond rather to those obtained after ignition (Figure 4-2b shows a representative spectrum which was constant over time during the oscillation period τ).

Turning back to the CO-IR intensity in Figure 4-1 (and 4-2a) one is tempted to simply take the CO intensity as a measure of the metal to oxide ratio (since it is a CO-Pd^0 band). However, the opposite is true! In region (A) of high catalytic activity the metallic Pd surface is oxygen-covered (coverage of O_2 ~2-times higher than that of CO, considering the

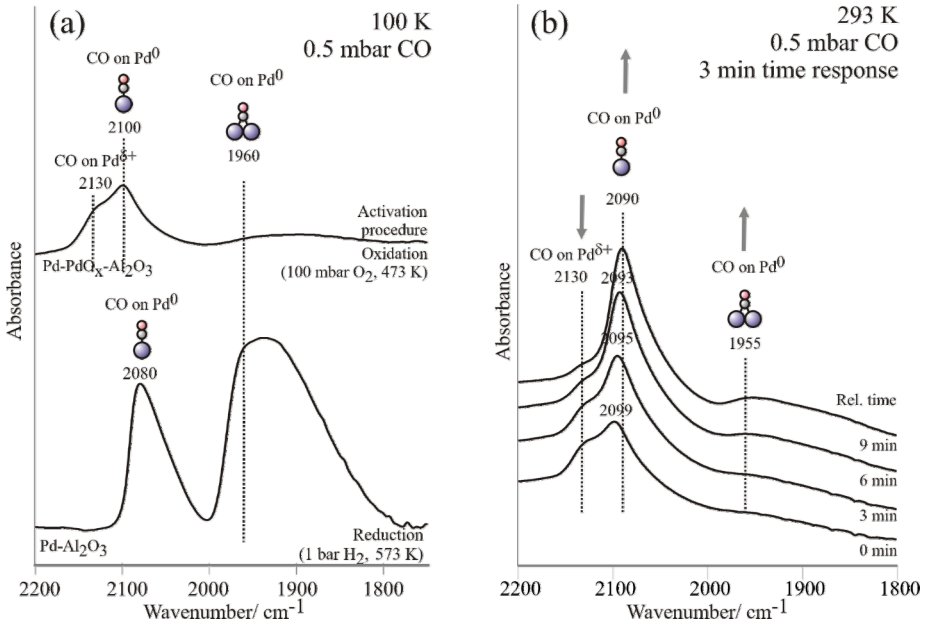

Figure 4-3 FTIR study of (a) CO adsorption at 100 K after oxidation at 473 K in 100 mbar O_2 (coexistence of Pd and PdO_x), and after reduction at 573 K in 1 bar H_2 (Pd); (b) CO adsorption at 293 K after oxidation at 473 K in 100 mbar. Reduction of Pd_5O_4–like surface oxide by CO (3 min time response).

higher sticking coefficient of O_2 at this high T [22, 23] and CO/O_2 partial pressure ratio), with the impinging CO molecules having a high reaction probability approaching 1, which leads to a low CO surface coverage. The high reaction rate leads to a CO conversion of (nearly) 100%, i.e. (nearly) all CO molecules are converted to CO_2. This is illustrated in Figure 4-4, step (1). The (lack of CO and) excess of oxygen then results in a slow oxidation of the Pd surface (during regime A). In the early stages of surface oxide growth (Figure 4-4, step 1) the CO_2 rate remains high because (i) most of the surface is still highly active oxygen-covered metal and (ii) also the oxide contributes to CO_2 formation (see below).

With increasing oxidization of the surface (Figure 4, step 2) not only the metallic areas shrink but – even more important– the overall (i.e. integrated over the whole catalyst area) sticking probability of oxygen vs. CO changes. On the metallic surface, oxygen has a higher sticking than CO (at this high temperature). In contrast, on a largely oxidized surface (with oxide and metal coexisting) CO has a higher (overall) sticking probability, because on the oxide islands that dominate the surface, CO has a higher sticking probability than oxygen (in between the Pd-oxide islands oxygen still has an inherently higher sticking probability). The CO molecules that adsorb on the oxide islands then diffuses to the metallic areas in between (via reverse spill-over) which increases the effective CO flux to the remaining metallic areas (note that the gas phase (feed gas) composition remains unaltered).

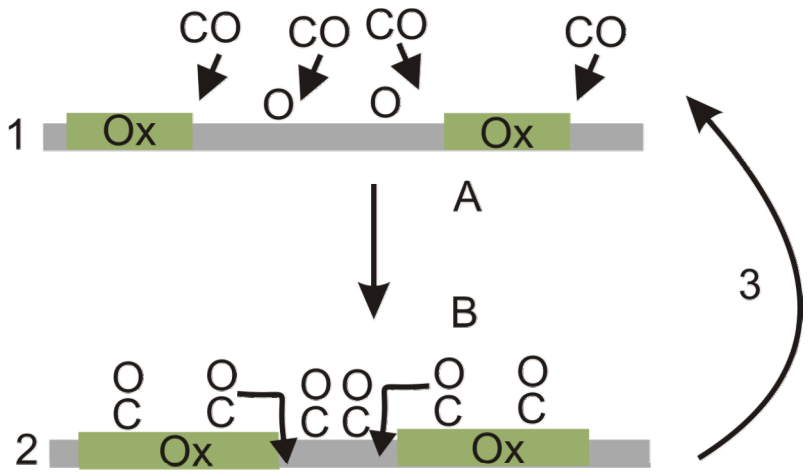

Figure 4-4 Illustration of surface states and phases present during oscillatory CO oxidation on Pd. Grey and green areas represent the Pd and Pd-oxide phase, respectively.

The effective CO flux per metal surface unit $n_{CO,total}$, including direct CO adsorption from the gas phase and the additional spill-over from the oxide, can be calculated as

$$n_{CO,total} = \frac{n_{CO,gas} * S_{CO,Pd} * (A_{total} - A_{PdO_x}) + n_{CO,gas} * S_{CO,PdO_x} * A_{PdO_x}}{A_{total} - A_{PdO_x}} \quad (4\text{-}1)$$

with $n_{CO,gas}$ being the CO flux from the gas phase, $S_{CO,Pd}$ and $S_{CO,PdOx}$ corresponding to the CO sticking coefficients on palladium and palladiumoxide respectively, A_{total} being the total palladium area (in either metallic or oxidic state; set as 1) and A_{PdOx} the palladiumoxide fraction. Thus, A_{total}-A_{PdOx} corresponds to the metal fraction.

As illustrated in Figure 4-5, the effective CO flux can strongly exceed the gas phase flux $n_{CO,gas}$. For example, for 80% surface oxidation the CO flux increases 5-times, assuming equal sticking coefficients for CO on the metal and on the oxide. The increased CO flux induces a kinetic phase transition on the metallic Pd areas, switching from active oxygen-covered (regime A) to inactive CO-covered (regime B). This effect is well-known from kinetic phase diagrams of CO oxidation on various noble metal surfaces [24-27].

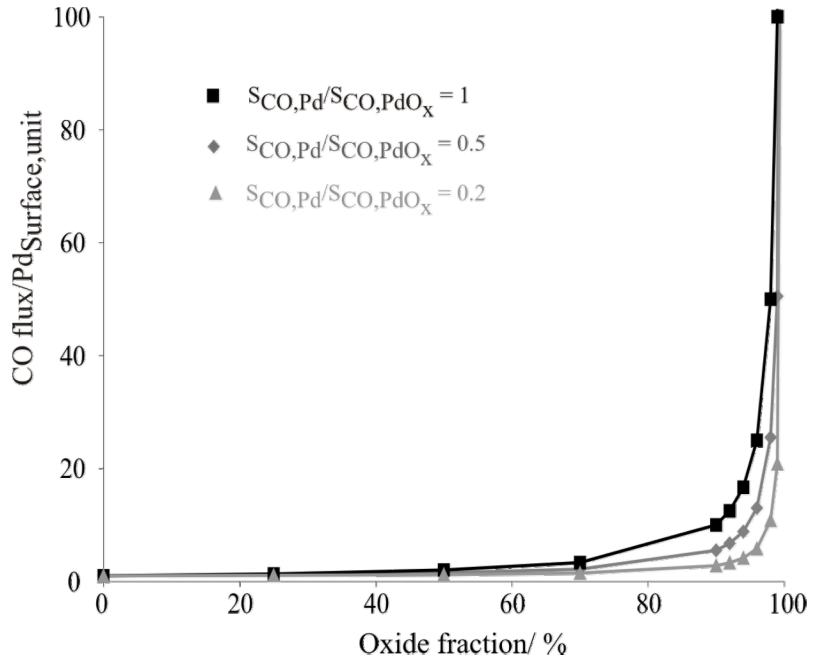

Figure 4-5 Influence of the oxide fraction on the effective CO flux per metal surface unit $n_{CO,total}$; Results for different CO sticking coefficient ratios on the oxide and on the metal $S_{CO,PdOx}/S_{CO,Pd}$ are shown.

The increased effective CO flux to the metal surface is equivalent to increasing the CO gas pressure which would poison the metallic surface. Note that in the present case the gas phase composition remains unaltered and the higher flux is induced only by the higher sticking probability of CO on the Pd oxide islands (compared to that of oxygen) and the diffusion across the phase boundaries. In this low activity state (regime B; Figure 4-4, step 2) the metallic areas are CO-covered as indicated by the high CO intensity in IR, which is almost comparable with the CO coverage before ignition (see Figure 4-2a).

If the Pd surface oxide would be inactive the catalyst would simply become deactivated. However, although CO can not react with oxygen from the gas phase anymore (because the CO-coverage prevents dissociative oxygen adsorption on the metal surface), CO can still react with the oxygen in the boundaries of the oxide islands. This reacts away and shrinks the oxide islands until they are small enough that the diffusional CO supply (spill-over) is no longer sufficient to keep the surface in a CO-covered state. Note, as known from kinetic phase diagrams [24-27], that a CO-covered surface remains stable even at CO pressures that would not be sufficient to convert an oxygen-covered surface to CO-covered (bistability region; hysteresis). At one point the metallic areas will switch back to the oxygen-covered highly active metallic state (Figure 4-4, step 3), as indicated by the rate increase and simultaneous decrease of CO-IR intensity, completing the oscillatory cycle. One should note that the variations in the CO-IR intensity in Figure 4-2a are not simply induced by changes in the local CO partial pressure (the CO-IR spectrum is almost unaffected upon pressure changes of two orders of magnitude; Figure 4-6), but clearly reflect the oscillating states of the catalyst surface.

Assuming that the ratio of the CO bands in the inactive (CO-poisoned) and active (oxygen-covered) state in Figure 4-2a corresponds to the ratio of the effective CO fluxes, one can estimate the oxide fraction that leads to CO poisoning (according to equation (4-1) and Figure 4-5). Up to an oxide fraction of 50% the metallic surface remains in the oxygen-covered high activity state. When the oxide fraction exceeds ~70 %, CO poisoning of the metal surface occurs, leading to low catalytic activity. Finally, when the oxide fraction reaches ~95%, CO reacts away the oxide and catalytic activity is restored.

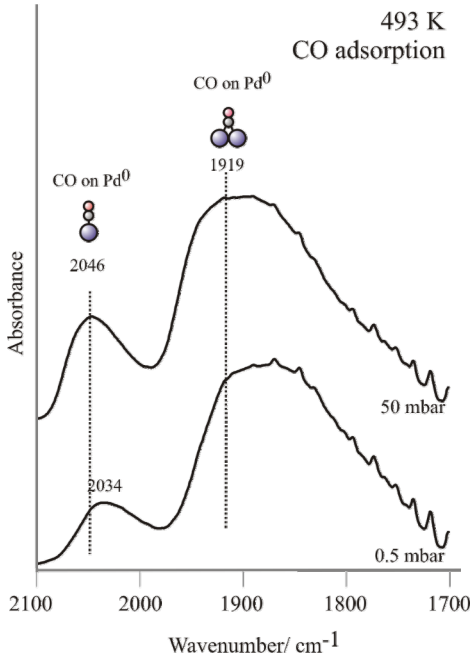

Figure 4-6 Pressure dependence of the FTIR spectrum of CO adsorbed on Pd-Al_2O_3. FTIR acquired at 493 K spectra at 0.5 mbar and 50 mbar CO pressure.

Apparently, relatively strong oxidic contributions (>70%) are required to switch the metallic areas from the active (oxygen-covered) state to the CO-poisoned inactive state. These values were estimated for equal CO sticking coefficients on the metal and palladium oxide ($S_{CO,PdOx} = S_{CO,Pd}$), but for $S_{CO,PdOx} < S_{CO,Pd}$ [12, 22, 23] even higher oxide fraction is necessary to induce CO-poisoning of metallic areas (Figure 4-5, shown e.g. for $S_{CO,PdOx} = ½ S_{CO,Pd}$). The required strong oxide contribution may explain why during oscillations the structural changes were not observed by *in situ* QEXAFS, which always indicated coexisting metal and oxide. Even when the degree of surface oxidation of the Pd nanoparticles changes during oscillations, the "bulk" of the nanoparticles would remain oxidic, rendering detection of surface reduction/oxidation difficult for QEXAFS.

The vibrational frequency of adsorbed CO, characteristic of CO affected by (co-adsorbed) oxygen, is rather unaffected by the oscillations. This may be explained by the presence of subsurface oxygen in both states (Figure 4-4, steps 1 and 2). Compared to spectra of (pure) CO on Pd nanoparticles (Figure 4-6), neighboring oxygen not only shifts the frequencies but also modifies the relative intensities of the different CO bands (hollow, bridge, on-top sites). This may indicate morphological changes (refacet-

ting/reshaping) of Pd (PdO_x) nanoparticles, as previously observed by HRTEM [28] and STM [29] in the presence of oxygen. Switching to pure CO atmosphere revealed that the frequency changes were reversible (not shown), which also agrees with by HRTEM observations of Pd nanoparticles on MgO single crystals, which regained their initial morphology upon hydrogen reduction [30].

The proposed reaction scheme also explains observations reported in the literature of high rates accompanied/followed by surface oxide formation. In these (batch-reactor) studies the decreasing rate after oxide formation was attributed to lack of CO (most had been consumed prior/during oxide formation), and re-dosing CO immediately reduced the postulated highly active surface oxide.

Coming back to the processes observed during oscillations, at this point one may provocatively ask: Considering 100% CO conversion and a quasi-oxygen atmosphere in the high activity regime (A), which process can cause a decreasing rate? The only process that can apparently take place is Pd (surface) oxidation! If the surface oxide would be so active, how can it form at all? Why should the surface oxidation by oxygen be initially faster than the reduction by CO? And why is the reduction by CO then suddenly faster than oxidation? The answer to all these questions is that the formation of Pd surface oxide happens *because* of the oxygen-coverage and high activity of the metallic surface but oxide formation is not the *cause* of high activity.

Oscillatory behavior, per definition requires a more active *and* a less active state, as well was a *feedback* mechanism [2, 31]. In the present case, the effective CO flux to the catalysts represents the switch which steers the state of the active metallic Pd surface: when the oxide islands are small and the CO flux corresponds to the gas phase CO flux, the metallic areas are oxygen-covered. Upon increasing oxidation (growth of oxide islands) the effective CO flux increases due to CO spill-over and the metallic areas switch to CO-covered. Reaction of CO with the Pd-oxide (while O_2 can not adsorb on CO-Pd^0 and Pd-oxide) islands then re-establishes the original situation.

It is interesting to note the analogy to Ertl´s Pt(110). On the unreconstructed Pt surface (or the not-oxidized Pd surface) oxygen adsorption dominates, whereas on the reconstructed Pt surface (or the oxidized Pd surface) CO adsorption prevails. Turner, Sales and Maple reported already in 1981 that oscillations in CO oxidation on Pt, Pd and Ir [32-35] were caused by the reversible formation of a less-active oxide. However, they suggested as a feedback mechanism that CO adsorption is favored with decreasing metal surface (caused by oxide formation), simply because of lower space requirement of CO in comparison to dissociative oxygen adsorption. Variations in the relative sticking coefficients were neglected, though.

Basset *et al.* [36] assigned oscillations of CO oxidation on Pd(110) to the effect of subsurface oxygen (because no surface reconstruction occurs on the single crystal). Although these studies were performed under UHV and no surface oxide was formed, the basic mechanism is the same. The produced and decomposed (surface) palladium oxide on small palladium nanoparticles seems to behave like subsurface oxygen (observed on single crystals) rather then fully oxidized Pd bulk oxides. This explains the relative high activity of surface oxides (which was shown to be only ~5 times lower than for chemisorbed oxygen on Pd(111) [12]).

A final issue concerns the state of the catalytic surface under excess oxygen (e.g. $CO:O_2$=1:5) at higher temperature, i.e. after ignition, when oscillatory behavior is absent. Under these conditions IR is almost unable to detect adsorbed CO species whereas EXAFS still detects coexisting oxidic and metallic Pd (Figure 4-2). Apparently, at higher temperature the small remaining metal surface and the Pd-oxide (with reduction and oxidation occurring at the same rate) are active enough to maintain high catalytic activity. Under conditions when the particles are fully oxidized, the mechanism must change to a direct reaction between CO and Pd-oxide.

4.4 Conclusions

The mechanism of oscillatory behaviour during CO oxidation on Pd-Al_2O_3 was investigated using *in situ* FTIR and *in situ* QEXAFS spectroscopy, combined with gas chromatographic and mass spectrometric gas phase analysis. A continuous formation of Pd surface oxide occurs in the active regime and leads to a decreasing reaction rate. Spill-over of CO from the surface oxide islands to the metallic areas in between leads to a higher effective CO flux that induces a conversion of metallic areas from O-covered to CO-covered. Because CO poisons oxygen adsorption, CO rather rapidly reduces the partially oxidized surface, thus shrinking the oxide islands and reducing the CO spill-over, re-establishing the original oxygen-covered active (metallic) areas. This leads to oscillatory behavior which allowed an unambiguously comparison of the specific activities of metallic and oxidic palladium. Conclusive evidence was found for identifying the oxygen-covered metallic surface as the more active phase for CO oxidation.

References

[1] M. Bowker, I.Z. Jones, R.A. Bennett, F. Esch, A. Baraldi, S. Lizzit, and G. Comelli, Catalysis Letters 51 (1998) 187.

[2] R. Imbihl, and G. Ertl, Chemical Reviews 95 (1995) 697.

[3] B.L.M. Hendriksen, S.C. Bobaru, and J.W.M. Frenken, Catalysis Today 105 (2005) 234.

[4] M.D. Ackermann, T.M. Pedersen, B.L.M. Hendriksen, O. Robach, S.C. Bobaru, I. Popa, C. Quiros, H. Kim, B. Hammer, S. Ferrer, and J.W.M. Frenken, Physical Review Letters 95 (2005).

[5] B.L.M. Hendriksen, S.C. Bobaru, and J.W.M. Frenken, Topics in Catalysis 36 (2005) 43.

[6] B.L.M. Hendriksen, and J.W.M. Frenken, Physical Review Letters 89 (2002).

[7] J. Gustafson, R. Westerstroem, A. Mikkelsen, X. Torrelles, O. Balmes, N. Bovet, J.N. Andersen, C.J. Baddeley, and E. Lundgren, Physical Review B 78 (2008).

[8] J. Gustafson, R. Westerstrom, O. Balmes, A. Resta, R. van Rijn, X. Torrelles, C.T. Herbschleb, J.W.M. Frenken, and E. Lundgren, Journal of Physical Chemistry C 114 (2010) 4580.

[9] J. Gustafson, R. Westerstrom, A. Resta, A. Mikkelsen, J.N. Andersen, O. Balmes, X. Torrelles, M. Schmid, P. Varga, B. Hammer, G. Kresse, C.J. Baddeley, and E. Lundgren, Catalysis Today 145 (2009) 227.

[10] B.L.M. Hendriksen, S.C. Bobaru, and J.W.M. Frenken, Surface Science 552 (2004) 229.

[11] R. van Rijn, O. Balmes, R. Felici, J. Gustafson, D. Wermeille, R. Westerstrol̂m, E. Lundgren, and J.W.M. Frenken, The Journal of Physical Chemistry C 114 6875.

[12] H. Gabasch, A. Knop-Gericke, R. Schlögl, M. Borasio, C. Weilach, G. Rupprechter, S. Penner, B. Jenewein, K. Hayek, and B. Klotzer, Physical Chemistry Chemical Physics 9 (2007) 533.

[13] T. Schalow, B. Brandt, M. Laurin, S. Schauermann, J. Libuda, and H.J. Freund, Journal of Catalysis 242 (2006) 58.

[14] F. Gao, M. Lundwall, and D.W. Goodman, Journal of Physical Chemistry C 112 (2008) 6057.

[15] F. Gao, S.M. McClure, Y. Cai, K.K. Gath, Y. Wang, M.S. Chen, Q.L. Guo, and D.W. Goodman, Surface Science 603 (2009) 65.

[16] F. Gao, Y. Wang, Y. Cai, and D.W. Goodman, Journal of Physical Chemistry C 113 (2009) 174.

[17] F. Gao, Y.L. Wang, Y. Cai, and W. Goodman, Surface Science 603 (2009) 1126.

[18] S.M. McClure, and D.W. Goodman, Chemical Physics Letters 469 (2009) 1.

[19] M.W. Tew, J.T. Miller, and J.A. van Bokhoven, Journal of Physical Chemistry C 113 (2009) 15140.

[20] R. Frahm, Nuclear Instruments & Methods in Physics Research Section a-Accelerators Spectrometers Detectors and Associated Equipment 270 (1988) 578.

[21] R. Frahm, Review of Scientific Instruments 60 (1989) 2515.

[22] T. Engel, and G. Ertl, Journal of Chemical Physics 69 (1978) 1267.

[23] B. Klötzer, K. Hayek, C. Konvicka, E. Lundgren, and P. Varga, Surface Science 482 (2001) 237.

[24] M. Berdau, A. Karpowicz, G.G. Yelenin, K. Christmann, and J.H. Block, Journal of Chemical Physics 106 (1997) 4291.

[25] Y. Suchorski, R. Imbihl, and V.K. Medvedev, Surface Science 401 (1998) 392.

[26] Y. Suchorski, R. Wrobel, S. Becker, and H. Weiss, Journal of Physical Chemistry C 112 (2008) 20012.

[27] V.P. Zhdanov, and B. Kasemo, Surface Science Reports 20 (1994) 111.

[28] O. Demoulin, G. Rupprechter, I. Seunier, B. Le Clef, M. Navez, and P. Ruiz, Journal of Physical Chemistry B 109 (2005) 20454.

[29] T. Schalow, B. Brandt, D.E. Starr, M. Laurin, S. Schauermann, S.K. Shaikhutdinov, J. Libuda, and H.J. Freund, Catalysis Letters 107 (2006) 189.

[30] H. Graoui, S. Giorgio, and C.R. Henry, Surface Science 417 (1998) 350.

[31] L.F. Razon, and R.A. Schmitz, Chemical Engineering Science 42 (1987) 1005.

[32] B.C. Sales, J.E. Turner, and M.B. Maple, Surface Science 112 (1981) 272.

[33] J.E. Turner, B.C. Sales, and M.B. Maple, Surface Science 103 (1981) 54.

[34] B.C. Sales, J.E. Turner, and M.B. Maple, Surface Science 114 (1982) 381.

[35] J.E. Turner, B.C. Sales, and M.B. Maple, Surface Science 109 (1981) 591.

[36] M.R. Bassett, and R. Imbihl, Journal of Chemical Physics 93 (1990) 811.

5

CO OXIDATION ON AU-TITANIA

5.1 Introduction

Gold has long been regarded as an inactive catalytic material due to the inert nature of macroscopic (bulk) gold. Early work by Bond *et al.* [1] reported unexpected activity of Au on boehmite for alkyne hydrogenation. However, only after Haruta´s report in the late 1980ies [2] of small gold particles being able to catalyze the CO oxidation reaction at temperatures as low as 203 K, extensive research on nanosized gold catalysts started.

The reason for the exceptional high catalytic activity is still a matter of controversial debate and was explained by the peculiar nature of smallest gold nanoparticles [2, 3]: high density of defect states [4-7] and/or a change of the electronic structure (of gold atoms) for very small gold particles [8], and/or support effects. The support may affect the reaction directly via transfer of activated oxygen to the gold particles [9], or indirectly via strain effects (i.e. lattice distortions of gold particles induced by adopting the substrate lattice) [10, 11] or by simply stabilizing small gold particles [12]. Whereas it is generally agreed that the CO adsorption site is located on the Au particles, the oxidation state of the catalytically active gold species is still debated: gold in zero-valent Au^0 oxidation state [13-15] and oxidized $Au^{\delta+}$ [16-18] were suggested as active sites.

Additionally, several models have been proposed for the oxygen adsorption site that could be either located on the gold particles [2, 8, 19, 20], on the support, or on the support-particle interface [13, 21, 22] and no consensus has been reached whether dissociative or molecular adsorption takes place.

Finally, the influence of moisture on the catalytic activity is another controversial aspect. Even though the beneficial influence of water on catalytic activity is recognized the

exact origin is poorly understood. The two most prominent explanations are that water i) decomposes/removes carbonates that would lead to deactivation [23-28] or ii) enhances oxygen adsorption and/or activation [22, 29, 30]. However, a third and often disregarded model is the direct involvement of support OH-groups in the CO oxidation reaction.

Such an involvement was proposed by Bond and Thompson [31] via a phase-boundary mechanism (a similar "active site" model was later on also proposed by Costello *et al* [32]): According to this mechanism (as schematically shown in Figure 5-1), OH-groups of the support move onto the gold particles (which consist of both zero-valent gold Au^0 atoms and Au^{III} cations). CO, which is adsorbed molecularly on the reduced Au^0 particles, is attacked by the OH group forming a carboxyhydroxyl- intermediate (-COOH; or hydroxycarbonyl). Oxygen adsorbed at anion vacancies V_S^- of the titania support creates a superoxide anion O_2^- which oxidizes the carboxyhydroxyl intermediate to CO_2 and hydroxyperoxide (HOO^-). Hydroxyperoxide itself is also able to oxidize another carboxyhydroxyl intermediate leading to CO_2 and a hydroxyl group on the support. Therefore, hydroxyl groups on the support surface are not consumed but are restored upon completing the catalytic cycle.

Nevertheless, the mechanism suggested by Bond and Thompson [31] was based on literature evaluation rather than direct experimental evidence of the involvement of hydroxyl groups or of the presence of hydroxycarbonyl intermediates.

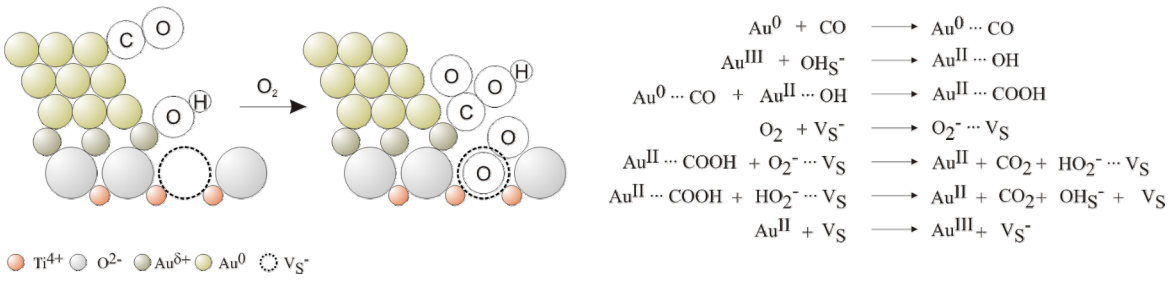

Figure 5-1 Schematic representation of the phase-boundary mechanism proposed by Bond and Thompson [31].

Therefore, the CO oxidation mechanism was investigated using *in situ* FTIR spectroscopy, combined with gas phase analysis (gas chromatography), on a commercial Au-TiO_2 catalyst. Adsorption experiments of CO and CO_2 (isotopic-labelled and unlabelled) followed by FTIR spectroscopy were performed to study the interaction of the catalyst surface with CO as the reactant and CO_2 as the product. Special attention was thus directed towards the role of hydroxyl groups as reactants and carbonates/carboxylates/carboxyhydroxyls as intermediates, in an effort to examine the *direct* involvement of hydroxyl groups in CO oxidation and to critically assess the relevance of the periphery mechanism proposed by Bond and Thompson [31].

5.2 Experimental

Catalyst preparation

All experiments were performed with a commercial AURO*lite*^{TM} gold catalyst from AuTEK, with a gold loading of 0.8 wt% on TiO_2 (anatase content >70 wt%), exhibiting a specific surface area of 43 m^2/g and specific pore volume of 0.3-0.4 cm^3/g. The catalyst was received as 1.5–1.6 mm extrudates that were ground to powder and stored in a refrigerator (cool, dark and moisture-free). Prior to characterization and catalytic measurements the catalyst was heated in Helium up to 373 K. Reference measurements with the pure commercial TiO_2 support (from AuTEK) were also performed.

Characterization methods

The BET surface area of the catalysts was measured with a Quantasorb apparatus. The gold particle size distribution was determined from analysis of HAADF-STEM (high-angle annular dark-field scanning transmission microscopy) images obtained after *ex situ* activation, i.e. the catalyst was supported on a holey-carbon covered microscope grid after heating in He at 373 K for 1 h.

FTIR spectroscopy of the adsorption of isotopically-labelled and unlabelled CO and CO_2 was applied for mechanistic studies and for characterization of the intermediates observed under reaction conditions. After *in situ* pre-treatment, adsorption experiments

were carried out under static pressure in high vacuum (HV; background pressure $<10^{-5}$ mbar) at 293 K. Infrared spectra were recorded by a Bruker IFS 28 FTIR spectrometer equipped with an MCT detector (resolution 4 cm^{-1}). The samples were prepared as self-supporting wafers (0.8 cm diameter, <0.5 mm thickness and typically 8-10 mg/cm^2), placed inside an IR cell (HV to 1 bar; 100 K to 873 K). Additionally, *in situ* FTIR spectra were collected in an IR flow cell, combining time-resolved IR spectroscopy with on-line gas chromatography, using HP-PLOT MoleSieve and HP-PLOT Q columns and a thermal conductivity detector.

Activity measurements

The catalytic performance of CO oxidation was investigated in a fixed-bed flow reactor. Activation procedures were performed *in situ* and the reaction was carried out at atmospheric pressure (reaction mixture: 50 mbar CO, 50 mbar O_2, He added up to 1 bar). The water content in the reactant mixture was varied by addition of water via a saturator kept at different temperatures: in the temperature range 273-293 K the H_2O partial pressure was varied between 6 and 23 mbar [33]. The influence of the water content was studied via isothermal kinetic measurements performed at 333 K (in order to assure precise temperature control of to the strong exothermic reaction). The flow of CO relative to the gold load was $1.8*10^{-2}$ mol/(g s) which, for 3.8 nm Au particles, is equivalent to 11.4 CO molecules/(Au surface atom s). The outlet gas composition was analyzed by on-line gas chromatography, using HP-PLOT MoleSieve and HP-PLOT Q columns and a thermal conductivity detector.

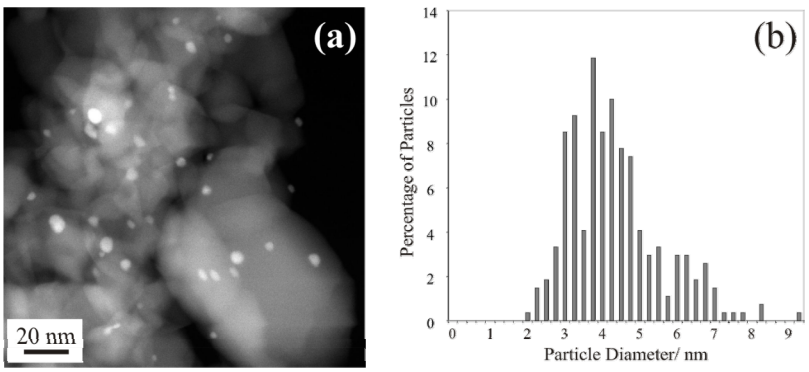

Figure 5-2 (a) Representative STEM-HAADF image and (b) corresponding particle size distribution of the AURO*lite*™ Au-TiO_2 catalyst after activation in Helium at 373 K.

5.3 Results and Discussion

This study was performed using a commercial AURO*lite*™ 0.8 w% Au-TiO_2 catalyst with a mean gold particle size of 3.8 nm (see Figure 5-2), determined by STEM-HAADF analysis. In the following the mechanism of CO oxidation on Au-TiO_2 is discussed on the basis of the following aspects:

The nature and location of the CO and O_2 adsorption sites, the involvement of surface hydroxyl groups during CO oxidation, the nature and role of carbonate-like surface species observed under reaction conditions and the influence of water on the catalyst properties and the promotional and/or inhibiting effect on catalytic activity.

5.3.1 Location of CO and oxygen adsorption sites

a) The CO adsorption sites

A typical infrared spectrum, collected under reaction conditions (50 mbar CO, 50 mbar O_2, balance He at 333 K), is shown in Figure 5-3a. An absorption band at 2113 cm^{-1}, assigned to CO adsorbed on metallic gold (see [34] and references therein), was superimposed with CO gas phase bands at 2177 and 2117 cm^{-1} (yielding a minimum at 2143 cm^{-1}). Absorption bands of CO between 2188-2160 cm^{-1}, characterizing oxidized $Au^{\delta+}$ sites, were not observed on the active catalyst under reaction conditions.

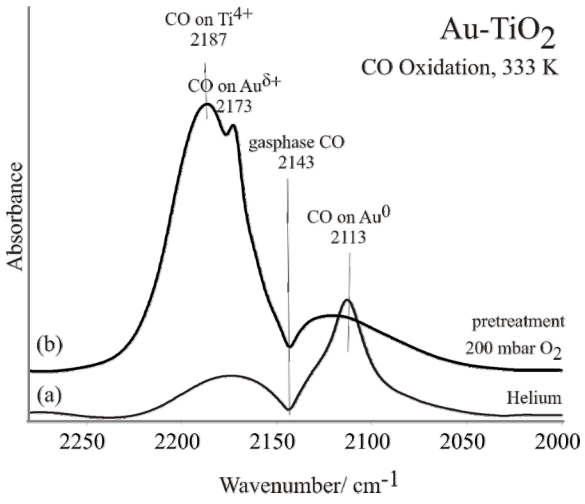

Figure 5-3 *In situ* FTIR spectra of Au-TiO_2 collected during CO oxidation after (a) usual activation in 1 bar helium at 373 K and (b) oxidative pre- treatment in 200 mbar O_2 (balance helium to 1 bar) at 373 K.

However, an oxidative pre-treatment (heating to 373 K in 200 mbar oxygen, helium balance to 1 bar) led to an almost complete loss of catalytic activity (the conversion decreased from 30% to 0.2% upon pre-oxidation) and the corresponding *in situ* FTIR spectrum is shown in Figure 5-3b. Two new CO absorption bands can be identified at 2187 cm^{-1} and at 2173 cm^{-1}, with the first being due to CO adsorbed on Ti^{4+} of the support [34] (supported by reference measurements on the pure TiO_2 support; not shown), and the latter being due to CO adsorbed on oxidized $Au^{\delta+}$ (not observed for the pure TiO_2 support). Therefore it can be concluded, that the major CO adsorption sites on the active Au-TiO_2 catalyst are zero-valent gold atoms and that oxidation to $Au^{\delta+}$ leads to deactivation.

b) The oxygen adsorption sites

Figure 5-4a compares the CO adsorption bands on Au-TiO_2 in the presence and absence of oxygen. In the presence of oxygen (under reaction conditions of 50 mbar CO, 50 mbar O_2, balance He) the C-O stretching frequency was found at 2113 cm^{-1}. This spectrum was collected during 20% CO conversion (at 323 K), i.e. the effective CO partial pressure was reduced to 40 mbar under reaction conditions. Accordingly, the comparative measurement in the absence of oxygen was performed at the same CO background pressure (40 mbar CO in helium balanced to 1 bar) to avoid pressure-dependent band shifts caused by different CO coverage. The absorption spectrum in the absence of oxygen (Figure 5-4) showed a strong red shift of the CO absorption band down to 2103 cm^{-1} or, in other words, the presence of oxygen leads to a strong blue shift of the CO absorption band. Hartshorn *et al.* [35] investigated CO adsorption on the same commercial AURO*lite*™ catalyst by infrared transmission spectroscopy in the pressure range 10–0.05 Torr at 295 K and observed a similar frequency shift due to variable CO coverages. With decreasing CO pressure the CO peak position shifted from 2106 to 2113 cm^{-1}, as typically observed for CO adsorption on gold [34]. (Note that a red-shift with decreasing coverage is rather characteristic of CO adsorbed on metals [34, 36]). However, this was paralleled by a ~5-fold decrease in intensity. The strong blue shift in the presence of O_2 can thus

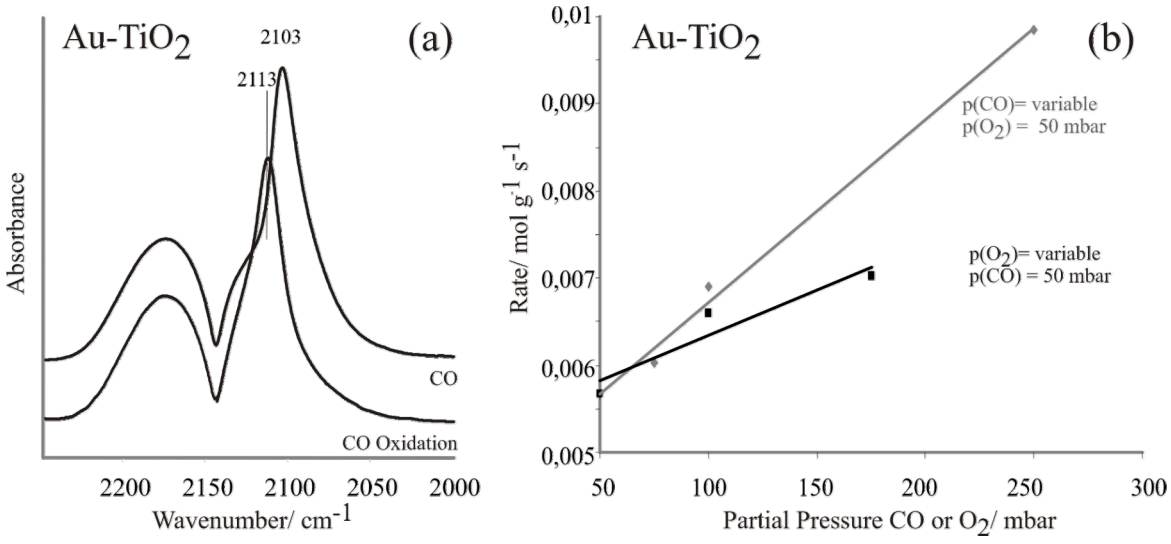

Figure 5-4 FTIR and *in situ* FTIR spectra of Au-TiO_2: (a) Comparison of the CO absorption band in absence (CO/He- flow) and presence of oxygen (usual reaction conditions) and (b) influence of the oxygen and CO partial pressure on the catalytic activity.

not be explained by a reduction in CO coverage but rather points to coadsorption of CO and oxygen on the gold particles affecting the CO frequency, e.g. by creating positively charged gold species upon transfer of electron density from gold to O_2 [37, 38]. Coadsorption of oxygen and CO can lead to even stronger blueshifts up to ~2138 cm^{-1} [20, 39]. Kinetic measurements performed with variable $p(CO)/p(O_2)$- ratio (see Figure 5-4b) clearly showed a positive reaction order in oxygen and in CO (in the range examined). The activity increase for both reactants demonstrates a non- competitive adsorption behaviour (also found by Bollinger *et al.* [13]) indicating that CO and oxygen possess different adsorption sites. Apparently, the electronic properties of the gold particles are strongly influenced by O_2 adsorption, either upon O_2 adsorption *directly* on the particles or on the support (such as at the boundary with the particles). Below it is demonstrated that the catalytic activity decreased when molecular water accumulated on the TiO_2 support. Although CO adsorption (the CO band position) was unaffected by the accumulating water, deactivation was nevertheless observed. This indicates that oxygen rather than CO adsorption was inhibited, therefore suggesting that the O_2 adsorption sites were located on the (water "poisoned") support.

5.3.2 Nature of surface species- before and during reaction

Before discussing the role of hydroxyl groups and the nature of possible intermediates during the CO oxidation reaction, a general overview on the various types of surface species (present before and during the CO oxidation reaction) is essential:

a) Nature of surface species before reaction

The FTIR spectra (dotted lines) in Figure 5-5 were collected at 333 K directly after activation of (a) Au-TiO_2 and (b) the TiO_2 support in Helium flow at 373 K.

Very weak absorption bands were observed at 1800-1200 cm^{-1} and could be assigned to carbonate species [34, 40, 41]. Their presence (even though in very low quantity) on both samples indicated that the carbonates were located on TiO_2 and that they were quite stable, being still present after heating to 373 K.

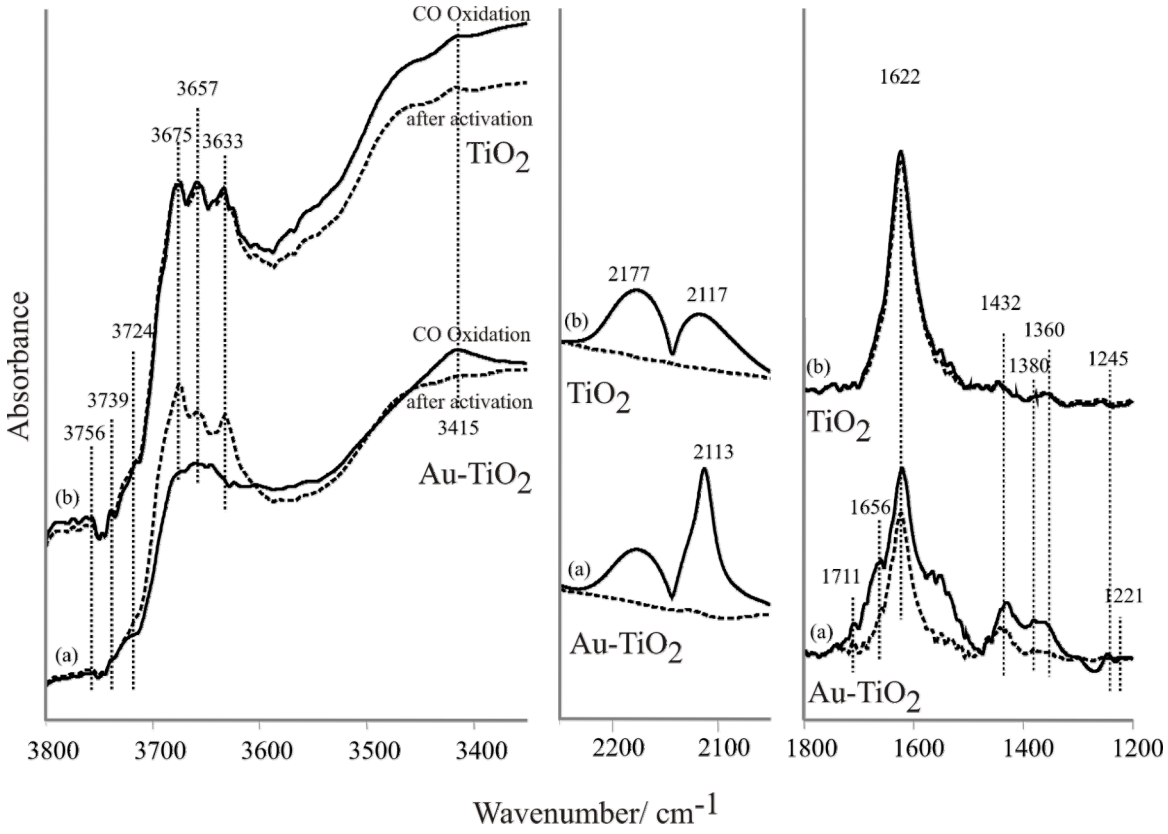

Figure 5-5 FTIR spectra collected at 333 K of (a) Au-TiO_2 and (b) TiO_2 after activation in Helium (dotted line) and *in situ* FTIR spectra during CO oxidation (solid line).

Both samples possess a significant amount of molecularly adsorbed water, indicated by the H-O-H deformation mode at 1622 cm^{-1} and the broad band in the O-H stretching region below 3600 cm^{-1} (with the broadening indicating that water molecules strongly interact via hydrogen bonding). Additionally, intense OH bands above 3600 cm^{-1} were visible, characteristic of terminal (>3700 cm^{-1}) and bridged (<3700 cm^{-1}) OH groups [42, 43] with stretching frequencies at 3756, 3739, 3724, 3675, 3657 and 3633 cm^{-1}.

This points out that water (adsorbed both molecularly and dissociatively as hydroxyls) is present under reaction conditions- even without additional water feed- and that OH groups represent the major surface species after activation.

b) Nature of surface species during CO oxidation reaction

Upon addition of the reaction mixture to Au-TiO_2 at 333 K (solid spectrum in Figure 5-5a), a CO conversion of 30% was observed, corresponding to a turnover frequency of ~3.5 CO molecules per surface gold atom and per second (for 3.8 nm gold particles). The intense OH bands above 3600 cm^{-1} strongly decreased in the first 10 minutes and finally reached an intensity as displayed in the spectrum in Figure 5-5a.

Additionally, CO adsorbed on Au^0 (2113 cm^{-1}) was observed and several intense bands appeared at 1800-1200 cm^{-1}, indicating the formation of carbonate and/or carboxylate and/or hydroxycarbonyl-species (referred to all as “carbonate-like” species in the following) under reaction condition. Due to the absence of C-H- stretching frequencies (around 2900 cm^{-1}) we can exclude the presence of formates (that would induce bands in this region [44]). Nevertheless, the exact assignment of the observed species will be discussed in more detail below.

In contrast, when the CO+O_2 mixture was fed to the pure TiO_2 support (with gas phase analysis detecting no CO oxidation activity) the OH-groups were unaffected and no additional carbonate- like species were formed (see solid line in Figure 5-5b).

Catalytic activity is thus paralleled by a strong decrease of surface (terminal and bridged) OH-groups and by the formation of carbonate-like species. The nature and role of both species is discussed in the following.

5.3.3 The role of hydroxyl groups and carbonate-like intermediates

As mentioned, catalytic activity is apparently connected to a strong decrease of surface hydroxyl groups and the formation of carbonate-like species. In an effort to proof i) whether these OH-groups are able to oxidize CO and ii) whether carbonate-like species are reactive intermediates, we have carefully analyzed the interaction of CO and CO_2 with Au-TiO_2 (in the absence of oxygen) by FTIR spectroscopy.

Blank measurements with the pure support were performed in addition, to discriminate between processes on gold and on TiO_2. Finally, the results were compared to the *in situ* FTIR measurements performed during CO oxidation on Au-TiO_2, in order to assign and identify the surface species present under "working" conditions.

a) Interaction (reaction) of Au-TiO_2 with CO

The adsorption of CO on Au-TiO_2 led to a strong decrease of hydroxyl groups, as evident from the negative bands in the OH stretching region of the difference spectrum (dotted line in Figure 5-6a).

Additionally, CO_2 was observed at 2346 cm^{-1} (not shown) which indicated the formation of CO_2 upon interaction (reaction) of CO with Au-TiO_2. Simultaneously, carbonate-like species appeared, indicated by the intense absorption bands at 1800-1200 cm^{-1} (dotted line in Figure 5-6a).

This experiment indicated the formation of CO_2 and carbonate-like species upon interaction/reaction with CO (in the absence of oxygen) via consumption of OH. However, carbonate formation is a well-known effect on oxide supported metal-nanoparticles that can also occur on the bare support.

The exact mechanism is not clear but carbonate formation may proceed via (adsorbed) CO_2 as intermediate which further reacts with the support forming variable types of carbonates and bicarbonates.

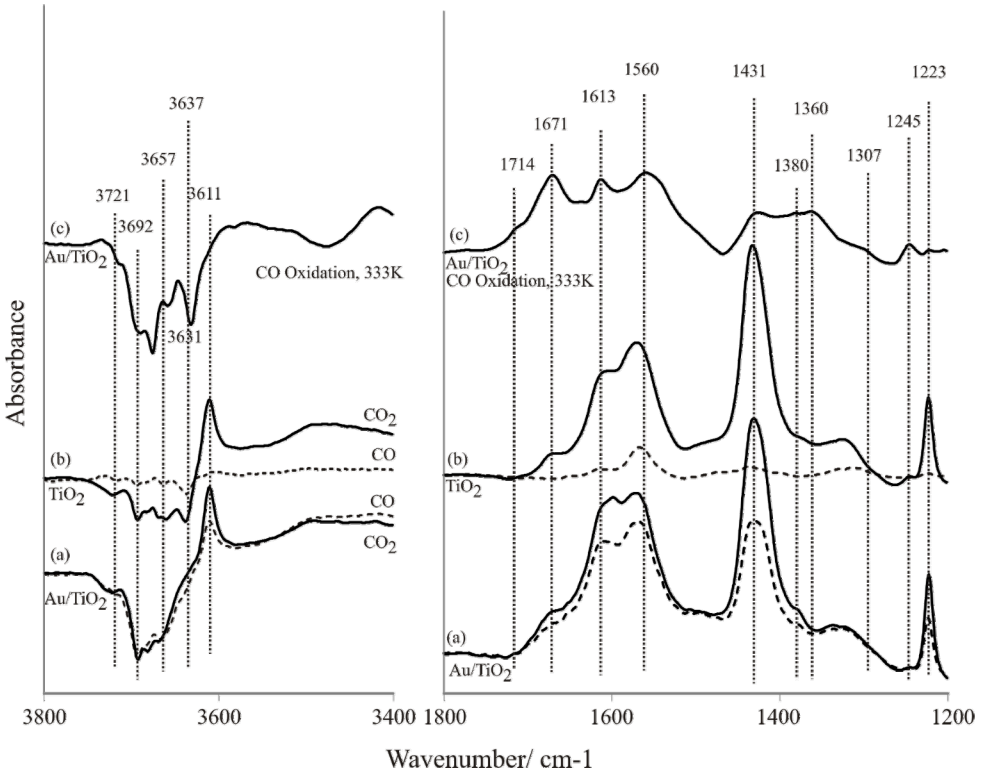

Figure 5-6 Carbonate species and OH stretching region on (a) Au-TiO_2 and (b) TiO_2 upon CO adsorption (dotted line) and CO_2 adsorption (solid line) in comparison to (c) the surface species present during the CO oxidation reaction on Au-TiO_2. All spectra shown are difference spectra (referenced to the corresponding spectra taken before admission of CO, CO_2 and CO/O_2).

Therefore, in a next step we compare the observed interaction of CO and CO_2 with Au-TiO_2 with that on (pure) TiO_2 support, in order to i) investigate if the observed CO_2 formation is related to gold or rather to the TiO_2 support and ii) to further characterize the carbonate-like species formed under reaction conditions.

b) Interaction of CO and CO_2 with Au-TiO_2 and TiO_2

Figure 5-6a compares the FTIR spectra obtained upon CO (dotted line) and CO_2 adsorption (solid line) on (a) Au-TiO_2 and (b) TiO_2 with the *in situ* spectrum (c) obtained during CO oxidation (all spectra are difference spectra).

Carbonate formation upon CO and CO_2 adsorption: In the carbonate-region bands appear at 1671, 1613, 1560, 1431, 1380, 1245 and 1223 cm^{-1} both for Au-TiO_2 and TiO_2. The fact that each carbonate-like species formed upon CO adsorption is also present upon CO_2 adsorption (even in higher quantity) confirms CO_2 being an intermediate for

the formation of the observed species. This further shows that carboxyhydroxyl-species are not involved because this would require a reduction of CO_2 to be observed upon CO_2 adsorption.

Shubina *et al.* [45] calculated the vibrational frequencies of carboxyhydroxyl (COOH) adsorbed on Au(110) using DFT: δ_{OH} = 1245 cm^{-1}, ν_{CO} = 1748 cm^{-1} and ν_{OH} = 3518 cm^{-1}. In fact, Henao *et al.* [46] observed a species at 1246 cm^{-1} and assigned it to carboxyhydroxyl on gold. Even though a band at 1245 cm^{-1} was observed under reaction conditions (Figure 5-6c), it cannot be assigned to a carboxyhydroxyl species on gold because i) it was formed upon CO_2 adsorption as well (Figure 5-6a- solid spectrum) and b) it also occurred on the pure TiO_2 support (Figure 5-6b- solid spectrum).

A comparison with the CO_2 adsorption experiment on TiO_2 (solid line in Figure 5-6b) yields exactly the same type and also a similar amount of carbonate-like species on the pure TiO_2 support. This reveals that carbonate species observed on Au-TiO_2 are located on the support and no intermediates can thus be related to gold. However, CO adsorption on pure TiO_2 (dotted line in Figure 5-6b) led to almost no carbonate formation. This indicates that a much smaller amount of carbonates is formed upon direct reaction between CO and the (pure) support and TiO_2 apparently has a very low CO_2 formation ability. Therefore, CO_2 formation upon CO adsorption on Au-TiO_2 must be related to gold.

No other intermediates were identified at 1800-1200 cm^{-1} and all observed carbonates demonstrate re-adsorption products of CO_2. Their assignment is not straightforward because these carbonates may (co-)exist in very different structures. According to the literature [34, 40, 41] the bands at 1613, 1431 and 1223 cm^{-1} can be assigned to bicarbonates since they appear together with an OH stretching frequency at 3611 cm^{-1} (also visible in Figure 5-6). Additionally, bridged bidentate carbonates (1711 cm^{-1}), chelating bidentate carbonates (1674 and 1245 cm^{-1}) and monodentate carbonates (1560, 1380 and 1360 cm^{-1}) may be present as well. Boccuzzi *et al.* [47] assigned the bands at 1674 and 1245 cm^{-1} to carboxylate COO^- intermediates adsorbed on Ti^{3+} close to gold particles. However, this assignment can also be excluded because this species was observed i) also upon CO_2 adsorption and ii) also on the pure TiO_2 support (see Figure 5-6).

Decreasing OH species upon CO and CO_2 adsorption: Upon CO adsorption on Au-TiO_2, as already discussed, decreasing OH bands were observed. However, upon CO_2 adsorption the OH bands also strongly decreased. The formation of bicarbonates (that are created upon reaction between CO_2 and OH-groups producing bands at 3611, 1613, 1431 and 1223 cm^{-1}) or the displacement of surface OH-groups (via water desorption) by carbonates could explain this behaviour.

A comparison of the relative amount of the consumed/desorbed OH-groups (integrated band area 3600-3800 cm^{-1}) and the formed carbonates on Au-TiO_2 upon CO and CO_2 adsorption (integrated band area 1800-1200 cm^{-1}) shows that upon CO adsorption on Au-TiO_2 ~10% more OH-groups were consumed, as compared to CO_2 adsorption leading to the same amount of carbonates.

This increase is even stronger when we neglect OH replacement/desorption and assume that the OH band decrease upon CO_2 adsorption is caused by the formation of bicarbonates only. Comparing the relative amount of bicarbonates (taking the integrated area of the band at 1431 cm^{-1}) with the relative amount of OH-groups consumed (integrated band area 3600-3800 cm^{-1}), then a 50% higher OH-group consumption is observed upon CO adsorption in comparison to CO_2 adsorption. This indicates an involvement of OH-groups in CO_2 formation but also shows that re-adsorption of CO_2 leads to further decrease via the formation of bicarbonates and/or carbonates.

c) Identification of carbonate-like species under reaction conditions

Figure 5-6 compares the *in situ* FTIR spectrum (c) collected under typical reaction conditions with the CO and CO_2 adsorption spectra of (a) Au-TiO_2 and (b) TiO_2, that were already discussed. Obviously, exactly the same species are present under reaction conditions (no new species were identified in the presence of oxygen) and only the relative concentrations/contributions of the particular species were different.

This demonstrates that all carbonate species present under reaction conditions were located on the titania support, no carboxyhydroxyl intermediate was detected and each carbonate observed under reaction conditions was a consequence of CO_2 (product) re-

adsorption and did not represent carbonate intermediates (which was also proposed in [9]).

Additionally, no correlation was found between the total amount of surface-carbonates and the activity, i.e. no deactivation was observed upon carbonate formation, as has been reported in literature [24-26]. However, assuming 3.8 nm Au particles, ~ 99.2 % of the total catalyst surface area corresponds to the support and a minor blocking of the available support surface by carbonates is probably insignificant. This may not be true for e.g. model catalysts for which the re-adsorption of the product CO_2 may have deactivating character (as e.g. reported in [26]). Additionally, the Au-TiO_2 catalyst used in this study possesses a significant amount of water on the surface even under "dry" (i.e. without additional water supply) reaction conditions. This may inhibit the formation and thus observation of "deactivating carbonates".

Also, the strong negative OH bands at 3800-3600 cm^{-1} indicated a decreasing quantity during CO oxidation. Comparing again the relative OH band intensity (integral band area 3800-3600 cm^{-1}) with the carbonate band intensity (integral band area 1800-1200 cm^{-1}) a 60% stronger decrease of the OH band as compared to CO_2 adsorption (normalized to an equal amount of carbonates) is observed. This again verifies that the decrease of the support OH species cannot only be explained by re-adsorption of CO_2 but that the OH groups are additionally decreased during the CO_2 formation reaction.

It can be summarized that CO and CO_2 adsorption experiments on Au-TiO_2 and TiO_2 clearly showed enhanced CO_2 and consequently carbonate formation on Au-TiO_2 upon interaction with CO (in the absence of oxygen), which was not observed for pure TiO_2. The formation of carbonates upon direct reaction of CO with the pure support proceeds with very low efficiency (Figure 5-6b). It can therefore be concluded that the carbonates observed in the region (1800-1200 cm^{-1}) mainly occur upon CO_2 re-adsorption on TiO_2.

The enhanced CO_2 formation in the presence of gold together with the decreased intensity of the hydroxyl-bands indicates that the OH-groups of the support are able to oxidize CO via a "water gas shift" type reaction: $CO + OH \rightarrow CO_2 + ½\ H_2$.

However, disproportionation of CO (2 CO $\rightarrow$ CO_2 + C), which may take place on reduced titania [48] could be an alternative reaction that would also lead to CO_2 in the absence of oxygen. Enhanced CO adsorption on the gold particles and a spill-over of CO to the support could also explain increased CO_2 production with respect to the pure support.

In order to differentiate between these two mechanisms and to proof the ability of OH-groups on Au-TiO_2 for CO oxidation, adsorption experiments of isotopically labelled CO and CO_2 were performed and are described in the following section.

d) Mechanism of CO_2 and carbonate formation on Au-TiO_2 in the absence of oxygen

In order to exclude CO disproportionation on reduced TiO_2 as pathway for CO_2 formation, the adsorption of isotopically labelled $^{13}C^{18}O$ was performed: CO_2 formation upon disproportionation should lead to $^{13}C^{18}O_2$ (2 $^{13}C^{18}O \rightarrow {}^{13}C^{18}O_2 + {}^{13}C$) with characteristic $^{13}C^{18}O_2$ gas phase absorption bands. In case of $^{13}C^{18}O_2$ re-adsorption (upon further reaction with the support) the obtained carbonate species should mainly show $^{13}C^{18}O$ vibrations. In contrast, a "water gas shift"- type reaction should lead to $^{13}C^{18}O^{16}O$ ($^{13}C^{18}O + {}^{16}OH \rightarrow {}^{13}C^{18}O^{16}O + ½\ H_2$) and thus $^{13}C^{18}O^{16}O$ gas phase absorption bands and the carbonate species should possess both $^{13}C^{18}O$ and $^{13}C^{16}O$- vibrational bands. In order to assign and confirm the observed frequencies, reference adsorption experiments were performed with $^{13}C^{18}O_2$ and $^{13}C^{16}O_2$ ($^{13}C^{18}O^{16}O$ was not available). In case the CO_2 formation would be caused by CO disproportionation the infrared spectrum after $^{13}C^{18}O$ adsorption should basically resemble that after $^{13}C^{18}O_2$ adsorption on Au-TiO_2.

Upon exposure of 1 mbar $^{13}C^{18}O$ (Figure 5-7b) to Au-TiO_2 a small double-peak with maxima at 2281 cm^{-1} and 2264 cm^{-1} appeared which can be assigned to gas-phase $^{13}C^{18}O^{16}O$. This clearly supports the "water gas shift"-type reaction between CO and surface OH groups as CO_2 formation pathway. Additionally, carbonate bands appearing at 1616, 1565, 1524, 1381 and 1217 cm^{-1} did not match with the vibrational bands observed after adsorption of $^{13}C^{18}O_2$ (Figure 5-7a).

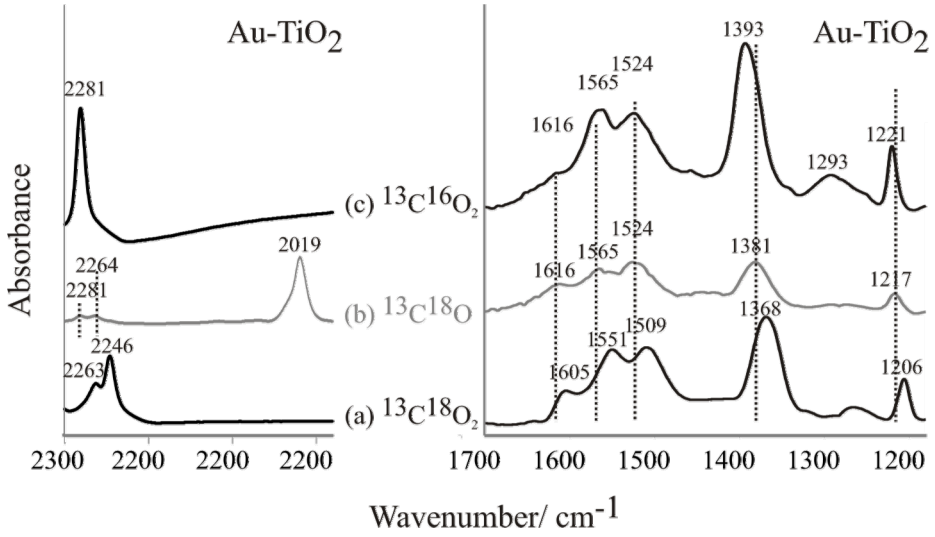

Figure 5-7 Adsorption of 1 mbar (a) $^{13}C^{18}O_2$, (b) $^{13}C^{18}O$ and (c) $^{13}C^{16}O_2$ at 293 K on Au-TiO_2: Difference spectra of the carbonate region obtained by subtracting the corresponding spectra acquired before gas exposure.

Therefore, disproportionation can be excluded as CO_2 formation mechanism. The obtained spectrum is rather similar to that after $^{13}C^{16}O_2$ adsorption (Figure 5-7c) or represents absorption bands between those observed during $^{13}C^{18}O_2$ and $^{13}C^{16}O_2$ adsorption. This indicates re-adsorption of $^{13}C^{18}O^{16}O$ and therefore supports the "water-gas shift" route as mechanism for CO_2 formation on Au-TiO_2.

5.3.4 The influence of water on the catalytic performance

The results already presented indicated that CO can be oxidized via a "water gas shift-type" reaction on Au-TiO_2. If OH groups were directly involved in the CO oxidation mechanism, an increased number of available OH-groups on the support (catalyst surface) would have a beneficial effect on catalytic activity. Since TiO_2 is known for its excellent ability for water dissociation [42, 49], an increase of the catalytic activity in the presence of water could be explained by an increased amount of OH-groups, created upon water dissociation on the TiO_2 support. In order to proof this hypothesis, the CO oxidation performance of Au-TiO_2 was investigated with and without additional water supply (variable amount of water added via a saturator) by *in situ* FTIR spectroscopy/GC.

a) Kinetic measurements during water addition

Figure 5-8 displays (a) the catalytic activity versus time-on-stream as a function of water addition and (b) the corresponding *in situ* FTIR spectra collected during the reaction. The reaction was started under "dry" reaction conditions (at this point one has to mention that according to the specification of the used gases the reaction mixture may contain up to $3x10^{-3}$ mbar water vapour). The addition of 21 mbar water (after 55 min) led to an ~two-fold increase of the catalytic activity per gold weight, i.e. from 0.004 mol/s g to 0.007 mol/s g. However, no constant catalytic activity was reached but the activity subsequently decreased continuously with time-on-stream and levelled off around ~1.5 times higher than under dry conditions. As soon as the water supply was stopped (110 min) another increase followed by a gradual decrease in activity was observed (after 270 min still being 1.3 times higher as before water supply). The decreasing catalytic activity during water supply together with the increase as soon as the water supply was stopped indicates that only small amounts of water are needed to enhance the catalytic activity. Too much water decreases the catalytic activity, even though it may still be higher than the initial "dry activity". This experiment was repeated with variable water content.

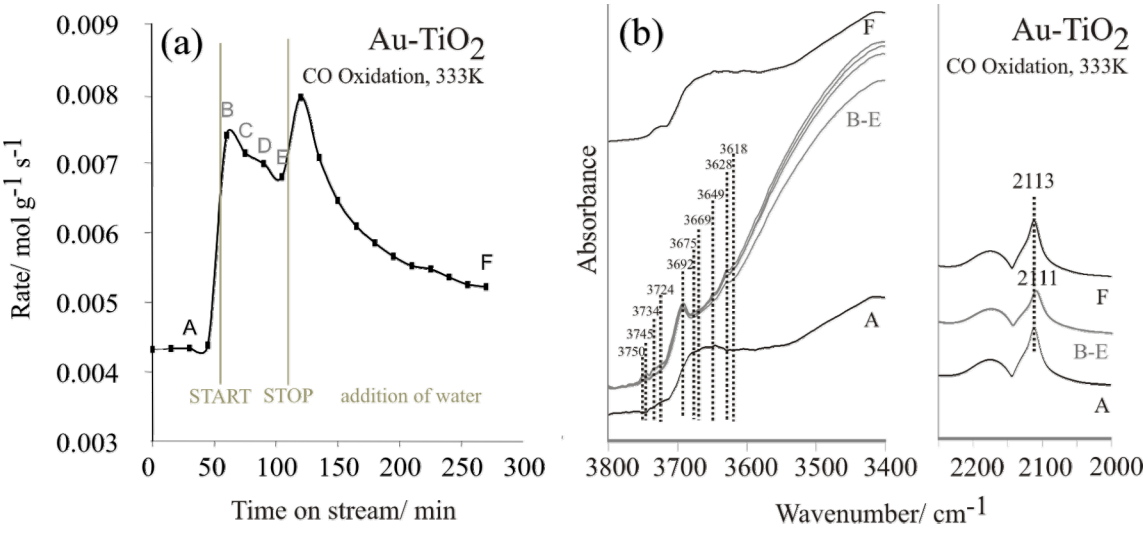

Figure 5-8 *In situ* FTIR spectroscopy of CO oxidation combined with gas phase analysis before, during and after water addition on Au-TiO_2: (a) Time dependence of catalytic activity and (b) corresponding *in situ* FTIR spectra collected under dry reaction conditions (A), during 21 mbar water supply (B-E) and after the switch back again to dry conditions (F); The spectra are labelled with capital letters in (a) to indicate the time of IR spectra collection.

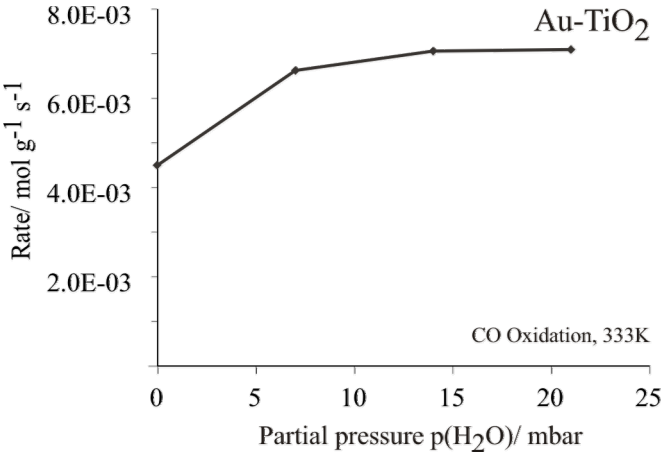

Figure 5-9 Influence of the water partial pressure in the reactant mixture on the catalytic activity on Au-TiO_2.

Figure 5-9 shows the catalytic activity under variable water partial pressure in comparison to "dry" reaction conditions (the values correspond to the averaged catalytic activity over 1.5h moisture exposure- since in every experiment the same time dependence as demonstrated in Figure 5-8a was obtained- not shown). Apparently (at least up to 21 mbar water content), the increase in catalytic activity was independent of the water partial pressure in the reactant mixture (within the experimental error). Similar behaviour was observed by Date and Haruta [50] showing that rather the amount of adsorbed water on the catalyst surface was essential for catalytic performance and not so much the moisture content in the feed. Obviously, the amount of adsorbed water was independent from the water partial pressure in the investigated parameter range. The slow decrease of the reaction rate when the water addition was stopped indicates water desorption with time-on-stream, therefore water adsorption (molecular and/or dissociative) is widely reversible.

b) *In situ* FTIR spectroscopy during water addition

Figure 5-8b displays the corresponding *in situ* FTIR spectra collected upon water addition during CO oxidation on Au-TiO_2. The spectra were marked with capital letters to identify the time of data collection in Figure 5-8a. Under dry reaction conditions (spectrum A) decreased bands in the OH-stretching region were again observed (in comparison to the fresh activated catalyst (see again Figure 5-5a) indicating the involvement of

OH-groups in the CO oxidation reaction. Additionally, the CO band located at 2113 cm^{-1} was visible- corresponding to CO adsorbed on zero-valent gold.

The addition of water (spectrum B, collected after 5 minutes of water supply) leading to increased activity, was accompanied by the formation of additional bands in the OH-stretching regions with the most intense species located at 3750, 3745, 3734, 3724, 3692, 3675, 3669, 3649, 3628 and 3618 cm^{-1}. This shows that additional terminal (>3700 cm^{-1}) and bridged OH-groups (<3700 cm^{-1}) were created via water dissociation on the TiO_2 support. Additionally, a broad O-H absorption band centered at 3400 cm^{-1} was observed which corresponds to molecular water adsorbed on the catalyst surface (accompanied by the H-O-H deformation band at 1622 cm^{-1}; not shown).

Interestingly, the CO absorption band was shifted from 2113 cm^{-1} to 2111 cm^{-1} and decreased in intensity. One may have expected a blue shift of the CO stretching frequency, caused by a lower CO coverage due to the higher catalytic activity. However, the opposite was observed which indicates that the CO adsorption properties are altered upon water addition. Electron density transfer from the OH groups to the gold may explain the red shift observed: increased electron density on the gold surface decreases the extend of 5σ donation from CO to Au [51]: this reduced stabilization of the 5σ orbital weakens the C-O bonding (red shift of the CO stretching frequency) which indicates an adsorption of OH-groups on or at least in the vicinity (at the periphery) of the gold particles.

Spectra C-E (collected after 20, 35 and 50 min water supply respectively) show several interesting results. First of all, the intensity of the new created OH-bands (3600-3800 cm^{-1}) remained constant after 20 min but the broad band centred at 3400 cm^{-1} continuously increased with TOS water supply. Obviously, the maximum number of terminal and bridged OH-groups was already obtained after 20 minutes and cannot be increased upon further water supply. This does not hold for molecular water that accumulated on the catalyst surface with time-on-stream water supply.

Interestingly, neither the CO stretching frequency nor the CO absorption band intensity changed upon further water supply, which showed that the continuously increased

amount of molecular water on the catalyst surface did not influence the CO adsorption properties. Apparently, the gold particles remained unaffected by the accumulating molecular water, even though a stepwise decreasing catalytic activity was observed. This suggests that the accumulating water alters, or in other words, blocks the oxygen adsorption sites by the increasing amount of molecular water on the support surface, which again indicates that the oxygen adsorption sites are located on the TiO_2 support.

At this point one should mention that without oxygen supply (with a reactant mixture of $CO/H_2O/He$) no activity was observed in the temperature range 273-423 K, i.e. oxygen supply was essential for catalytic activity. (According to the phase-boundary mechanism proposed by Bond and Thompson [31] oxygen is necessary to oxidize the carboxyhydroxyl intermediate.) Finally, no correlation between the absolute amount of carbonates and catalytic activity and no decrease in the amount of carbonates was observed upon water supply (as reported e.g. by Hao *et al* [28]) that could cause a higher catalytic activity.

It can be summarized that the increased reaction rate upon water addition can be explained by the formation of additional terminal and bridged hydroxyl groups on the catalyst surface, which supports the involvement of OH-groups in the CO oxidation mechanism. However, further water supply leads to a continuous decrease of the reaction rate caused by the blockage of the O_2 adsorption sites by the accumulating water on the TiO_2 support.

5.4 Conclusions

i) Zero-valent gold atoms Au^0 were identified as the main CO adsorption sites under high catalytic activity whereas the detection of significant amounts of oxidized $Au^{\delta+}$ was paralleled by deactivation.

ii) The non-competitive adsorption properties of CO and O_2, together with the fact that molecular water (accumulated on the support surface upon water addition) did not influence the CO adsorption properties on the gold particles but led to significant deacti-

vation (indicating a blocking of oxygen adsorption), suggested that the oxygen adsorption sites were located rather on the TiO_2 support than on the gold particles.

iii) Adsorption experiments with isotopically labelled and unlabelled CO and CO_2 clearly demonstrated that (support) OH groups are able to oxidize CO to CO_2 (even though no steady state activity was observed in the absence of oxygen). The promotional effect of water traces on the catalytic activity was explained by an increased amount of terminal OH-groups (detected by FTIR spectroscopy) created via water dissociation on TiO_2.

iv) All observed carbonates were generated upon re-adsorption of the product (CO_2) on the support and did not cause deactivation.

v) No carboxyhydroxyl-intermediates were detected via FTIR spectroscopy, which suggest their formation as being the rate limiting step.

Finally, even though no carboxyhydroxyl intermediates and oxidized $Au^{\delta+}$ were detected, strong evidence for a phase-boundary mechanism proposed by Bond and Thompson [31] was found since the involvement of OH-groups during CO oxidation was identified and the oxygen adsorption site was localized on the support. However, a direct reaction of CO (adsorbed on gold) with oxygen (dissociating on the support at the periphery to the gold particles) occurring in parallel cannot be excluded.

References

[1] G.C. Bond, P.A. Sermon, G. Webb, D.A. Buchanan, and P.B. Wells, Journal of the Chemical Society-Chemical Communications (1973) 444.

[2] M. Haruta, N. Yamada, T. Kobayashi, and S. Iijima, Journal of Catalysis 115 (1989) 301.

[3] M. Haruta, S. Tsubota, T. Kobayashi, H. Kageyama, M.J. Genet, and B. Delmon, Journal of Catalysis 144 (1993) 175.

[4] H. Falsig, B. Hvolbaek, I.S. Kristensen, T. Jiang, T. Bligaard, C.H. Christensen, and J.K. Norskov, Angewandte Chemie-International Edition 47 (2008) 4835.

[5] C. Lemire, M. Randall, S. Shamil, and F. Hans-Joachim, Angewandte Chemie International Edition 43 (2004) 118.

[6] N. Lopez, T.V.W. Janssens, B.S. Clausen, Y. Xu, M. Mavrikakis, T. Bligaard, and J.K. Nørskov, Journal of Catalysis 223 (2004) 232.

[7] I.N. Remediakis, N. Lopez, and J.K. Norskov, Angewandte Chemie-International Edition 44 (2005) 1824.

[8] M. Valden, X. Lai, and D.W. Goodman, Science 281 (1998) 1647.

[9] M.M. Schubert, S. Hackenberg, A.C. van Veen, M. Muhler, V. Plzak, and R.J. Behm, Journal of Catalysis 197 (2001) 113.

[10] M. Mavrikakis, P. Stoltze, and J.K. Norskov, Catalysis Letters 64 (2000) 101.

[11] Y. Xu, and M. Mavrikakis, Journal of Physical Chemistry B 107 (2003) 9298.

[12] W. Yan, S.M. Mahurin, B. Chen, S.H. Overbury, and S. Dai, The Journal of Physical Chemistry B 109 (2005) 15489.

[13] M.A. Bollinger, and M.A. Vannice, Applied Catalysis B-Environmental 8 (1996) 417.

[14] J.D. Grunwaldt, M. Maciejewski, O.S. Becker, P. Fabrizioli, and A. Baiker, Journal of Catalysis 186 (1999) 458.

[15] J. Van Bokhoven, A. , C. Louis, J. Miller, T., M. Tromp, O. Safonova, V., and P. Glatzel, Angewandte Chemie International Edition 45 (2006) 4651.

[16] M.A.P. Dekkers, M.J. Lippits, and B.E. Nieuwenhuys, Catalysis Letters 56 (1998) 195.

[17] M.A.P. Dekkers, M.J. Lippits, and B.E. Nieuwenhuys, Catalysis Today 54 (1999) 381.

[18] E.D. Park, and J.S. Lee, Journal of Catalysis 186 (1999) 1.

[19] V.A. Bondzie, S.C. Parker, and C.T. Campbell, J. Vac. Sci. Technology A 17 (1999) 1717.

[20] S. Minico, S. Scire, C. Crisafulli, A.M. Visco, and S. Galvagno, Catalysis Letters 47 (1997) 273.

[21] J.D. Grunwaldt, and A. Baiker, Journal of Physical Chemistry B 103 (1999) 1002.

[22] H. Liu, A.I. Kozlov, A.P. Kozlova, T. Shido, K. Asakura, and Y. Iwasawa, Journal of Catalysis 185 (1999) 252.

[23] M. Azar, V. Caps, F. Morfin, J.L. Rousset, A. Piednoir, J.C. Bertolini, and L. Piccolo, Journal of Catalysis 239 (2006) 307.

[24] C.K. Costello, J.H. Yang, H.Y. Law, Y. Wang, J.N. Lin, L.D. Marks, M.C. Kung, and H.H. Kung, Applied Catalysis a-General 243 (2003) 15.

[25] M. Date, H. Imai, S. Tsubota, and M. Haruta, Catalysis Today 122 (2007) 222.

[26] T. Diemant, J. Bansmann, and R.J. Behm, Vacuum 84 (2009) 193.

[27] B. Schumacher, Y. Denkwitz, V. Plzak, M. Kinne, and R.J. Behm, Journal of Catalysis 224 (2004) 449.

[28] Y. Hao, M. Mihaylov, E. Ivanova, K. Hadjiivanov, H. Knozinger, and B.C. Gates, Journal of Catalysis 261 (2009) 137.

[29] F. Boccuzzi, and A. Chiorino, Journal of Physical Chemistry B 104 (2000) 5414.

[30] A. Bongiorno, and U. Landman, Physical Review Letters 95 (2005).

[31] G.C. Bond, and D.T. Thompson, Gold Bulletin 33 (2000) 41.

[32] C.K. Costello, M.C. Kung, H.S. Oh, Y. Wang, and H.H. Kung, Applied Catalysis A: General 232 (2002) 159.

[33] D.R. Lide, Handbook of Chemistry and Physics. Chemical Rubber Company Florida 2000.

[34] K.I. Hadjiivanov, and G.N. Vayssilov, Advances in Catalysis, Vol 47 47 (2002) 307.

[35] H. Hartshorn, C.J. Pursell, and B.D. Chandler, Journal of Physical Chemistry C 113 (2009) 10718.

[36] G. Rupprechter, Advances in Catalysis, Academic Press. 133.

[37] F. Boccuzzi, A. Chiorino, S. Tsubota, and M. Haruta, Journal of Physical Chemistry 100 (1996) 3625.

[38] L.M. Molina, M.D. Rasmussen, and B. Hammer, Journal of Chemical Physics 120 (2004) 7673.

[39] F. Boccuzzi, A. Chiorino, S. Tsubota, and M. Haruta, Catalysis Letters 29 (1994) 225.

[40] A.A. Davydov, Infrared Spectroscopy of Adsorbed Species on the Surface of Transition Metal Oxides. Wiley, Chichester, 1990.

[41] L. Hair, Infrared Spectroscopy in Surface Chemistry. Marcel Dekker, New York, 1967.

[42] K.S. Finnie, D.J. Cassidy, J.R. Bartlett, and J.L. Woolfrey, Langmuir 17 (2001) 816.

[43] M.A. Henderson, Langmuir 12 (1996) 5093.

[44] G. Busca, J. Lamotte, J.C. Lavalley, and V. Lorenzelli, Journal of the American Chemical Society 109 (1987) 5197.

[45] T.E. Shubina, C. Hartnig, and M.T.M. Koper, Physical Chemistry Chemical Physics 6 (2004) 4215.

[46] J.D. Henao, T. Caputo, J.H. Yang, M.C. Kung, and H.H. Kung, Journal of Physical Chemistry B 110 (2006) 8689.

[47] F. Boccuzzi, A. Chiorino, M. Manzoli, D. Andreeva, and T. Tabakova, Journal of Catalysis 188 (1999) 176.

[48] K. Hadjiivanov, J. Lamotte, and J.-C. Lavalley, Langmuir 13 (1997) 3374.

[49] U. Diebold, Surface Science Reports 48 (2003) 53.

[50] M. Date, and M. Haruta, Journal of Catalysis 201 (2001) 221.

[51] M. Chen, Y. Cai, Z. Yan, and D.W. Goodman, Journal of the American Chemical Society 128 (2006) 6341.

6

CONCLUSIONS

The objective of this thesis was to study the mechanism of CO oxidation on industrial-grade palladium and gold nanoparticles under technical relevant reaction conditions. Combining *in situ* EXAFS and *in situ* FTIR spectroscopy provided simultaneous information on the local structural properties of the active catalyst and the adsorbed surface species (reactants, intermediates). A simultaneous determination of the catalytic activity via gas phase analysis by gas chromatography (GC) or mass spectroscopy (MS), allowed a direct assignment of specific catalytic activities to specific structural (or chemical) properties. High-resolution Transmission Electron Microscopy (HRTEM), X-Ray Diffraction (XRD), Chemisorption of Hydrogen or CO and CO adsorption followed by FTIR spectroscopy have been applied as complementary methods for comprehensive (*ex situ*) characterization of the noble metal catalysts. For selected systems Density Functional Theory (DFT) studies enabled a correlation of structure with adsorption properties.

Motivated by the controversially discussed topic whether metallic palladium or a palladium(sub)oxide is more active for CO oxidation under technical relevant reaction conditions, CO oxidation was investigated on industrial-grade Pd nanoparticles.

A comprehensive study of the behaviour of Pd-Al_2O_3 in different oxidative atmospheres revealed the coexistence of metallic Pd and PdO_x over a wide oxygen pressure and temperature range. However, limited Pd oxidation was observed, and temperatures as high as 673 K in 1 bar O_2 were required to obtain substoichiometric PdO_x ($x<1$) particles (with no metallic Pd left). Furthermore, fully oxidized Pd(II)oxide particles were obtained only above 1073-1273 K in 1 bar O_2.

The different PdO_x (x=0-1) nanoparticles, prepared by variable oxidative and reductive pre-treatments, were comprehensively characterized and their catalytic activity for CO oxidation was determined. Substoichiometric PdO_x (x<1) nanoparticles were characterized by a CO absorption band at ~2148 cm^{-1}, corresponding to CO adsorbed on $Pd^{\delta+}$. PdO_x and metallic Pd nanoparticles exhibited comparable high catalytic activity, due to the facile reduction of PdO_x to Pd upon CO exposure (already at 293 K), as demonstrated by FTIR spectroscopy. In contrast, stoichiometric palladium(II)oxide nanoparticles showed no CO adsorption capacity and a lower catalytic activity, explained by the higher stability towards reduction by CO (up to 533 K).

The CO band assignments were corroborated by DFT calculations of CO adsorption on different Pd single crystal facets, their corresponding surface oxides and bulk PdO.

In situ EXAFS and *in situ* FTIR spectroscopy during steady state CO oxidation on Pd-Al_2O_3 detected a partial oxidation of the metal nanoparticles, i.e. a coexistence of metallic palladium and substoichiometric palladiumoxide PdO_x, in the high activity regime. This coexistence circumvented a clear assignment of the catalytic activity to either of these two phases. However, the highly dynamic behaviour of partial PdO_x formation, that can be easily decomposed/reduced (at low temperature) in the presence of CO to metallic palladium, led to oscillatory behaviour under specific conditions.

In situ FTIR and *in situ* EXAFS spectroscopy of oscillatory CO oxidation allowed an unambiguous comparison of the catalytic activities of metallic and oxidic palladium under equal reaction conditions. Conclusive evidence for the oxygen-covered metallic Pd being the more active phase for CO oxidation was found. The *in situ* spectroscopic study of CO oxidation on Pd-Al_2O_3 therefore indicated metallic Pd being essential for the activation of CO (and oxygen) and thus for high catalytic activity.

In order to elucidate the nature of the catalytically active site and the mechanism of **CO oxidation on Au nanoparticles**, CO oxidation was studied on industrial-grade Au-TiO_2 under technical relevant conditions. CO adsorption studies followed by FTIR spectroscopy identified zero-valent gold atoms Au^0 as the main CO adsorption sites under high

catalytic activity. This was further confirmed by *in situ* FTIR spectroscopy indicating deactivation in the presence of significant amounts of oxidized $Au^{\delta+}$.

In contrast, non-competitive adsorption properties of CO and O_2, combined with exclusive blocking of the O_2 adsorption sites (leaving the CO adsorption sites unaffected) when molecular water accumulated on TiO_2, identified the support as oxygen adsorption site.

Adsorption experiments with isotopically labelled and unlabelled CO and CO_2 clearly demonstrated the involvement of support hydroxyl groups in the catalytic reaction. This explained the increase in catalytic activity upon addition of small amounts of water that dissociated on titania producing an increased number of terminal OH groups. The results of the *in situ* FTIR spectroscopy study of CO oxidation on Au-TiO_2 strongly supported a "phase boundary-mechanism", with the reaction taking place at the metal/oxide interface.

PUBLICATIONS

JOURNAL ARTICLES

1. K. Zorn, J.A. Perez-Omil, J.J. Calvino, G. Rupprechter

   In situ FTIR spectroscopic study of the CO oxidation mechanism on industrial-grade Au-TiO_2

   In preparation

2. K. Zorn, K. Föttinger, J.A. van Bokhoven, Y. Suchorski, G. Rupprechter

   Oscillatory CO Oxidation on Pd-Al_2O_3 studied by in situ FTIR and EXAFS spectroscopy

   to be submitted

3. K. Zorn, S. Giorgio, E. Halwax, C. R. Henry, H. Grönbeck, G. Rupprechter

   CO oxidation on industrial-grade Pd-Al_2O_3 catalysts: oxidation state and activity

   Journal of Catalysis, submitted

4. M. Lomoschitz, H. Peterlik, K. Zorn, S. O. Baumann, U. Schubert

   Titanium alkoxo oximates, with surfactant-like properties of the oximate ligands, as precursors for porous TiO_2 and mixed oxide sol-gel films

   Journal of Materials Chemistry, submitted

5. S. Loiha, K. Föttinger, K. Zorn, W. Klysubun, G. Rupprechter, J. Wittayakun

   Catalytic enhancement of platinum supported on zeolite beta for toluene hydrogenation by addition of palladium

   Journal of Industrial and Engineering Chemistry, 15 (2009), 6; S. 819-823.

6. K. Zorn, K. Föttinger, H. Vinek:

   Active sites on Pt containing sulfated zirconia

   Topics in Catalysis, 46 (2007), 93.

7. K. Föttinger, K. Zorn, H. Vinek

   Influence of the sulfate content on the activity of Pt containing sulfated zirconia

   Applied Catalysis A: General, 284 (2005), 69-75.

ORAL PRESENTATIONS AND POSTERS

1. K. Zorn, S. Giorgio, C. Henry, J.A. van Bokhoven, G. Rupprechter
   In situ spectroscopy of active phases during CO oxidation on Pd/Al_2O_3
   Presentation: COST Action D 41 Annual Meeting of the COST Action 2009 Inorganic Oxides: Surfaces and Interfaces (CORR), Institut des Nanosciences de Paris, Paris, France; 22.10.2009 - 24.10.2009; in: "*Book of Abstracts*", (2009).

2. K. Zorn, M. Tew, J. Bokhoven van, S. Giorgio, C. Henry, G. Rupprechter
   In situ investigation of the structure and CO oxidation activity of Pd/Al_2O_3
   Poster: EuropaCat IX 2009, Salamanca, Spain; 30.08.2009 - 04.09.2009; in: "*EuropaCat IX, Catalysis for a Sustainable World*", (2009).

3. K. Zorn, D. Thompson, G. Rupprechter
   CO oxidation on technical gold catalysts
   Presentation: 13th Austrian Chemistry Days 2009, Joint Meeting of the Czech, Slovak & Austrian Chemical Societies, Wien; 24.08.2009 - 27.08.2009; in: "*13th Austrian Chemistry Days 2009, Joint Meeting of the Czech, Slovak & Austrian Chemical Societies*", (2009), S. 9.

4. K. Zorn, C. Weilach, K. Föttinger, G. Rupprechter
   Methanol decomposition on Palladium- Comparison between technical and model catalysts
   Poster: 108. Bunsentagung der Deutschen Bunsen-Gesellschaft für Physikalische Chemie,, Köln; 21.05.2009 - 23.05.2009; in: "*Physical Chemistry of Solids: the Science behind Materials Engineering*", (2009), S. 340.

5. K. Zorn, C Weilach, K. Föttinger, G. Rupprechter
   Methanol decomposition on Palladium-Comparison between technical and model catalysts
   Poster: COST Action D41 Winter School 2009 "Methods to characterize oxide surfaces" corr, Berlin, Germany; 23.02.2009 - 27.02.2009.

6. K. Zorn, S. Giorgio, C. Henry, G. Rupprechter
   Active phases during CO oxidation on Pd catalysts
   Poster: Cost Action D41 Inorganic Oxides: Surfaces and Interfaces, 2008 Annual Meeting of the COST Action, Faculty of Chemistry, Universitat de Barcelona, 08028 Barcelona, Spanien; 16.10.2008 - 18.10.2008.

7. K. Zorn, S. Giorgio, C. Henry, G. Rupprechter
   CO-oxidation on technical palladium catalysts in different oxidation states
   Presentation: 9th Pannonian International Symposium on Catalysis, Strbske Pleso, Slowakei; 08.09.2008 - 12.09.2008; in: "*9th Pannonian International Symposium on Catalysis*", Slovak University of Technology, Bratislava (2008), ISBN: 978-80-227-2923-9; S. 51 - 52.

8. K. Zorn, S. Giorgio, C. Henry, G. Rupprechter
CO Oxidation on Pd/Al2$_2$O$_3$: Correlation between Pd- oxidation state and activity
Poster: 5th International Conference on Environmental Catalysis, Belfast, Großbritannien; 31.08.2008 - 03.09.2008; in: "*5th International Conference on Environmental Catalysis*", (2008), S. 262.

9. K. Zorn, S. Giorgio, C. Henry, G. Rupprechter
Investigation of Pd/Al$_2$O$_3$ for CO oxidation: correlation of palladium oxidation state and activity
Poster: 107. Bunsentagung der Deutschen Bunsen-Gesellschaft für Physikalische Chemie,, Saarbrücken; 01.05.2008 - 03.05.2008; in: "*Analyse, Manipulation und Simulation auf der Nanometerskala*", (2008), S. 186.

10. K. Zorn, S. Giorgio, C. Henry, G. Rupprechter
Active phases during CO oxidation on Pd catalysts
Poster: COST D41 Workgroup 3 Meeting, Marseille, France; 24.04.2008 - 25.04.2008; in: "*Workgroup 3 meeting of COST Action D41 (Inorganic Oxides: Surface and Interfaces)*", (2008), S. 39.

11. K. Zorn, S. Giorgio, C. Henry, G. Rupprechter
CO oxidation on model and technical Pd/Al$_2$O$_3$ catalysts: oxidation state and activity
Presentation: COST Action D41, Inorganic Oxides: Surfaces and Interfaces, 2007 Annual Meeting of the COST Action, Berlin; 21.10.2007 - 23.10.2007.

12. K. Zorn, S. Giorgio, C. Henry, G. Rupprechter
Investigation of Pd/Al$_2$O$_3$ for CO Oxidation: Correlation of Palladium Oxidation State and Activity
Poster: 1.Göch- Symposium, Wien; 19.10.2007 - 20.10.2007; in: "*1. Göch-Symposium 2007 "Physikalische Chemie in Österreich""*", (2007), S. 12 - 13.

13. K. Zorn, S. Giorgio, C. Henry, G. Rupprechter
Investigation of Pd/Al$_2$O$_3$ for CO Oxidation: Correlation of Palladium Oxidation State and Activity
Presentation: 12.Österreichische Chemietage, Klagenfurt; 10.09.2007 - 13.09.2007; in: "*12. Österreichische Chemietage: Book of Abstracts*", (2007).

14. K. Zorn, U J Quaade, G. Rupprechter
Exploring new microreactors for CO oxidation on palladium catalysts in different oxidation states
Poster: 8th European Conference on Catalysis, Turku, Finland; 26.08.2007 - 31.08.2007; in: "*Proceedings of 8th European Conference on Catalysis*", (2007).

15. K. Zorn, K. Föttinger, U J Quaade, G. Rupprechter
New Microreactors for Catalytic Tests
Poster: Bunsentagung 2007, Graz; 16.05.2007 - 18.05.2007; in: "*Proceedings Bunsentagung 2007*", (2007).

16. G. Rupprechter, K. Föttinger, K. Zorn, E Emhofer
Pd nanoparticles on different oxide surfaces: Real versus model catalysts
Presentation: COST D41 Workgroup 3 Meeting, Erlangen, Germany; 13.04.2007; in: "*Proceedings of COST D41 Workgroup 3 Meeting*", (2007), S. 1 - 2.

17. K. Zorn, K. Föttinger, U J Quaade, G. Rupprechter
Mikroreaktoren zur Untersuchung von stark exothermen Reaktionen: CO-Oxidation an Pd/Al2O3
Poster: Jahrestagung Deutscher Katalytiker 2007, Weimar; 14.03.2007 - 16.03.2007; in: "*Proceedings Jahrestagung Deutscher Katalytiker 2007*", (2007), S. 437 - 438.

18. G. Rupprechter, K. Föttinger, K. Zorn
Vibrational spectroscopy on alumina supported Pd nanoparticles: Real vs. model catalysts
Presentation: COST D41 Kick-off Meeting, Wien; 04.11.2006; in: "*Proceedings COST D41 Meeting*", (2006), S. 29.

19. G. Rupprechter, K. Föttinger, K. Zorn
High pressure studies of real and model Pd-alumina catalysts under oxidative conditions
Presentation: NanO2 Workshop, Kloster Irsee, Germany, Irsee; 30.09.2006; in: "*Proceedings NanO2 Workshop, Kloster Irsee, Germany*", (2006), S. 90.

20. K. Zorn, K. Föttinger, H. Vinek
Investigation of active sites on Pt containing sulfated zirconia
Presentation: 4th EFCATS School on Catalysis, St. Petersburg, Russia; 22.09.2006; in: "*Proceedings EFCATS School on Catalysis, St. Petersburg*", (2006), S. 67.

21. K. Zorn, K. Föttinger, H. Vinek
Characterization and catalytic properties of Pt containing sulfated zirconia and sulfated titania
Poster: 105. Bunsentagung, Erlangen, Germany; 25.05.2006 - 27.05.2006; in: "*Heterogene Katalyse: Brücke zwischen Ideal- und Realsystemen*", (2006).

22. K. Zorn, K. Föttinger, H. Vinek
Einfluss der Pt-Verteilung auf die Aktivität von sulfatisiertem Zirkonoxid
Poster: 39. Jahrestreffen Deutscher Katalytiker, Weimar, Germany; 15.03.2006 - 17.03.2006; in: "*39. Jahrestreffen Deutscher Katalytiker*", (2006), S. 325 - 326.

23. K. Zorn, K. Föttinger, H. Vinek
Influence of the sulfate content on the activity of Pt containing sulfated zirconia
Poster: 11. Österreichische Chemietage, Leoben, Österreich; 19.09.2005 - 22.09.2005; in: "*11. Österreichische Chemietage*", (2005).

CURRICULUM VITAE

Personal details

Full Name	Katrin Maria Zorn
Date and place of birth	March 12, 1980; Wels, Austria
Citizenship	Austrian
Address	Kalvarienberggasse 18/1/3;
	1170 Wien, Austria
Email	kzorn@imc.tuwien.ac.at

Education

10/2000-04/2006	Studies of Technical Chemistry, Vienna University of Technology, Austria
04/2006	Dipl.Ing. (M.Sc.), Vienna University of Technology, Austria; Thesis: "Hydroisomerisierung von n-Alkanen über platinierte und sulfatisierte Zirkonoxidkatalysatoren"
since 07/2006	Ph.D. studies in technical chemistry, Vienna University of Technology, Austria; Supervisor: Günther Rupprechter

Research at other Institutions

11/2006	Technical University of Denmark in Kongens Lyngby, Denmark (Prof. U. Quaade)
04/2007	Chemical Research Center of the Hungarian Academy of Science in Budapest, Hungary (Dr. T. I. Koranyi, Prof. J. Valyon)
11/2007, 04/2008	CNRS, Campus de Luminy in Marseille, France (Prof. J. C. Henry)
07/2007, 07/2008	Universidad Rovira i Virgili in Tarragona, Spain (Prof. F. Medina)
10/2008, 09/2009	Eidgenössische Technische Hochschule in Zürich and Swiss Light Source (SLS) in Villigen, Switzerland (Prof. J. A. van Bokhoven).